Entanglement entropy of an analogue black hole

S.J. Hakvoort

Supervisor: Prof. dr. ir. H.T.C. Stoof

Institute of Theoretical Physics
Utrecht University

This dissertation is submitted for the degree of
Master of Science

Utrecht University July 2024

"And the days and the nights
passed
in the company of the Problem."

Cédric Villani

Acknowledgements

First and foremost, I would like to thank Henk Stoof, without whom this project would not have been possible. His enthusiasm and intuition always proved to be a great aid, and whenever the project found itself in murky waters, he managed to motivate me and give me a push in the right direction. I also owe a word of thanks to Ro Jefferson. Despite the fact that we did not collaborate much on the project itself, your research on the intersection of quantum field theory and machine learning truly sparked a new passion of mine, to which I hope to contribute in the near future. Lastly, I want to extend my professional gratitude to César Agón and Pablo Bueno. Without our email correspondence, some of the simulations would not have worked out as well as they did.

But not all support I received over the last year was on a professional level. The countless afternoons and evenings spent in the master's room, university library and abandoned lecture halls would have been a lot less enjoyable were it not for the company of my fellow students. We worked together, ploughed together, struggled together, but most of all succeeded together. Thank you for your endless friendship and support. But lest I forget, I want to extend the most deepfelt gratitude to my family. Without their words of wisdom, kindness and willingness to provide an uninterrupted supply of coffee and tea, this thesis might still be in the making. Finally, I want to extend my gratitude to all those whom I have failed to mention, but nevertheless aided me in writing this thesis.

Abstract

This thesis investigates the two seemingly unrelated topics of analogue black holes and entanglement entropy. After a review of the basic mechanisms behind earlier water-based analogues and analogue black holes in Bose-Einstein condensates, we retrace the ideas behind a recently proposed analogue black hole in a Bose-Einstein condensate of light, in which the authors demonstrate that the acoustic horizon emits phononic radiation. It is suggested that the creation of entangled phonon pairs at the horizon might be behind this phenomenon, which could potentially be confirmed by calculating the entanglement entropy of the acoustic radiation. As the phonons are governed by the equation of motion for free, massless scalar fields, we consider a treatment of entanglement entropy based on the discretization of scalar fields in the direction normal to the entangling surface. The regularized theory is mapped to a finite one-dimensional chain of harmonic oscillators, for which the reduced density matrix is known exactly. This result is used to numerically predict the entanglement entropy of oscillator-chains representing scalar fields in $d \in \{1, 2, 3\}$ spatial dimensions on flat backgrounds, in preparation of the method's future extension to curved spacetimes. We confirm that the analytical results for a (1+1)-dimensional scalar field are approximated by this numerical method, and proceed to verify the area-law for scalar fields in $d = 3$ spatial dimensions. The approach is extended to a method which requires only the position and momentum correlators restricted to subsystems of the full lattice, which allows us to obtain improved results for the studied cases. It is shown that this method can be efficiently used to study the entanglement entropy of scalar fields mapped to square lattices, which we demonstrate explicitly for a discrete circle as a function of its perimeter, and compare its predictions to those of the one-dimensional chain representation of scalar fields.

Table of contents

Chapter 1

Introduction

Generations of physicists have marvelled over the two seemingly unrelated topics of black holes and Bose-Einstein condensates. The former a pinnacle of high-energy physics, while the latter is a favourite among the condensed matter community. It is only on rare occasions that high-energy and condensed matter merge, yet when they do, the results are often interesting and unexpected. One such subdomain crafted from both pillars of physics, are analogue black holes. Though the debate on whether or not these analogues properly capture the inner workings of astrophysical black holes is still ongoing [3, 73], occasionally making the subject slightly controversial, they are nevertheless interesting quantum objects in their own right, which are both theoretically and experimentally realizable and comprehensible. In fact, in recent years multiple experimental realizations have emerged [12], including magnonic analogues in superfluid helium [20] and analogue black-hole lasers [71], with some publications claiming to have measured the acoustic equivalent of Hawking radiation [55].

Before we embark upon developing an understanding of the novel analogue black hole suggested in [48], which lies at the heart of the first part of this thesis, we allow ourselves the freedom to first explore some of the easier analogues, which we do by roughly following the historical developments in this domain. Chapter 3 will commence with a description of the mathematics behind the classical, hydrodynamic models inspired by Unruh's seminal work [75], which is one of the earliest publications on the topic (but inarguably the most significant). However, it will not be long before we tread into the modern world of analogue black hole physics, by fusing these ideas and concepts with Bose-Einstein condensates in the hydrodynamic regime, which have been realized in various experiments, cf. [71, 23]. We explore the general framework and physics behind analogues in Bose-Einstein condensates, and demonstrate the coupling of phonons to an effective metric mimicking curved backgrounds and the existence of an acoustic event horizon. After this brief excursion, we shall return to [48], from which we reproduce its reasoning and mathematics, and demonstrate the presence of acoustic Hawking radiation.

In recent years, there has been considerable attention for measuring acoustic Hawking radiation experimentally [71]. In part because constructing an analogue capable of this phenomenon is a great experimental achievement, but also to elucidate and capture the mechanism underlying the production of thermalized radiation emitted by the acoustic horizon. Some sources for quantum-based analogues, such as the experiment proposed in [48], suggest that the acoustic Hawking radiation is caused by entangled phonon pairs created at or near the acoustic horizon. An advantage of these systems, however, is the fact that the inner region is not 'off-limits' or demanding to describe. The experimentalist can easily peek behind the acoustic event horizon to see what precisely is going on, while perhaps performing a few measurements on the go. It would therefore be interesting to ask ourselves whether one could potentially mathematically demonstrate that the supersonic region ('inner region') and the emitted acoustic radiation are entangled. Sadly, after posing this interesting question, we depart from analogue black holes for the remainder of our story, as we must first construct and test several formalisms to predict the entanglement entropy.

The second part of the thesis is devoted to determining the entanglement entropy of free, massless scalar fields. There are multiple routes to achieve this goal, yet in our case we are particularly interested in a numerical approach known as the 'real time formalism' [58]. The earlier works on this Hamiltonian approach, most notably [69], discretise the field theory to a lattice of shells, which are then reduced to a chain of coupled harmonic oscillators, where the coupling constants are a remnant of the geometry of the original theory. As the Hamiltonian of the (discrete) system is known, the corresponding joint-state wave function, and hence its reduced density matrix, can be found analytically. In Chapter 5 we present the derivation behind this statement and describe an algorithm which extracts the entanglement entropy of the chain by means of the reduced density matrix. Following this derivation, we will test our algorithm on various free, massless scalar fields, in particular those for which some results are known, and demonstrate that the entanglement entropy is seen to scale with the boundary of the subregion when $d > 1$ [26]. In Chapter 6 we turn to yet another route of deriving the entanglement entropy from the Hamiltonian formulation, but this time one where the explicit calculation of a series of auxiliary matrices is unnecessary [15]. We subject the resulting algorithm to the same tests as employed in Chapter 5, and compare their predictions. The additional freedom of the approach from Chapter 6 will then be used to determine the entanglement entropy of subregions of square lattices, on which we position a discrete circle, which is compared to predictions for the actual circle obtained by means of radial discretisation.

The theory necessary to understand the aforementioned chapters will be discussed in Chapter 2, which briefly (yet thoroughly) introduces the concept of entanglement and von Neumann

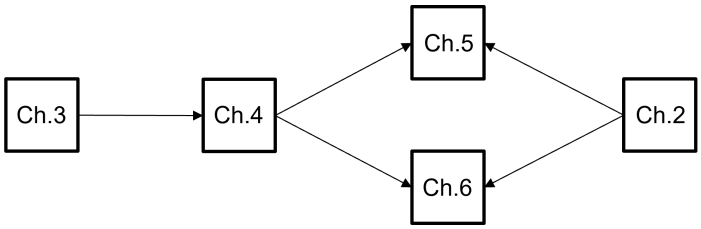

Fig. 1.1 This figure provides a simple overview of the interconnections between the chapters.

entropy from an information theoretic perspective. This chapter is meant to be a gentle introduction, with as a key takehome message the requirements needed to find the von Neumann entropy. Lastly, we address the aim of Chapter 4, which discusses the Schrödinger representation for scalar fields on curved spacetimes. Since the calculation of the entanglement entropy in Chapter 5 and Chapter 6 proceed through a Hamiltonian route, where the ground state wave function of the joint-system can be explicitly computed, it is interesting to wonder whether finding the continuum-spacetime kernel and subsequent discretization gives a correction to the approach described so far (discretization followed by finding the kernel). This, in a nutshell, is the aim of Chapter 4. It describes a formalism which allows us to write down a wide variety of continuum-spacetime kernels for scalar fields, of which the radially discretized forms are exploited in Chapter 6. We also use this formalism to examine a possible expression for the ground state wave functional of the analogue black hole from [48]. This expression will not return in Chapter 5 and Chapter 6, yet upon verification could also be subjected to radial discretization and considered in the context of our algorithms.

After skim-reading the table of contents, the chapters may seem rather disjoint at first. In a way, this is indeed the case. Despite our review of analogue black holes and the description of the analogue suggested in [48], our construction of the entanglement entropy algorithms more or less stands on its own, where it serves to ultimately unite the two topics, but does not manage to do so in this dissertation. Yet this does not mean that a connection between the two is absent. In fig.(1.1) we give a rough outline of how the chapters are connected, where Chapter 2 covers the prerequisites of Chapter 5 and Chapter 6, while the results from Chapter 3 are used to study the analogue's possible ground state wave functional in Chapter 4. The latter also covers some of the kernels for our fields on flat backgrounds, and as such directly provides some of the results needed in Chapter 5 and Chapter 6. As a small last aide on the reader's behalf, we note that the reader on a tight schedule benefits most from studying Chapter 5 and Chapter 6, as these last two chapters reflect best the work we conducted on this interesting and perhaps even under-represented technique in calculating entanglement entropy. The other two chapters are recommended for readers with slightly more time, as it connects the calculation of the entanglement entropy for general scalar fields to how we ultimately hope to determine the entropy of the analogue from [48].

Chapter 2

Entanglement Entropy

"...no one really knows what entropy really is, so in a debate you will always have the advantage."
Claude Shannon on JvN

2.1 A simple quantum mechanical perspective

Before we turn to measures for the entanglement entropy, we will briefly consider a simple quantum mechanical interpretation of entanglement. There are many excellent reviews available on this topic, and in our case we base our discussion on [58]. Before providing some physical intuition, we aim for a slightly more mathematical treatment. Consider a pure state $|\Psi\rangle \in \mathcal{H}$, where we write the total Hilbert space $\mathcal{H} = \mathcal{H}_A \otimes \mathcal{H}_B$ in terms of subsystems A and B. The Hilbert space $\mathcal{H}_A$ is spanned by the states $\{|\psi\rangle_a \,|\, a \in \mathbb{N}\}$, while the orthonormal set $\{|\phi\rangle_b \,|\, b \in \mathbb{N}\}$ spans $\mathcal{H}_B$. We may therefore write the pure state in $\mathcal{H}$ as

$$|\Psi\rangle = \sum_{a,b} c_{ab} \, |\psi\rangle_a \otimes |\phi\rangle_b \,. \tag{2.1}$$

There are two distinct situation that one must consider. It may be possible that the matrix elements $c_{ab} = c_a c_b$ are separable, in which case the state can be rewritten as a product of two pure states in the separate Hilbert spaces, *i.e.* one would find $|\Psi\rangle = |\psi\rangle \otimes |\phi\rangle$, where $|\psi\rangle \in \mathcal{H}_A$ and $|\phi\rangle \in \mathcal{H}_B$. Note that in this situation performing a measurement on subsystem A would tell us nothing about subsystem B. Such states are known as 'separable' or 'product states'. Our analysis becomes more interesting when we take $c_{ab} \neq c_a c_b$, such that the pure state of the composite system can no longer be separated into pure states in $\mathcal{H}_A$ and $\mathcal{H}_B$. These states are known as 'entangled'. Let us now develop some physical intuition by studying the popular example of the Bell state. Following [58], we denote this pure state as $|\Psi\rangle \in \mathcal{H}_A \otimes \mathcal{H}_B$, where the Hilbert spaces of the subsystems are given by $\mathcal{H}_A = \{|0\rangle, |1\rangle\}$

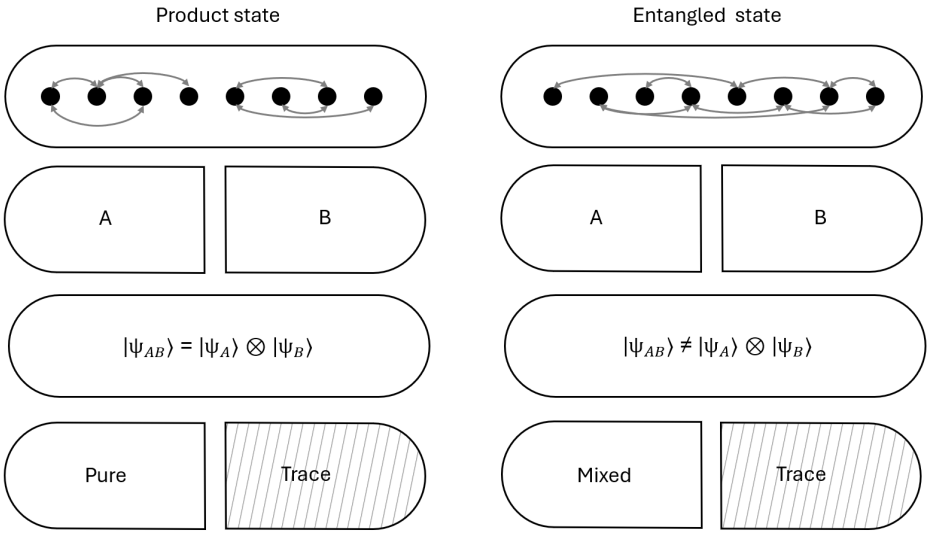

Fig. 2.1 This figure is an adaptation from [41]. On the left it shows a composite system where A and B are not entangled, and as such has pure reduced density matrices, and is described by a separable state. On the right we show the opposite situation, where A and B are entangled, and the reduced density matrices of the subsystems are mixed. These two cases have a vanishing and non-vanishing entanglement entropy, respectively.

and $\mathcal{H}_B = \{|0\rangle, |1\rangle\}$, yet for this particular example we restrict our gaze to the state

$$|\Psi\rangle = \frac{1}{\sqrt{2}}(|01\rangle - |10\rangle), \tag{2.2}$$

where we use the shorthand $|ij\rangle = |i\rangle_A \otimes |j\rangle_B$. This state is inseparable, and hence an example of an entangled state. But what can we say about the 'amount' of entanglement between the subsystems? Let us assume we perform a measurement on subsystem A, which returns the eigenvalue 1. This immediately fixes the eigenvalue of the cubit of system B to 0. Hence, observing subsystem A reduces our uncertainty of subsystem B. The influence a measurement on one subsystem has on the 'uncertainty' of the other subsystem is reminiscent of the context in which Shannon entropy is typically defined (the interested reader is referred to appendix C). Yet despite this interesting observation, we are still not capable of quantitatively describing the 'amount' of entropy between the subsystems. The required machinery for this task is developed in the next section, where the parallel with Shannon entropy is solidified.

2.2 Entanglement entropy

Now that we have developed a basic understanding of entanglement, we return to our previous question of the entanglement measure. It turns out that this question is most easily answered by representing quantum states in terms of density matrices. In fact, one can show [57] that each ensemble of states $\{p_i, |\psi_i\rangle\}$, with p_i the probability of measuring $|\psi_i\rangle$, has a density

matrix

$$\rho = \sum_i p_i \left|\psi_i\right\rangle \left\langle\psi_i\right|, \tag{2.3}$$

for which the relation $\mathrm{Tr}(\rho) = 1$ is ensured through normalization of the probability distribution function. One can easily demonstrate that if the ground state is pure, *i.e.* if one can write $|\Psi\rangle = |\psi\rangle \otimes |\phi\rangle$, the density matrix should obey $\mathrm{Tr}(\rho^2) = 1$. However, if the state is non-separable, we are able to show that $\mathrm{Tr}(\rho^2) < 1$. This leads us to define a quantum-equivalent of the Shannon entropy, which is known as the von Neumann entropy, and given by

$$S(\rho) = -\mathrm{Tr}(\rho \log \rho) = -\sum_i \lambda_i \log \lambda_i, \tag{2.4}$$

where λ_i are the eigenvalues of the density matrix ρ. This expression is zero for pure states, where the density matrix has eigenvalues one, yet becomes positive for mixed states. Despite the strides that we have just made, one may wonder if this expression carries any predictive power for *e.g.* the Bell state we studied earlier, where we were particularly interested in studying the entanglement of one subregion with respect to its complement. This extension can be achieved by defining the reduced density matrix

$$\rho_A = \mathrm{Tr}_B(\rho), \tag{2.5}$$

where the partial trace Tr_B is defined such that it traces over all degrees of freedom of subsystem B (it acts only on the Hilbert space $\mathcal{H}_B$). Similarly, one may define the reduced density matrix for region B as $\rho_B = \mathrm{Tr}_A(\rho)$. Replacing the density matrices in Eq.(2.4) by the reduced density matrix for region A leads to the entanglement entropy of this particular subsystem:

$$\begin{aligned} S_A \equiv S(\rho_A) &= -\mathrm{Tr}(\rho_A \log \rho_A) \\ &= -\sum_i \lambda_i^A \log \lambda_i^A, \end{aligned} \tag{2.6}$$

where λ_i^A are the eigenvalues of the reduced density matrix ρ_A. Similarly, one could write down the entanglement entropy for subsystem B, which follows from

$$\begin{aligned} S_B \equiv S(\rho_B) &= -\mathrm{Tr}(\rho_B \log \rho_B) \\ &= -\sum_i \lambda_i^B \log \lambda_i^B, \end{aligned} \tag{2.7}$$

where λ_i^B are the eigenvalues of the reduced density matrix ρ_B. An interesting situation to consider is when the state $|\Psi\rangle$ is pure, as is the case for the ground states we will later encounter in Ch.5 and Ch.6. By means of a Schmidt decomposition, one can show that the entanglement entropy for the subsystems of a bipartite composite system in a pure state are

identical [57, 58]; we may therefore add the useful relation $S_A = S_B$ to our armoury, which we will use extensively in Ch.5. In fig.(2.1) we illustrate the relation between the reduced density matrix and separable or entangled states. In fact, one could easily demonstrate that $\mathrm{Tr}(\rho_A^2) = 1$ (*i.e.* the reduced density matrix is pure) when the composite system is separable, whereas $\mathrm{Tr}(\rho_A^2) < 1$ for entangled states. As a simple example, let us consider the Bell state Eq.(2.2) again, but this time determine the reduced density matrix for cubit A, as in [58]. It can easily be shown that $\rho_A = \frac{1}{2}\mathbb{1}$, which implies that the condition $\mathrm{Tr}(\rho_A^2) < 1$ is satisfied, and hence leads us to classify the state as mixed. Inserting the eigenvalues of ρ_A into the entanglement entropy Eq.(2.6) yields a non-zero result; the subsystems are entangled, as we set about to proof.

In Ch.6 we will occasionally refer to the Rényi entropy, which can be related to the definition of the von Neumann entropy. It would be outside the scope of this thesis to discuss this measure in detail, and as such we simply provide the required expression. The Rényi entropy is given by [54]

$$S_\alpha(\rho) = \frac{1}{1-\alpha}\log(\mathrm{Tr}[C\rho^\alpha]), \tag{2.8}$$

where the order $\alpha \in (0,1) \cup (1,\infty)$ and C is a normalization constant of the density matrix. In Ch.6 we will demonstrate explicitly that the $\alpha \to 1$ limit of the Rényi entropy is equivalent to the von Neumann entropy, as described by *e.g.* [68].

As a final comment, we want to share that a discussion as brief as ours hardly does the extensive subject of quantum information theory justice. This section was roughly based on [57, 37, 25, 80, 58], and the interested reader is encouraged to explore the discussions in these sources further, as they provide a wealth of extra information on this topic and its connection with classical information theory,

Chapter 3

Analogue black holes

"They all confirm that a black hole ought to emit particles and radiation as if it were a hot body..."
Stephen Hawking

3.1 Sonic black holes

Before discussing the analogue black hole proposed in [48], which lies at the heart of this dissertation, we will revisit some of the early work on analogue black holes. In particular, we aim to retrace the mathematics and ideas behind Unruh's seminal 1981 work [75], which catalyzed the research into black hole analogues, and provided a simple set of principles still used for nearly every analogue experiment today. The general idea behind this early type of analogue black hole is perfectly captured by Unruh's description of the event horizon to an audience of black-hole layman in the early '70s [3]. He presented his audience with the simple case of a stream of water, a small brook if you wish, which eventually terminates in a drop and becomes a waterfall. The fluid velocity of the stream increases as it approaches the drop, and for convenience we assume that it adheres to a linearly increasing velocity profile over the full domain, as depicted in fig.(3.1b). The sound velocity in the stream is constant, which we denote by c_s. Now suppose we find ourselves on the bank of this stream and release a 'fish' (or any other transmitter) into the water, which is programmed to send us sound signals, as shown in fig.(3.1a). The fish does not swim itself but simply 'rests'; it is dragged along by the stream at velocity v, while transmitting acoustic signals to us from its current position. As long as the transmitter is in the subsonic region, where $v < c_s$, the signal will reach us as expected, albeit being 'red-shifted'. Yet once the fish enters the waterfall, the stream velocity becomes $v > c_s$, *i.e.* it enters the supersonic region, such that its signals will no longer reach us, or for that matter even reach the top of the waterfall. Unruh described this 'point of no return' at $v = c_s$ as being equivalent to an event horizon. Effectively, from

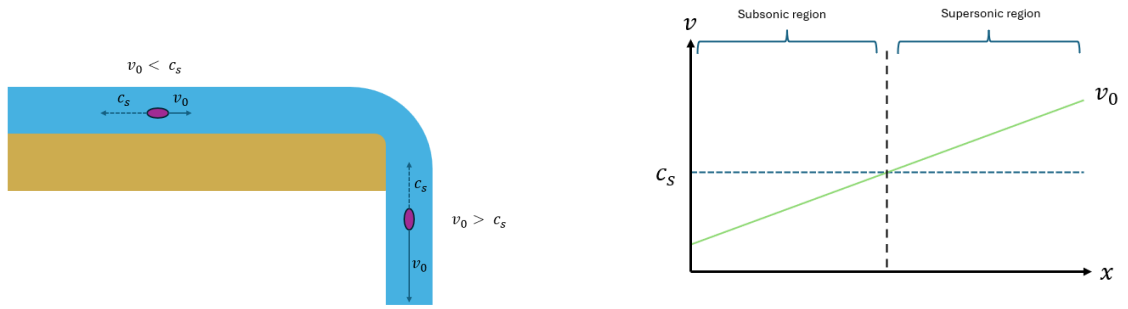

(a) (b)

Fig. 3.1 Figure (a) shows a transmitter in a stream of water with increasing fluid velocity. The velocity profile of the fluid and its division into a subsonic and supersonic region compared to the sound velocity c_s is shown in (b).

the perspective of the acoustic waves the increasing gradient in the stream velocity mimics the geometric properties of the curved spacetime it represents.

This example is of course a grave oversimplification of how modern analogues are constructed, yet formalizing the discussion above through some basic hydrodynamics provides a stepping stone to modern, BEC-based analogues. There is an abundance of literature available on this topic, some involving highly complicated hydrodynamic derivations, yet we will confine ourselves to the earlier, slightly simpler papers on its foundations (as this dissertation is not aimed at providing a detailed description of state-of-the-art water-based sonic black holes). We will not outline the full proof, but rather provide a review of [75, 74, 76, 78, 79], since the general outline is very similar to the BEC-analogue derivation we aim to explore next. The crux of the derivation lies in the assumption that the fluid is inviscid, vorticity free (and hence locally irrotational), barotropic and the flow is steady [78, 79]. Using the notation from [46], we commence by finding the continuity equation

$$\frac{\partial \rho}{\partial t} + \nabla \cdot (\rho \mathbf{v}) = 0, \tag{3.1}$$

while the Euler equation can be written as

$$\frac{\partial \mathbf{v}}{\partial t} = -\nabla(\frac{1}{2}v^2 + \phi + \Phi + h(p)), \tag{3.2}$$

with $v^2 = \mathbf{v} \cdot \mathbf{v}$ the inner product of the fluid velocity. The Euler equation contains a Newtonian gravitational potential ϕ and a driving force potential Φ. Furthermore, it contains a quantity $h(p)$, which in [75, 78, 79] is defined as

$$h(p) = \int_0^p \frac{\mathrm{d}p'}{\rho(p')}, \tag{3.3}$$

and relates to the assumption that the density is only dependent on the pressure. The assumption that the fluid is free of vortices allows us to write $\mathbf{v} = -\nabla\psi$, with ψ the velocity potential. As such, the Euler equation is seen to reduce to the expression

$$\frac{\partial\psi}{\partial t} = -(\frac{1}{2}(\nabla\psi)^2 + \phi + \Phi + h(p)). \tag{3.4}$$

These equations are all one needs to solve for and obtain the hydrodynamic variables (ρ, p, ψ), which characterize the full system. So far, we have not encountered anything too surprising. But things get slightly more interesting once we linearize these variables around a background fluid (ρ_0, p_0, ψ_0), as in [75], such that the hydrodynamic variables become $\rho = \rho_0 + \delta\rho$, $p = p_0 + \delta p$ and $\psi = \psi_0 + \delta\psi$, where $\delta\rho \ll \rho_0$, $\delta p \ll p_0$ and $\delta\psi \ll \psi_0$. The fluctuations characterized by $(\delta\rho, \delta p, \delta\psi)$ describe acoustic waves propagating in the background fluid [46], whose hydrodynamic equations will lead to interesting new physics. Thus, without further ado, let us substitute the linearized hydrodynamic variables into the continuity equation Eq.(3.1) and the Euler equation Eq.(3.4), the former of which splits into the two equations

$$\frac{\partial\rho_0}{\partial t} - \nabla(\rho_0\nabla\psi_0) = 0, \tag{3.5}$$

which describes the background contribution and

$$\frac{\partial\delta\rho}{\partial t} - \nabla(\delta\rho\nabla\psi_0 + \rho_0\nabla\delta\psi) = 0, \tag{3.6}$$

which captures the continuity equation for the fluctuations up to first-order. The reader is encouraged to show this themselves, yet [78, 79] greatly aids the reader in a haste. Similarly, the Euler equation Eq.(3.4) splits into the two expressions

$$\frac{\partial\psi_0}{\partial t} = -(\frac{1}{2}(\nabla\psi_0)^2 + \phi + \Phi + h(p_0)) \tag{3.7}$$

for the background contribution and

$$\frac{\partial\delta\psi}{\partial t} = \mathbf{v}_0 \cdot \nabla\delta\psi - \frac{\delta p}{\rho_0} \tag{3.8}$$

for the acoustic waves. Note that these equations fix both (ρ_0, p_0, ψ_0) and $(\delta\rho, \delta p, \delta\psi)$, and solving for ψ_0 and $\delta\psi$ allows us to obtain all other hydrodynamic variables. Next, following [78, 79], we invert Eq.(3.8) for $\delta p/\rho_0$, insert it into Eq.(3.6), and use Eq.(3.3), which gives the wave equation for the acoustic fluctuations

$$\frac{\partial}{\partial t}(\frac{\partial\rho}{\partial p}\rho_0(\frac{\partial\delta\psi}{\partial t} + \mathbf{v}_0 \cdot \nabla\delta\psi)) - \nabla \cdot (\rho_0\nabla\delta\psi - \frac{\partial\rho}{\partial p}\rho_0\mathbf{v}_0(\frac{\partial\delta\psi}{\partial t} + \mathbf{v}_0 \cdot \nabla\delta\psi)) = 0. \tag{3.9}$$

This slightly daunting looking equation is all that we require, as we will show without further delay. We simplify the notation by adopting the definition of the sound velocity [46] $c_s^2 = \partial p/\partial\rho$, and define a metric

$$g_{\mu\nu} = \frac{\rho_0}{c_s}\begin{pmatrix} -(c_s^2 - v_0^2) & -\mathbf{v}_0^T \\ -\mathbf{v}_0 & \mathbb{1} \end{pmatrix}. \tag{3.10}$$

The wave equation Eq.(3.9) can then be cast into the suggestive form

$$\hat{\Box}\delta\psi = \frac{1}{\sqrt{|g|}}\partial_\mu(\sqrt{|g|}g^{\mu\nu}\partial_\nu\delta\psi) = 0, \tag{3.11}$$

which is the equation of motion for a scalar field on a general curved spacetime [14]. Hence, we conclude that the background fluid couples to the Minkowski metric, while the acoustic waves couple to a non-trivial metric and effectively 'mimics' a free scalar field on a curved background. Let us examine the metric Eq.(3.10) a bit closer, as to gauge the type of propagation the acoustic waves are subjected to. The infinitesimal line-element can be written as

$$ds^2 = \frac{\rho_0}{c_s}[-c_s^2dt^2 + (d\mathbf{x} - \mathbf{v}_0dt)^2]. \tag{3.12}$$

For our convenience, we cast this expression into a more familiar form through using the coordinate-transformation specified in [76, 78, 79], which is given by

$$d\tau = dt + \frac{\mathbf{v}_0 \cdot \mathrm{d}\mathbf{x}}{c_s^2 - v_0^2}. \tag{3.13}$$

Substitution into the line-element and subsequently rewriting it in terms of spherical coordinates gives

$$ds^2 = \frac{\rho_0}{c_s}[-(c_s^2 - v_0^2)d\tau^2 + (1 - \frac{v_0^2}{c_s^2})^{-1}dr^2 + r^2d\Omega^2], \tag{3.14}$$

which is of a Schwarzschild-*like* form. Despite the fact that it does not exactly capture a Schwarzschild-geometry, which is spoiled by the element g_{00} from our metric, it does capture the basic characteristics. We note that the metric becomes singular for $v_0 = c_s$, and that the time-like Killing vector changes sign when the acoustic wave leaves the subsonic region and enters the supersonic region. In between these regions the Killing vector becomes null, marking an acoustic horizon. It also seems to capture the correct signature of a scalar field. A more detailed digression into the similarities between actual scalar fields on Schwarzschild-geometries and our acoustic waves can be found in [78, 79], and we will now proceed to study a system underlying the paper we hope to describe soon. The key takeaway from this section is that, under the correct assumptions, the hydrodynamic equations of simple acoustic fluctuations are capable of 'mimicking' the basic properties of free scalar fields on non-trivial backgrounds.

3.2 BEC-based analogues

The previous section demonstrated how a classical (hydrodynamic) system, when assumed to be non-viscid, barotropic and irrotational, is able to mimic the behaviour of a scalar field on a curved background. Yet the more subtle effects associated with an acoustic horizon, such as the phononic Hawking radiation, suffer from experimental constraints when considering typical fluids. For example, most fluids which are experimentally accessible are in fact not perfectly non-viscous, and therefore break the gravitational analogy [43]. Another severe difficulty resides in the background noise and impurities that most (classical) fluids suffer from, such that measuring the acoustic Hawking radiation is potentially obscured, and might in fact become fully indistinguishable from the noise [43]. A promising alternative is offered by superfluids, which are known to experience a frictionless flow [66], hence being effectively non-viscous, and are typically very pure [43]. Since Bose-Einstein condensates (BECs) are conceptually well-understood and can be accurately controlled experimentally [32], this section aims at demonstrating that a BEC in the hydrodynamic regime can be shown to support a modified version of the acoustic metric Eq.(3.10). We will start our discussion by (very) briefly recalling some of the basic ideas behind Bose-Einstein condensation. Subsequently, we derive the Gross-Pitaevskii equation, which acts as the starting point for our proof.

Some might consider it a blatant crime to reduce the topic of Bose-Einstein condensation to a few sentences, but as our discussion of analogue gravity is only in its infancy, we make haste and mention only a few important facts to get us started. Heuristically, a bosonic many-body system undergoes Bose-Einstein condensation when a macroscopic amount of the bosons occupy the ground state governed by some external trapping potential [72, 43]. The order-parameter of this phase transition is given by $\langle N_0 \rangle / \langle N \rangle$, where $\langle N_0 \rangle$ is the average number of particles in the condensate. It can be shown that, below the critical temperature T_c, the order-parameter is non-vanishing in the thermodynamic limit, and hence $\langle N_0 \rangle$ is of the same order as $\langle N \rangle$ [18]. Similarly, one could state that the density $\langle N_0 \rangle / V$ does not vanish in the thermodynamic limit [72]. This fixes our definition of a 'macroscopic amount' of bosons occupying the lowest-energy state. In general, one can argue (cf. [72]) that the non-commutativity of fields is irrelevant due to the large particle number, and as such the order parameter of the transition can equally well be taken to be $\phi_0(\mathbf{x}, t) = \langle \hat{\Psi}(\mathbf{x}, t) \rangle$, which is known as the macroscopic wavefunction of the condensate, with a normalization factor $\langle N_0 \rangle = \int \mathrm{d}\mathbf{x} |\phi_0(\mathbf{x}, t)|^2$. At this point we temporarily depart from the theory of BECs and consider arbitrary bosonic fields, yet one could always substitute the macroscopic wavefunction into the following expressions to obtain a zeroth-order approximation, which describes the classical condensate. In a while, however, we introduce fluctuations around the macroscopic wave function, which will emerge as our gateway to the hydrodynamic equations.

A convenient starting point to derive the quantum-equivalents of the hydrodynamic equations is the many-body Hamiltonian

$$H = \int \mathrm{d}\mathbf{x}\hat{\Psi}^\dagger(t,\mathbf{x})[-\frac{\hbar^2}{2m}\nabla + V_{\mathrm{ext}}(\mathbf{x})]\hat{\Psi}(t,\mathbf{x}) + \frac{1}{2}\int \mathrm{d}\mathbf{x}\mathrm{d}\mathbf{x}'\hat{\Psi}^\dagger(t,\mathbf{x})\hat{\Psi}^\dagger(t,\mathbf{x}')V(\mathbf{x}-\mathbf{x}')\hat{\Psi}(t,\mathbf{x}')\hat{\Psi}(t,\mathbf{x}), \quad (3.15)$$

where $\hat{\Psi}$ are bosonic fields obeying the standard commutation relations and $V(\mathbf{x}-\mathbf{x}')$ is a generic interatomic potential. The two terms of first integrand stem from the single-particle Hamiltonian. The evolution of the fields is governed by the Heisenberg equation

$$i\hbar\frac{\partial}{\partial t}\hat{\Psi}(t,\mathbf{r}) = [\hat{\Psi}(t,\mathbf{r}), H], \quad (3.16)$$

which will eventually lead us to the Gross-Pitaevskii equation. For clarity, we consider the terms from the single-particle Hamiltonian and the interaction terms separately, with the former giving

$$\begin{aligned} i\hbar\frac{\partial}{\partial t}\hat{\Psi}(t,\mathbf{r}) &= -\frac{\hbar}{2m}\int \mathrm{d}\mathbf{r}'[\hat{\Psi}(t,\mathbf{r}),\hat{\Psi}^\dagger(t,\mathbf{r}')(\nabla^2 + V_{\mathrm{ext}}(\mathbf{r}'))\hat{\Psi}(t,\mathbf{r}')] \\ &= -\frac{\hbar}{2m}\int \mathrm{d}\mathbf{r}'\delta(\mathbf{r}-\mathbf{r}')(\nabla^2 + V_{\mathrm{ext}}(\mathbf{r}'))\hat{\Psi}(t,\mathbf{r}') = -\frac{\hbar}{2m}(\nabla^2 + V_{\mathrm{ext}}(\mathbf{r}))\hat{\Psi}(t,\mathbf{r}), \end{aligned} \quad (3.17)$$

where from the first to second line we have used the Leibniz-rule equivalent for commutators, and for the last equality we have simply used the commutation relations of the fields repeatedly. The interaction term is slightly more labour-intensive, but after sharing a little taster through the single-particle term, we leave the remainder for the interested reader. We find

$$\begin{aligned} i\hbar\frac{\partial}{\partial t}\hat{\Psi}^\dagger(t,\mathbf{r}) &= \frac{1}{2}\int \mathrm{d}\mathbf{r}'\mathrm{d}\mathbf{r}''V(\mathbf{r}'-\mathbf{r}'')[\hat{\Psi}(t,\mathbf{r}),\hat{\Psi}^\dagger(t,\mathbf{r}')\hat{\Psi}^\dagger(t,\mathbf{r}'')\hat{\Psi}(t,\mathbf{r}')\hat{\Psi}(t,\mathbf{r}'')] \\ &= \int \mathrm{d}\mathbf{r}[\hat{\Psi}^\dagger(t,\mathbf{r}')V(\mathbf{r}'-\mathbf{r})\hat{\Psi}(t,\mathbf{r}')]\hat{\Psi}(t,\mathbf{r}), \end{aligned} \quad (3.18)$$

which merely requires repeatedly using the commutation relations and relabeling indices of the fields. Combining Eq.(3.17) and Eq.(3.18) then leads to the Heisenberg equation for the fields:

$$i\hbar\frac{\partial}{\partial t}\hat{\Psi}(t,\mathbf{r}) = \left[-\frac{\hbar}{2m}\nabla^2 + V_{\mathrm{ext}}(\mathbf{r}) + \int \mathrm{d}\mathbf{r}'\hat{\Psi}^\dagger(t,\mathbf{r}')V(\mathbf{r}'-\mathbf{r})\hat{\Psi}(t,\mathbf{r}')\right]\hat{\Psi}(t,\mathbf{r}). \quad (3.19)$$

We replace the interatomic potential by a point-interaction term $V(\mathbf{r}-\mathbf{r}') = \frac{4\pi\hbar^2 a}{m}\delta(\mathbf{r}-\mathbf{r}') \equiv \lambda\delta(\mathbf{r}-\mathbf{r}')$, which according to [72] is allowed when the interatomic interaction is fully characterized by the s-wave scattering length a. Since binary collisions characterized by

s-wave scattering are the most important interactions in cold dilute gases [43], we remark that said replacement is justified. Note that introducing this pseudopotential simplifies Eq.(3.19) considerably, which leads to the expression

$$i\hbar\frac{\partial}{\partial t}\hat{\Psi}(t,\mathbf{r}) = \left[-\frac{\hbar}{2m}\nabla^2 + V_{\text{ext}}(\mathbf{r}) + \lambda|\hat{\Psi}(t,\mathbf{r})|^2\right]\hat{\Psi}(t,\mathbf{r}). \tag{3.20}$$

Enter stage the macroscopic wavefunction $\phi_0(\mathbf{x},t)$. By considering a Bogoliubov shift, where we expand the fields in terms of the macroscopic wavefunction of the condensate and fluctuations $\delta\phi(\mathbf{x},t)$ [72], we write

$$\hat{\Psi}(\mathbf{x},t) = \phi_0(\mathbf{x},t) + \delta\phi(\mathbf{x},t), \tag{3.21}$$

where we recall that $\phi_0(\mathbf{x},t) = \langle\hat{\Psi}(\mathbf{x},t)\rangle$. The fluctuations describe phonons (quantized acoustic waves) in the condensate. We will in time get to treat those more carefully, but let us for now focus on the former, which leads to

$$i\hbar\frac{\partial}{\partial t}\phi_0(t,\mathbf{x}) = \Big[-\frac{\hbar^2}{2m}\nabla^2 + V_{\text{ext}}(\mathbf{x}) + \lambda n_0\Big]\phi_0(t,\mathbf{x}), \tag{3.22}$$

where $n_0 = |\phi_0(\mathbf{x},t)|^2$ is the condensate density, and is implicitly dependent on the position and time. This result is known as the time-dependent Gross-Pitaevskii equation and governs the evolution of the classical condensate [62, 63]. A similar expression can be found for the fluctuations, which up to first-order is given by

$$i\hbar\frac{\partial}{\partial t}\delta\phi(t,\mathbf{r}) = \Big[-\frac{\hbar^2}{2m}\nabla^2 + V_{\text{ext}}(\mathbf{r}) + 2\lambda n_0\Big]\delta\phi(t,\mathbf{r}) + \phi_0(t,\mathbf{r})^2\delta\phi^\dagger(t,\mathbf{r}). \tag{3.23}$$

As mentioned in [5], the Gross-Pitaevskii equation for the classical condensate can equally well be obtained from the time-dependent Landau-Ginzburg action

$$S = \int \mathrm{d}t\mathrm{d}\mathbf{r}\left[\phi_0^\dagger(\mathbf{r},t)\{i\hbar\partial_t + \frac{\hbar^2}{2m}\nabla^2 - V_{\text{ext}}(\mathbf{r})\}\phi_0(\mathbf{r},t) - \frac{1}{2}\lambda|\phi_0(\mathbf{r},t)|^4\right]. \tag{3.24}$$

But let us not wander off too much, and return to the Gross-Pitaevskii equation. First, we separate the phase and real amplitude of the condensate wave function by means of the Madelung representation [5, 63], given by

$$\phi_0(t,\mathbf{x}) = \sqrt{n_0}e^{-i\theta(\mathbf{x},t)/\hbar}, \tag{3.25}$$

with n_0 as defined before. The phase is given by the expression

$$\theta(\mathbf{r},t) = (\frac{1}{2}mv^2 + \mu)t - m\mathbf{v}\cdot\mathbf{x}, \tag{3.26}$$

as discussed in [63, 82]. Next, we aim to derive the hydrodynamic equations for this system by means of the Gross-Pitaevskii equation, for which we closely follow the discussion by [5, 6]. Our first step is to insert the Madelung representation in the Gross-Pitaevskii equation Eq.(3.22), which governs the classical condensate. Separating the imaginary and real parts of the resulting expression leads to the quantum equivalent of the continuity equation

$$\frac{\partial}{\partial t}n_0 = -\frac{\hbar}{m}\nabla\cdot(n_0\nabla\theta) \equiv -\nabla\cdot(n_0\mathbf{v}_s), \tag{3.27}$$

where we identify the superfluid velocity $\mathbf{v}_s = \frac{\hbar}{m}\nabla\theta$. We furthermore obtain an equivalent of the Hamilton-Jacobi equation

$$\frac{\partial}{\partial t}\theta = -\frac{1}{2m}(\nabla\theta)^2 - \lambda n_0 - V_{\text{ext}} + \frac{\hbar^2}{2m}\frac{\nabla^2\sqrt{n_0}}{\sqrt{n_0}}. \tag{3.28}$$

The latter trivially leads to the quantum equivalent of the Euler equation by taking the gradient, such that

$$m\frac{\partial}{\partial t}\mathbf{v}_s = -\nabla(\frac{1}{2}mv_s^2 + V_{\text{ext}} + \lambda n_0 - \frac{\hbar^2}{2m}\frac{\nabla^2\sqrt{n_0}}{\sqrt{n_0}}), \tag{3.29}$$

where $v_s^2 = ||\mathbf{v}_s||^2$. These are equivalent in shape to the hydrodynamic equations for the classical fluid we studied earlier, apart from the quantum potential in the Euler equation. Subsequently, we hope to find similar equations for the fluctuations, in line with the approach taken for the classical case. There are two distinct ways to arrive at the hydrodynamic equations for the fluctuations, where the most straightforward follows from taking $n_0 \to n_0+\delta n$ and $\theta \to \theta + \delta\theta$, as discussed in [72]. However, the analogue black hole literature seems to favour a different route, which considers an explicit expression for the fluctuations known as the quantum acoustic representation [5], given by

$$\delta\phi = (\frac{1}{2\sqrt{n_0}}\delta n - i\frac{\sqrt{n_0}}{\hbar}\delta\theta)e^{-i\theta/\hbar}. \tag{3.30}$$

Note that both approaches will ultimately yield the same result, and it therefore only depends on the reader's personal taste. Upon inserting this representation into Eq.(3.23), followed by a considerable amount of bookkeeping, one ends up with the results from [5, 6], where the continuity equation for the fluctuations is found to be

$$\frac{\partial}{\partial t}\delta n = -\frac{1}{m}\nabla\cdot(\delta n\nabla\theta + n_0\nabla\delta\theta), \tag{3.31}$$

while the Hamilton-Jacobi equation becomes

$$\frac{\partial}{\partial t}\delta\theta = \frac{\hbar^2}{2m}\hat{\mathcal{D}}\delta n - \frac{1}{m}\nabla\theta\cdot\nabla\delta\theta - \lambda\delta n. \tag{3.32}$$

In line with [5] we have defined the differential operator

$$\hat{\mathcal{D}}\delta n = -\frac{\delta n}{2n_0^{3/2}}\nabla^2\sqrt{n_0} + \frac{1}{2\sqrt{n_0}}\nabla^2(\frac{\delta n}{\sqrt{n_0}}). \tag{3.33}$$

As stated in [72], it is useful to consider the Thomas-Fermi limit, where the kinetic energy is small with respect to the interaction energy, such that Eq.(3.32) reduces to the more tractable expression

$$\frac{\partial}{\partial t}\delta\theta \approx -\frac{1}{m}\nabla\theta\cdot\nabla\delta\theta - \lambda\delta n. \tag{3.34}$$

The attentive reader will probably note a striking similarity with our derivation of the effective acoustic metric from the (classical) hydrodynamic equations. In fact, if we invert Eq.(3.34) for δn and then substitute this relation in the continuity equation Eq.(3.31), we end up with the wave equation

$$\frac{\partial}{\partial t}(\frac{\partial}{\partial t}\delta\theta + \frac{1}{m}\nabla\theta\cdot\nabla\delta\theta) - \frac{\lambda}{m}\nabla\cdot(n_0\nabla\delta\theta - \nabla\theta(\frac{1}{\lambda}\frac{\partial}{\partial t}\delta\theta + \frac{1}{m}\nabla\theta\cdot\nabla\delta\theta)) = 0, \tag{3.35}$$

which governs the fluctuations of the classical condensate. After some trial-and-error, the metric

$$g_{\mu\nu} = \frac{n_0}{mc_s}\begin{pmatrix} -(c_s^2 - v_s^2) & -\mathbf{v}_s^T \\ -\mathbf{v}_s & \mathbb{1} \end{pmatrix} \tag{3.36}$$

is identified as the one to cast Eq.(3.35) into the form

$$\frac{1}{\sqrt{|g|}}\partial_\mu(\sqrt{|g|}g^{\mu\nu}\partial_\nu\delta\theta) = 0, \tag{3.37}$$

where we have introduced the sound velocity $c_s^2 = \lambda n_0/m$. Hence, we conclude that, as for the classical hydrodynamic case, the fluctuations effectively mimic the propagation of a scalar field on a non-trivial background. Phrased differently, the classical condensate couples to the Minkowski metric, whereas the fluctuations couple to the non-trivial metric Eq.(3.36), while both are governed by the Gross-Pitaevskii equation. The coordinate-transformation Eq.(3.13) from the previous section casts the metric into the form

$$ds^2 = \frac{n_0}{mc_s}[-c_s^2(1 - \frac{v_s^2}{c_s^2})d\tau^2 + (1 - \frac{v_s^2}{c_s^2})^{-1}dr^2 + r^2d\Omega^2], \tag{3.38}$$

which has the same Schwarzschild-*like* shape as before, except for the conformal factor. The metric is seen to have the correct signature, and the time-like Killing vector becomes null at $v_s = c_s$, which marks the presence of an acoustic horizon. Transforming the theory into an experiment would require creating a velocity profile such that there exists a unique r_h for which $v_s(r_h) = c_s$. Furthermore, we should enforce the existence of a supersonic region $r < r_h$, where $v_s(r) > c_s$, and the existence of a subsonic region $r > r_h$, where $v_s(r) < c_s$. In the next

section we will describe a BEC-based experiment involving a radially-inward directed velocity profile. It can be shown that, in this experimental setup, an effective geometry exists in which the 'mismatch' between the actual Schwarzschild geometry and our Schwarzschild-*like* geometry largely disappears, and in which the existence of a supersonic and subsonic region emerge as a straightforward consequence of the velocity profile.

3.3 Analogue black hole in a BEC of light

In the previous section we have seen how a Bose-Einstein condensate in the hydrodynamic regime allows for the creation of an analogue black hole by means of a velocity profile supporting a subsonic and supersonic region with respect to the phonon velocity. This idea has been exploited in many experiments over the last decade or so, and it is far outside the scope of this thesis to provide an overview of these experimental developments and their underlying mechanisms. Instead, we will use the developed theory up to this point to describe a novel type of analogue suggested in [48], which lies at the heart of this thesis. The authors suggest creating an analogue black hole in a Bose-Einstein condensate of light, in which they aim to fabricate a non-rotating draining-bathtub model [7] with a radially-inward directed velocity flow [48], given by $\mathbf{v}_s = -\xi \frac{c_s c_0}{r} \hat{\mathbf{r}}$, where $\xi = \hbar/mc_s$ is the healing length (the distance needed to smoothen out sharp inhomogeneities of the density [43]). We consider c_0 an arbitrary positive constant. This velocity profile is a solution of the hydrodynamic equations emerging from the Gross-Pitaevskii equation, yet is not physically allowed due to the singularity at $r = 0$. The authors proceed by suggesting a 'sink' (or drain) at the origin, which removes the part of the velocity profile which renders the solutions unphysical. However, in order to avoid breaking the conservation of particle number, photons will be pumped into the medium, such that the continuity equations hold. The authors demonstrate that this particular analogue is capable of emitting a phononic equivalent of Hawking radiation, and simulates the presence of a greybody factor. In this section we aim to retrace these derivations and motivate why it might prove interesting to determine the entanglement entropy of the subsonic region with respect to the supersonic region of this particular type of analogue black hole.

3.3.1 Radial-vortex based analogue

As a starting point to this analysis we consider the effective acoustic metric Eq.(3.36). The authors from [48] take a different, yet equivalent approach by deriving the equation of motion for the phase fluctuations directly from the Gross-Pitaevskii equation. Note that both routes eventually end up at the same equation of motion, yet we will stay as close as we possibly can to the more geometrically-oriented line of approach we have taken so far. Considering the velocity profile denoted before, we find $v_s^2 = \xi^2 c_0^2 / r^2$, such that the infinitesimal line element

can be written as

$$ds^2 = \xi^2[-c_s^2(1-\frac{c_0^2}{r^2})d\tau^2 + (1-\frac{c_0^2}{r^2})^{-1}dr^2 + r^2 d\phi^2]. \tag{3.39}$$

By introducing the dimensionless variables $r \to \xi r$ and $t \to \xi t/c_s$, we obtain the metric

$$ds^2 = -f(r)d\tau^2 + f(r)^{-1}dr^2 + r^2 d\phi^2. \tag{3.40}$$

where the warping factor is given by $f(r) = 1 - c_0^2/r^2$. As promised in the previous section, we obtain a metric which is a (2+1)-dimensional equivalent of the Schwarzschild-metric, with an acoustic horizon located at $r = c_0$. The quantization of the phase fluctuations proceeds by allowing a decomposition of the field into its radial and angular variables, and assuming a complete basis of eigenfunctions $\{\psi_m(r;\omega)e^{-i\omega\tau+im\phi}\}$ exists. Furthermore, we define annihilation (creation) operators for both right-moving and left-moving scattering states, denoted by $a^{(\dagger)}_{mR}(\omega)$ and $a^{(\dagger)}_{mL}(\omega)$, respectively. The operators are assumed to obey the commutation relation

$$[a_{mR(L)}(\omega), a^\dagger_{m'R(L)}(\omega')] = \delta(\omega-\omega')\delta_{mm'}. \tag{3.41}$$

The phase fluctuations can then be expanded as in [48] and give

$$\delta\theta(r,\phi,\tau) = \int_0^\infty \mathrm{d}\omega \sum_{m=-\infty}^{\infty} \{\psi_m(r;\omega)e^{-\omega\tau+im\phi}a_{mR}(\omega) + \psi^*_m(r;\omega)e^{-i\omega\tau+im\phi}a_{mL}(\omega) + \text{h.c.}\}. \tag{3.42}$$

Subsequently, we consider the metric Eq.(3.40) and use the definition of the d'Alembertian to write the equation of motion. Acting with the time-derivative and angular-derivative on the expansion gives

$$\partial_r^2\psi_m(r;\omega) + f(r)^{-1}(\frac{f(r)}{r} + \partial_r f(r))\partial_r\psi_m(r;\omega) + f(r)^{-2}\omega^2\psi_m(r;\omega) - f(r)^{-1}\frac{m^2}{r^2}\psi_m(r;\omega) = 0. \tag{3.43}$$

This differential equation only has analytical solutions for $m = 0$, in which case we find radial modes of the form

$$\psi_0(r;\omega) = \mathcal{N}[c_1 I_{ic_0\omega}(i\omega\sqrt{r^2-c_0^2}) + c_2 e^{\pi c_0\omega}K_{ic_0\omega}(i\omega\sqrt{r^2-c_0^2})], \tag{3.44}$$

where $I_\nu(z)$ and $K_\nu(z)$ are modified Bessel functions of the first and second kind, respectively. The constants c_1 and c_2 are implicitly frequency-dependent. We consider Dirichlet boundary conditions on the acoustic horizon $r = c_0$ by choosing $c_1 \neq 0$ and $c_2 = 0$. Furthermore,

the second-order differential equation solved by the modified Bessel functions (appendix B) admits solutions with $\nu \to -\nu$ as well, when $\nu \in \mathbb{C}$. Hence, the full solution for the radial modes are given by

$$\psi_0(r;\omega) = \mathcal{N}[c_1 I_{-ic_0\omega}(i\omega\sqrt{r^2-c_0^2}) + c_2 I_{ic_0\omega}(i\omega\sqrt{r^2-c_0^2})]. \tag{3.45}$$

However, we have been a bit careless so far with the restrictions on r, since the above solution is in principle only valid for the outer region $r > c_0$. The inner region $r < c_0$ needs slightly more care and demands using the relation

$$I_{-i\nu}(-z) = e^{-\pi\nu} I_{-i\nu}(z), \tag{3.46}$$

which we proof in appendix (B.14). The radial modes in the region $r < c_0$ are therefore given by

$$\psi_0(r;\omega) = \mathcal{N} e^{-\pi c_0\omega}[c_1 I_{-ic_0\omega}(\omega\sqrt{c_0^2-r^2}) + c_2 e^{2\pi c_0\omega} I_{ic_0\omega}(\omega\sqrt{c_0^2-r^2})]. \tag{3.47}$$

It is trivial to show that, with the expressions given above, the commutators of the phase fluctuations vanish:

$$[\delta\theta(r,\phi), \delta\theta(r',\phi')] = 0 \quad \text{and} \quad [\delta\pi(r,\phi), \delta\pi(r',\phi')] = 0, \tag{3.48}$$

where $\delta\pi(r,\phi) = \partial_\tau \delta\theta(r,\phi)$ is the conjugate momentum. Lastly, we may determine the commutator of the phase fluctuations and their conjugate momentum, leading to

$$\begin{aligned}[\delta\theta(r,\omega), \delta\pi(r',\omega')] = i\int_0^\infty \int_0^\infty \mathrm{d}\omega \mathrm{d}\omega' \omega' \Big\{ &\psi_0(r;\omega)\psi_0^*(r';\omega')[a_{0R}(\omega), a_{0R}^\dagger(\omega')] \\ &+ \psi_0^*(r;\omega)\psi_0(r';\omega')[a_{0L}(\omega), a_{0L}^\dagger(\omega')] - \text{h.c.}\Big\}.\end{aligned} \tag{3.49}$$

Using the commutator and integrating over ω', one then obtains the relation

$$[\delta\theta(r,\omega), \delta\pi(r',\omega')] = 2i\int_0^\infty \mathrm{d}\omega\omega\Big\{\psi_0(r;\omega)\psi_0^*(r';\omega) + \text{c.c.}\Big\} \stackrel{!}{=} i\delta(r-r'). \tag{3.50}$$

According to [48], the last equality, which enforces the standard commutation relations, only holds if the normalization constant is taken to be $\mathcal{N} = 1/\sqrt{4\pi n_0}(e^{2\pi c_0\omega} - 1)$. The choice of coefficients c_1 and c_2 is particularly intricate and subjects the analogue black hole to specific boundary conditions. Using appendix (B.4), we note that the radial modes have the asymptotic form

$$\psi_0(r;\omega) \sim \mathcal{N}\sqrt{\frac{1}{2\pi\omega r}}\Big[(c_1+c_2)e^{i\omega r} + (c_1 + c_2 e^{-2\pi c_0\omega})e^{i\pi/2}e^{\pi c_0\omega}e^{-i\omega r}\Big]. \tag{3.51}$$

In comparison with appendix (B.4), there appears to be an extra factor $e^{i\pi/2}$ in our expressions, which must be noted to stem from the $1/i$ in the square root from the argument. Furthermore, we use the fact that $\sqrt{r^2-c_0^2} \approx r$ in the limit $r \to \infty$. We define two particular bases for the vacuum; an out-vacuum, where the flux at $r \to \infty$ is purely outgoing (*i.e.* right-moving) and an in-basis, which contains only outgoing flux at the horizon ($r \to c_0$). The former can be achieved by the choice $c_1 = -1$ and $c_2 = e^{2\pi c_0 \omega}$, such that Eq.(3.51) becomes

$$\begin{aligned} \psi_0^{\text{out}}(r;\omega) &= \mathcal{N}[e^{2\pi c_0\omega} I_{ic_0\omega}(i\omega\sqrt{r^2-c_0^2}) - I_{-ic_0\omega}(i\omega\sqrt{r^2-c_0^2})] \\ &\overset{r\to\infty}{\sim} \mathcal{N}\sqrt{\frac{1}{2\pi\omega r}}(e^{2\pi c_0\omega}-1)e^{i\omega r} \sim \sqrt{\frac{1}{2\pi\omega r}}e^{i\omega r}. \end{aligned} \tag{3.52}$$

Clearly, there are only outgoing waves asymptotically far from the horizon. Similarly, we may choose $c_1 = 0$ and $c_2 = e^{\pi c_0\omega}\sqrt{e^{2\pi c_0\omega}-1}$ for the in-basis, such that the radial modes for the outer region become

$$\begin{aligned} \psi_0^{\text{in}}(r;\omega) &= \mathcal{N}e^{\pi c_0\omega}\sqrt{e^{2\pi c_0\omega}-1} I_{ic_0\omega}(i\omega\sqrt{r^2-c_0^2}) \\ &\overset{r\to\infty}{\sim} \sqrt{\frac{1}{2\pi\omega r}}\frac{e^{\pi c_0\omega}}{\sqrt{e^{2\pi c_0\omega}-1}}\left(e^{i\omega r} + ie^{-\pi c_0\omega}e^{-i\omega r}\right). \end{aligned} \tag{3.53}$$

Contrary to before, the asymptotic region in this basis provides little information about whether there indeed is only outgoing flux at the horizon. As we will argue later, this flux composition in fact contains contributions from incident radiation, reflected radiation and transmitted radiation from the horizon. In the limit $r \to c_0^+$, one obtains (see appendix (B.4)) the expression

$$\psi_0^{\text{in}}(r;\omega) \overset{r\to c_0^+}{\sim} \frac{e^{\pi c_0\omega}}{\sqrt{e^{2\pi c_0\omega}-1}}(\sqrt{r^2-c_0^2})^{ic_0\omega} \sim e^{\frac{1}{2}ic_0\omega\log(r^2-c_0^2)}, \tag{3.54}$$

which we have denoted modulus a gamma factor $\Gamma(ic_0\omega+1)$. This captures both the purely outgoing character of the in-basis, and the phase singularity of the horizon; the phase fluctuations start oscillating infinitely fast once approaching the acoustic horizon. The asymptotic flux of the two solutions is shown in fig.(3.2). Before examining the flux profile in more detail, we will consider the phononic equivalent of Hawking radiation, for which the next section develops the required techniques.

3.3.2 Intermezzo: Bogoliubov transformations

In this brief intermezzo we aim to introduce the basics of the Bogoliubov transformation and its relation to the Hawking effect, which are based on the discussion in [10] and [52]. For convenience, we consider a massless, (1+1)-dimensional scalar field, for which the expansion

is given by

$$\hat{\psi}(r;\omega) = \int_0^\infty \frac{\mathrm{d}\omega}{\sqrt{4\pi\omega}} \left[u_\omega a_\omega + u_\omega^* a_\omega^\dagger \right], \tag{3.55}$$

where u_ω are orthonormal solutions to the wave equation. The operators a_ω annihilate the vacuum $|0\rangle_a$, and the construction of a Fock space proceeds as usual. However, we are not necessarily confined to this particular choice of vacuum. We consider a second set of orthonormal modes v_ω, and subsequently expand the scalar field as

$$\hat{\psi}(r;\omega) = \int_0^\infty \frac{\mathrm{d}\omega}{\sqrt{4\pi\omega}} \left[v_\omega b_\omega + v_\omega^* b_\omega^\dagger \right]. \tag{3.56}$$

This decomposition defines a vacuum state $|0\rangle_b$ unequal to $|0\rangle_a$, which is annihilated by the operators b_ω, and therefore has a different Fock space. It is interesting to investigate how these two vacua relate to each other. We note that, since both sets of solutions are orthonormal and complete, we may expand the modes $\{u_\omega\}$ and $\{v_\omega\}$ in terms of each other, such that

$$u_\omega = \alpha_\omega v_\omega + \beta_\omega v_\omega^\dagger, \tag{3.57}$$

with α_ω and β_ω the so-called Bogoliubov coefficients. This relation can easily be inverted [10] to obtain

$$v_\omega = \alpha_\omega^* u_\omega - \beta_\omega u_\omega^\dagger. \tag{3.58}$$

We must ensure that the expansion Eq.(3.57) is normalized, which is ensured by demanding [10, 52] the condition

$$|\alpha_\omega|^2 - |\beta_\omega|^2 = 1. \tag{3.59}$$

However, this discussion has still not answered the question of how the two vacua $|0\rangle_a$ and $|0\rangle_b$ are related. We proceed by following [52], where the two expressions for the field operator Eq.(3.55) and Eq.(3.56) are equated, and we subsequently insert the expression Eq.(3.57). After some simple bookkeeping, one obtains the Bogoliubov transformations

$$a_\omega = \alpha_\omega^* b_\omega + \beta_\omega b_\omega^\dagger \quad \text{and} \quad a_\omega^\dagger = \alpha_\omega b_\omega^\dagger + \beta_\omega^* b_\omega, \tag{3.60}$$

and similarly for the b-vacuum operators

$$b_\omega = \alpha_\omega a_\omega - \beta_\omega a_\omega^\dagger \quad \text{and} \quad b_\omega^\dagger = \alpha_\omega^* a_\omega^\dagger - \beta_\omega^* a_\omega. \tag{3.61}$$

The connection between the two vacua can be made explicit by considering the expectation value of the a-particle number operator $\hat{N}_a = a_\omega^\dagger a_\omega$ in the b-vacuum, which can be shown to yield

$$\langle \hat{N}_a \rangle_b = |\beta_\omega|^2 \delta(0). \tag{3.62}$$

The above calculation is precisely the way to go when one wants to obtain the Hawking radiation, which shows that a black hole emits heat radiation [36]. We will not provide a detailed derivation, but simply describe the mechanism from [52], in which they mention that a possible way to arrive at the Hawking radiation is by considering a field expansion in terms of lightcone tortoise-coordinates, with a vacuum $b_\Omega \left|0\right\rangle_B = 0$, which contains no particles according to an asymptotic observer. Similarly, we expand the fields in terms of the Kruskal-Szekeres coordinates, in which the observer does measure particles, with a vacuum state $a_\omega \left|0\right\rangle_K = 0$. The latter is considered to be the physical vacuum. If one uses the Bogoliubov discussion from before, one eventually ends up with the expectation value

$$\langle \hat{N}_\Omega \rangle_K = \frac{1}{e^{\Omega/T_H} - 1}\delta(0), \tag{3.63}$$

with T_H the Hawking temperature. This rather sketchy discussion on Hawking radiation provides us with a simple roadmap to show that, for our analogue black hole, a similar mechanism seems to exist.

3.3.3 Analogue Hawking spectrum

Now that we have developed the required machinery to relate different choices of the vacuum, it is a natural extension to consider how the in-basis vacuum, which we considered to be the 'general' vacuum, and out-basis vacuum compare. This may be achieved rather straightforwardly by expanding the out-basis modes in terms of the in-basis modes. Note that both the in-basis and out-basis vacuum are defined with respect to the same frequency and time-coordinate, such that we may write

$$\tilde{\psi}_0^{\text{out}}(r;\omega) = u_0 \tilde{\psi}_0^{\text{in}}(r;\omega) - v_0^* \tilde{\psi}_0^{\text{in}\,*}(r;\omega)), \tag{3.64}$$

where u_0 and v_0 are the Bogoliubov coefficients. These can be determined by inserting the expressions for the in-basis and out-basis solutions into the transformation, leading to the expression

$$\begin{aligned} e^{2\pi c_0\omega} I_{ic_0\omega}(i\omega\sqrt{r^2 - c_0^2}) - I_{-ic_0\omega}(i\omega\sqrt{r^2 - c_0^2}) \\ = e^{\pi c_0\omega}\sqrt{e^{2\pi c_0\omega} - 1}\left[u_0 I_{ic_0\omega}(i\omega\sqrt{r^2 - c_0^2}) - v_0^*(I_{ic_0\omega}(i\omega\sqrt{r^2 - c_0^2}))^*\right]. \end{aligned} \tag{3.65}$$

All we have to do at this point is subtracting the right-hand side from both sides and choosing the coefficients such that corresponding modified Bessel functions cancel. The coefficient u_0 is found most easily, following directly from

$$e^{\pi c_0\omega} I_{ic_0\omega}(i\omega\sqrt{r^2 - c_0^2}) = u_0\sqrt{e^{2\pi c_0\omega} - 1} I_{ic_0\omega}(i\omega\sqrt{r^2 - c_0^2}), \tag{3.66}$$

such that we may write

$$u_0 = \frac{e^{\pi c_0 \omega}}{\sqrt{e^{2\pi c_0\omega} - 1}} \quad \Rightarrow \quad |u_0|^2 = \frac{1}{1 - e^{-2\pi c_0\omega}}. \tag{3.67}$$

Similarly, we must choose the coefficient v_0 in such a way that the following expression holds:

$$I_{-ic_0\omega}(i\omega\sqrt{r^2 - c_0^2}) = v_0^* e^{\pi c_0\omega}\sqrt{e^{2\pi c_0\omega} - 1} I_{-ic_0\omega}(-i\omega\sqrt{r^2 - c_0^2}). \tag{3.68}$$

In appendix (B.14), we demonstrate the following identity for modified Bessel functions:

$$I_{-ic_0\omega}(-i\omega x) = e^{-\pi c_0\omega} I_{-ic_0\omega}(i\omega x), \tag{3.69}$$

for any $x \in \mathbb{R}, \omega \in \mathbb{R}$. Using this identity, we may rewrite Eq.(3.68) into an expression with modified Bessel functions of the same order and argument, such that

$$I_{-ic_0\omega}(i\omega\sqrt{r^2 - c_0^2}) = v_0^*\sqrt{e^{2\pi c_0\omega} - 1} I_{-ic_0\omega}(i\omega\sqrt{r^2 - c_0^2}). \tag{3.70}$$

From this expression the last Bogoliubov coefficient can be trivially deduced, and is seen to give

$$v_0^* = \frac{1}{\sqrt{e^{2\pi c_0\omega} - 1}} \quad \Rightarrow \quad |v_0|^2 = \frac{1}{e^{2\pi c_0\omega} - 1}. \tag{3.71}$$

Using these expressions, one is able to show that the condition $|u_0|^2 - |v_0|^2 = 1$ indeed holds. The connection with Hawking radiation follows quite naturally from the remainder of the intermezzo, by using the expansion for the creation (and annihilation) operators

$$\hat{a}^{\text{out}}_{0R(L)}(\omega) = u_0 \hat{a}^{\text{in}}_{0R(L)}(\omega) + v_0 \hat{a}^{\text{in}\dagger}_{0R(L)}(\omega). \tag{3.72}$$

We also introduce the vacuum states $\hat{a}^{\text{out}}_{0R(L)} |0\rangle_{\text{out}} = 0$ and $\hat{a}^{\text{in}}_{0R(L)} |0\rangle = 0$, where for the in-basis vacuum we dropped the subscript, as this vacuum is considered to be the general vacuum. The out-particle number operator is given by $\hat{N}_{\text{out}} = a^{\text{out}\dagger}_{0R(L)} a^{\text{out}}_{0R(L)}$, where we have suppressed the frequency dependence of all operators for brevity. The expectation value of this operator with respect to the in-basis can then be written as

$$\langle \hat{N}_{\text{out}} \rangle = \langle 0 | \hat{a}^{\text{out}\dagger}_{0R(L)}(\omega) \hat{a}^{\text{out}}_{0R(L)}(\omega) | 0 \rangle \,. \tag{3.73}$$

Inserting the Bogoliubov transformation Eq.(3.72), acting on the vacuum with the annihilation operator and using the commutation relations then allows us to write

$$\begin{aligned} \langle \hat{N}_{\text{out}} \rangle &= \langle 0 | (u_0^* \hat{a}^{\text{in}\dagger}_{0R(L)} + v_0^* \hat{a}^{\text{in}}_{0R(L)})(u_0 \hat{a}^{\text{in}}_{0R(L)} + v_0 \hat{a}^{\text{in}\dagger}_{0R(L)}) | 0 \rangle \\ &= |v_0|^2 \langle 0 | \hat{a}^{\text{in}}_{0R(L)} \hat{a}^{\text{in}\dagger}_{0R(L)} | 0 \rangle = |v_0|^2 \delta(0). \end{aligned} \tag{3.74}$$

The out-particle number density in the in-vacuum is therefore seen to yield

$$\langle \hat{n}_{\text{out}} \rangle = \frac{1}{e^{2\pi c_0 \omega} - 1}. \tag{3.75}$$

Similarly, the average number of out-particles is given by

$$\langle \hat{N}_{\text{out}} \rangle = \frac{1}{e^{\omega/T_H} - 1} \delta(0), \tag{3.76}$$

with $T_H = 1/(2\pi c_0)$ the Hawking temperature. An observer in the in-vacuum must therefore see a flux of particles with a thermal spectrum as described by Eq.(3.76). This result captures the acoustic equivalent of the Hawking effect.

3.3.4 Greybody factor, emitted particles, and correlators

In the previous section we managed to derive a spectrum for the particles emitted from the acoustic horizon. The seemingly trivial generalisation of this expression to the total number of emitted particles is a rather deceptive problem, as one ought to take into account the presence of an effective potential in front of the horizon, before we are in any way capable of measuring the emitted phonons in the asymptotic region (*i.e.* the boundary of our experiment). In line with [7, 8], we rewrite the equation of motion Eq.(3.43) as

$$\partial_r^2 R(r) + P(r)\partial_r R(r) + Q(r)R(r) = 0, \tag{3.77}$$

where in our case

$$P(r) = \frac{c_0^2 + r^2}{r(r^2 - c_0^2)} \tag{3.78}$$

$$Q(r) = -\frac{m^2 r^2 - r^4 \omega^2}{r^2(r^2 - c_0^2)}. \tag{3.79}$$

Note that we have not taken $m = 0$ in this particular instance. Our next step is to map the subsonic region of the analogue black hole (c_0, ∞) to $(-\infty, \infty)$ through an appropriately chosen coordinate transformation. Hence, in these new coordinates, an observer approaches the horizon $r \to c_0$ when $r^* \to -\infty$. This particular coordinate is known as the tortoise coordinate, which for our system takes the form

$$r^* = r - \frac{c_0}{2} \log \left| \frac{r + c_0}{r - c_0} \right|. \tag{3.80}$$

One can easily show that its derivative with respect to the original radial coordinate gives $dr^*/dr = f(r)^{-1} \equiv \Delta$. Next, we separate the function $R(r) = Z(r)H(r)$ into two non-equal

radial parts, which allows us to write the equation of motion as

$$\frac{\partial}{\partial r_*^2}H(r) + \frac{1}{\Delta^2 Z}\big[\Delta(2\frac{\partial}{\partial r_*}Z + PZ) + \frac{\partial \Delta}{\partial r_*}Z\big]\frac{\partial}{\partial r_*}H(r) + \frac{1}{\Delta^2 Z}(\frac{\partial^2}{\partial r_*^2}Z + P\frac{\partial}{\partial r}Z + QZ)H(r) = 0. \quad (3.81)$$

Note that all we have done so far is following the discussion from [7, 8], and accordingly we will now demand the coefficient of the first derivative of $H(r)$ to be zero:

$$\frac{\partial}{\partial r}Z(r) + \frac{1}{2}\big[P(r) + \frac{\partial}{\partial r}\log(\Delta)\big]Z(r) = 0. \quad (3.82)$$

This equation is solved by the simple expression

$$Z(r) = \frac{A}{\sqrt{r}}, \quad (3.83)$$

with A an arbitrary real number, which we will take to be $A = 1$. Inserting this into Eq.(3.81) leads to the effective Schrödinger equation

$$\frac{\partial^2}{\partial r_*^2}H(r) + \big[\omega^2 - V(r)\big]H(r) = 0, \quad (3.84)$$

which contains the effective potential

$$V(r) = \frac{f(r)^2}{r^2}\big[m^2 + \frac{5c_0^2}{4r^2} - \frac{1}{4}\big]. \quad (3.85)$$

Note that we implicitly assume $r = r(r^*)$, which is obtained by inverting Eq.(3.80) for fixed c_0. An important observation is that, for $r \to \infty$, the warping factor $f(r) \to 1$, which causes the potential to vanish. Furthermore, note that in this limit $r = r_*$. In line with the analytical approach to our analogue, we consider the $m = 0$ modes only, knowing that the remainder of the analysis can be done numerically if one wishes. A left-travelling incident wave of amplitude 1, which is reflected by the potential, is then seen to take the asymptotic form

$$H(r) \sim R_\omega e^{i\omega r_*} + e^{-\omega r_*}. \quad (3.86)$$

Here, R_ω is the reflection coefficient for the incident wave scattered by the effective potential. Similarly, in the event where there is only outgoing radiation at the boundary of the system, we may consider only right-moving radiation (from the horizon) while setting the transmission coefficient $T_\omega = 1$ and the reflection coefficient $R_\omega \neq 0$, which matches with the interpretation of Eq.(3.52). If we demand only outgoing radiation at the horizon, we could allow for both right-moving and left-moving waves, while taking $T_\omega = 1$ and $R_\omega = 0$, such that all incident radiation is reflected, but all emitted radiation is transmitted. This also sheds light on the

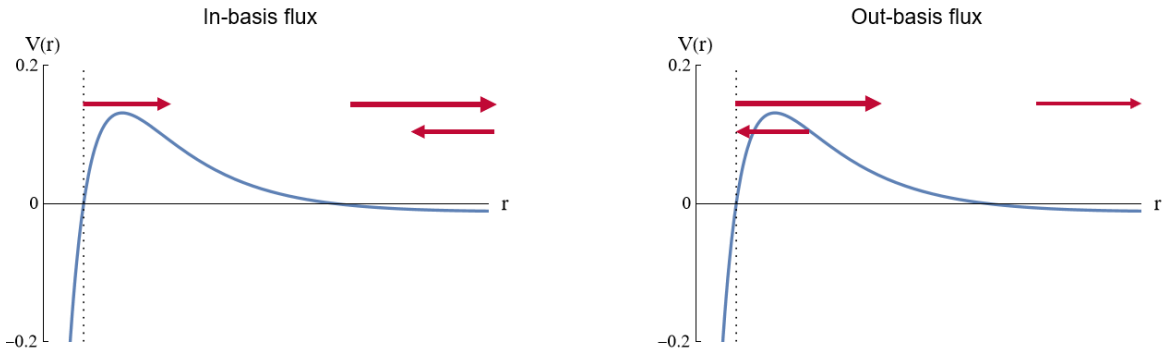

Fig. 3.2 This figure shows the effective potential $V(r)$ and the flux profiles for both the in-basis and out-basis solutions. The dotted line represents the acoustic horizon at $c_0 = 2$.

appearance of the in-basis asymptotic form Eq.(3.53). Fig.(3.2) depicts the in-basis and out-basis boundary conditions, including the effective potential. For convenience we have plotted the potential as a function of r, yet one should note that a correct depiction of the potential would 'smear' the potential out over the region $(-\infty, \infty)$. It is in principle possible to determine the greybody (or: the fraction of emitted radiation reflected by the potential) from these coefficients. One could, for example, also consider the limit $r^* \to -\infty$, which leads to a hypergeometric function [35], and then match this with the expression for $r \to \infty$. The explicit form of R_ω and T_ω are then all one needs to determine the greybody factor $\gamma(\omega)$. However, there exists a slightly easier route in our case, as the asymptotic solutions of the exact wave functions for $m = 0$ can be used to compute the ratio of the outgoing flux and ingoing flux at the horizon, after which one obtains [48]

$$\gamma_0(\omega) = \frac{\mathcal{F}_{\text{out}}}{\mathcal{F}_{\text{in}}} = 1 - e^{-\omega/T_H}. \tag{3.87}$$

The total amount of emitted particles is then found by integrating the acoustic Hawking spectrum over ω, while correcting for the fraction which is reflected by the potential, leading to [48]

$$N = \sum_m \int_0^\infty \frac{\mathrm{d}\omega\, \omega}{2\pi} \frac{\gamma_m(\omega)}{e^{\omega/T_H} - 1}. \tag{3.88}$$

In [48] the greybody factor is determined numerically for $m \in \{1, 2, 3\}$, from which they conclude that, in the low-frequency regime $\omega \ll 1$, the $m = 0$ mode is dominant. Hence, we may approximately write

$$\frac{\sum_m \gamma_m(\omega)}{e^{\omega/T_H} - 1} \approx \frac{1 - e^{-\omega/T_H}}{e^{\omega/T_H} - 1} \approx e^{-\omega/T_H}, \tag{3.89}$$

where in the last step we considered a Taylor expansion around $\omega \approx 0$. Therefore, the total number of emitted particles is altered by the effective potential emerging from the acoustic

geometry, and can be written in terms of a classical Maxwell-Boltzmann spectrum

$$N \approx \int_0^\infty \mathrm{d}\omega \frac{\omega}{2\pi} e^{-\omega/T_H}. \tag{3.90}$$

However, despite the fact that this scattering problem is interesting entirely for its own sake, we still have not shown why acoustic Hawking radiation should be studies from the lens of entanglement entropy. This connection becomes clear when computing the current-current correlation function, given by

$$\Pi^{\mu\nu}(\mathbf{r}, \mathbf{r}'; \tau - \tau') = \langle 0 | \hat{J}^\mu(\mathbf{r}, \tau) \hat{J}^\nu(\mathbf{r}', \tau') | 0 \rangle \,, \tag{3.91}$$

where (as before) we use the shorthand $|0\rangle = |0\rangle_{\text{in}}$. From the equation of motion, it is clear that a convenient choice for the conserved current is $\hat{J}^\mu(\mathbf{r}, \tau) = \nabla^\mu \delta\theta(\mathbf{r}, \tau)$. Substituting Eq.(3.42) and the Bogoliubov transform for $a^{(\dagger)}_{mR/L}(\omega)$, the authors show that the correlator is given by [48]

$$\Pi^{\mu\nu}(\mathbf{r}, \mathbf{r}'; \tau - \tau') = \int_0^\infty \mathrm{d}\omega \sum_m \chi_c(\omega) \left(\frac{1}{e^{\omega/T_H} - 1} + \frac{1}{2}\right) \times \nabla^\mu \{\psi^{\text{out}}_m(r; \omega) A(m, \tau)\} \nabla^\nu \{\psi^{\text{out}*}_m A^*(m, \tau')\}, \tag{3.92}$$

where $A(m, \tau) = e^{im\phi - i\omega\tau}$ and $\chi_c(\omega)$ is a cutoff function. The authors determined the density-density correlators Π^{tt} and velocity-velocity correlators Π^{rr} numerically, which lays bare the connection we are after. They found that both correlators for the out-basis solutions, measured in the in-basis, result in dominant correlation lines both for the case where r and r' are in the subsonic region, as well as when the phonon at r is supersonic while the phonon at r' is subsonic. The latter suggests that it might be plausible that entangled phonon pairs are created at or slightly before the acoustic horizon, after which one of the phonons transverses through the supersonic region, whereas the other enters the subsonic region. However, confirmation of this hypothesis requires one to explicitly determine the entanglement entropy of the supersonic region with respect to the subsonic region, or vice versa. We have now arrived at the goal of this thesis: developing a formalism to (numerically) determine the entanglement entropy of the supersonic (or subsonic) region. Ideally, one would obtain a vacuum wave functional in the Schrödinger representation for the out-basis solutions, after which one can determine the density matrix of the system and proceed to find the reduced density matrix of either of the aforementioned regions. The former, finding the vacuum wave functional for the analogue black hole, will be attempted in the next chapter. Developing a formalism to find the numerical entanglement entropy of scalar fields takes center stage in the last two chapters of this dissertation.

Chapter 4

Curved spacetime QFT in the Schrödinger representation

"I... a universe of atoms, an atom in the universe."
Richard Feynman

In the previous chapter we explored a proposal for an analogue black hole in a Bose-Einstein condensate of light by [48], which culminated in the authors concluding that entangled phonon pairs may be created at or near the acoustic horizon, and as such one could benefit from explicitly determining the entanglement entropy of the supersonic region (or *vice versa* the subsonic region). As we mentioned in Ch.2, one could go about this task in various ways, yet we will adhere to a numerical scheme which requires either knowledge of the Hamiltonian of the theory in question, or an explicit expression for its vacuum wave functional. Obtaining the former is a trivial task, yet the latter is more cumbersome, since studying scalar theories on curved backgrounds in the Schrödinger representation is not done too often. Luckily for us, there has been quite some activity in this particular subdomain in the '80s, '90s and early '00s, with [50, 51, 31] providing important resources. We will first very briefly derive the vacuum wave functional for a (2+1)-dimensional scalar field on a flat background. Next, we turn to the work by [50, 51], which is inarguably the backbone of the remainder of this chapter, and we will follow their derivations as closely as the length of this chapter can muster. We conclude the chapter by testing the developed formalism on two well-known examples, and ultimately on our analogue black hole, despite the fact that there are some important questions left to answer.

4.1 Minkowski spacetime

Since many of these arguments will seem familiar to the reader, with most them appearing once or twice in an introductory course on quantum field theory, we will keep this discussion brief. There are several ways to arrive at the vacuum wave functional of a free, massless scalar field in (2+1)-dimensions, and as such we list three of them, yet the reader is encouraged to explore more ways of arriving at the same conclusion. Perhaps the easiest (but least satisfactory) way of doing so is to heuristically argue that the ground state should adopt a form similar to

$$\Psi_0 \propto \exp\{-\frac{1}{2}\int \frac{\mathrm{d}\mathbf{k}}{(2\pi)^2}\,\omega(\mathbf{k})\phi(\mathbf{k})\phi(-\mathbf{k})\}, \tag{4.1}$$

where the dispersion $\omega(\mathbf{k}) = \pm|\mathbf{k}|$ is obtained from the equation of motion. Upon Fourier-transforming the fields $\phi(\mathbf{k}) = \int \mathrm{d}\mathbf{x}\, e^{-i\mathbf{k}\cdot\mathbf{x}}\phi(\mathbf{x})$, we obtain the intuitively obvious expression

$$\Psi_0 \propto \exp\{-\frac{1}{2}\int \mathrm{d}\mathbf{x}\int \mathrm{d}\mathbf{x}'\int \frac{\mathrm{d}\mathbf{k}}{(2\pi)^2}\,\omega(\mathbf{k})e^{-i\mathbf{k}\cdot(\mathbf{x}-\mathbf{x}')}\phi(\mathbf{x})\phi(\mathbf{x}')\}. \tag{4.2}$$

However easy this may seem, we cannot claim to have adhered to much rigour. Let us revisit the derivation, but this time around start from the expansion of the field operator, which we define in line with [70], and is given by

$$\hat{\phi}(\mathbf{x}) = \int \frac{\mathrm{d}\mathbf{k}}{(2\pi)^2 2\omega}\Big[a(\mathbf{k})e^{ikx} + a^\dagger(\mathbf{k})e^{-ikx}\Big]. \tag{4.3}$$

As discussed in [70], the field operator can be inverted for the annihilation operator, which gives

$$a(\mathbf{k}) = \int \mathrm{d}\mathbf{x}\, e^{-ikx}\Big[i\hat{\pi}(x) + \omega\hat{\phi}(x)\Big], \tag{4.4}$$

where $\hat{\pi}(x)$ is defined as the conjugate momentum of the field operator. This simple exercise is typically done in a first course on QFT, and as such we will simply stick to the statements above. Note that, as a shorthand, we have suppressed the $\mathbf{k}$-dependence of the dispersion. We recall that, in the Schrödinger picture, one represents the quantum states as the time-dependent wave functionals $\Psi[\phi(\mathbf{x}), t]$, and operators acting on these states are represented by $\mathcal{O}(\hat{\pi}(x), \hat{\phi}(x)) \sim \mathcal{O}(-i\delta/\delta\phi(\mathbf{x}), \phi(\mathbf{x}))$, a brief review for which in given in [50]. We consider the *Ansatz* for the ground state wave functional suggested in [50, 51], which is given by

$$\Psi_0[\phi(\mathbf{x}), t] = N_0 \exp\{-\frac{1}{2}\int \mathrm{d}\mathbf{x}\int \mathrm{d}\mathbf{x}'\phi(\mathbf{x})G(\mathbf{x},\mathbf{x}')\phi(\mathbf{x}')\} \equiv N_0\psi_0(\phi), \tag{4.5}$$

where $N_0 = \exp\{-iE_0t\}$. Replacing the operators in Eq.(4.4) by the corresponding functional derivatives or fields and acting on the *Ansatz*, while demanding that $a\psi_0 = 0$ is respected, allows us to write

$$G(\mathbf{x},\mathbf{x}') = \int \frac{\mathrm{d}\mathbf{k}}{(2\pi)^2}\,\omega e^{-i\mathbf{k}\cdot(\mathbf{x}-\mathbf{x}')}, \tag{4.6}$$

with $\omega = \pm|\mathbf{k}|$ from before. Inserting this kernel into the *Ansatz* returns the wave functional we found through our heuristic route. Similarly, as discussed in [50], one could also write down the time-dependent Schrödinger equation, which after the correct replacement of operators by functional derivatives and field eigenvalues returns the kernel equation [50]

$$\int \mathrm{d}\mathbf{x}'\, G(\mathbf{x},\mathbf{x}')G(\mathbf{x}',\mathbf{x}'') = -\nabla^2\delta(\mathbf{x}-\mathbf{x}''). \tag{4.7}$$

A simple Fourier transform of the kernel demonstrates that the equation is solved by Eq.(4.6), and hence yields the vacuum wave functional

$$\Psi_0 \propto \exp\{-\frac{1}{2}\int \mathrm{d}\mathbf{x}\int \mathrm{d}\mathbf{x}'\int \frac{\mathrm{d}\mathbf{k}}{(2\pi)^2}\,\omega e^{-i\mathbf{k}\cdot(\mathbf{x}-\mathbf{x}')}\phi(\mathbf{x})\phi(\mathbf{x}')\}. \tag{4.8}$$

However, for later purposes it will prove useful to write the expression in polar coordinates, as this will allow us to ultimately discretize the radial coordinate of the kernel. This is achieved by means of the Jacobi-Anger identity, which we discuss in appendix (A.2). In this appendix we also demonstrate that

$$e^{-i\mathbf{k}\cdot(\mathbf{x}-\mathbf{x}')} = \sum_m\sum_{m'}(-i)^m i^{m'} J_m(kr)J_{m'}(kr')e^{i\theta_k(m-m')}e^{-im\theta_r}e^{im'\theta_{r'}}. \tag{4.9}$$

We are now at liberty to evaluate the $\mathbf{k}$-dependent part of our kernel, which is seen to become

$$\int \mathrm{d}\mathbf{k}\,\omega e^{-i\mathbf{k}\cdot(\mathbf{x}-\mathbf{x}')} = \sum_{m,m'}\int \mathrm{d}k\int \mathrm{d}\theta_k\,\omega^2(-i)^m i^{m'}J_m(kr)J_{m'}(kr') \times e^{i\theta_k(m-m')}e^{-im\theta_r}e^{im\theta_{r'}}, \tag{4.10}$$

where ω^2 contains the contribution $|\mathbf{k}|$ from the measure. Integrating over the angular variable θ_k and eliminating the resulting delta-function by summing over m' yields

$$\int \mathrm{d}\mathbf{k}\,\omega e^{-i\mathbf{k}\cdot(\mathbf{x}-\mathbf{x}')} = 2\pi\sum_m\int \mathrm{d}k\,\omega^2 J_m(kr)J_m(kr')e^{im(\theta_{r'}-\theta_r)}. \tag{4.11}$$

We insert this expression back into the ground state wave functional and decompose the fields into a radial and angular part, *i.e.* we take $\phi(\mathbf{x}) = \sum_m \phi_m(r)Y_m(\theta_r)/\sqrt{r}$, such that we may write

$$\Psi_0 \propto \exp\{-\frac{1}{2}\sum_{m,m',m''}\int \mathrm{d}r\mathrm{d}r'\,\sqrt{rr'}\int \mathrm{d}\theta_r\mathrm{d}\theta_{r'}\,Y_{m'}(\theta_r)Y_{m''}(\theta_{r'}) \times \int \mathrm{d}k\,\omega^2 J_m(kr)J_m(kr')e^{im(\theta_{r'}-\theta_r)}\phi_{m'}(r)\phi_{m''}(r')\}. \tag{4.12}$$

We assume that there exist circular harmonics $Y_m(\theta_r)$ such that $\int \mathrm{d}\theta_r Y_{m'}(\theta_r)e^{-im\theta_r} = \delta_{m,m'}$, for example by choosing $Y_m(\theta) = e^{\pm im\theta}$. If the previous harmonics are allowed, then the wave functional can be shown to reduce to

$$\Psi_0 \propto \exp\{-\frac{1}{2}\sum_m \int \mathrm{d}r\mathrm{d}r' \sqrt{rr'} \int \mathrm{d}k\, \omega^2 J_m(kr)J_m(kr')\phi_m(r)\phi_m(r')\}, \tag{4.13}$$

of which the kernel can easily be discretized in the radial coordinate. In the next section we aim to generalize this discussion to curved backgrounds. We will demonstrate that the formalism from [50, 51] will in fact simplify the derivation above considerably, which will ultimately aid us in studying the ground state wave functional of the analogue black hole.

4.2 Generalization to curved backgrounds

The discussion for Minkowski spacetime can, with some effort, be generalized to globally hyperbolic spacetimes with a (global) timelike vector field. The key in this whole procedure is choosing an appropriate foliation of the manifold and connecting this with the derivation from before. However, this description would be a notoriously labour-intensive pursuit, while containing many elements which are wholly irrelevant to the remainder of the thesis, and as such we will simply state a result from [50] which acts as a convenient starting point, while keeping the geometric prerequisites to a bare minimum. Since this source gives an excellent review of the subject, we will follow the relevant derivations very closely, reproducing some of their key results, and elaborate on them where possible (filling in the mathematical blanks, so to speak). The Schrödinger equation for a scalar field on a general curved (globally hyperbolic) spacetime is given by the expression

$$i\frac{\partial}{\partial s}\Psi[\phi(\zeta), s] = \int_\Sigma \mathrm{d}\zeta\{\frac{1}{2}N\sqrt{-h}(\frac{1}{h}\frac{\delta^2}{\delta\phi^2} - h^{ij}\partial_i\phi\partial_j\phi + (m^2 + \xi R)\phi^2) \\ - iN^i\partial_i\phi\frac{\delta}{\delta\phi}\}\Psi[\phi(\zeta), s]. \tag{4.14}$$

Before diving into a small explanation of the expression above, we note that we are at liberty to set $m = 0$ and $\xi = 0$, as we are primarily interested in a massless, minimally-coupled scalar field. In the notation of [50], ζ_i are the coordinates of a family of spacelike hypersurfaces Σ, while considering their evolution along curves $\partial/\partial s$. Furthermore, N and N^i denote shift and lapse functions, yet the only relevant feature for us, is that in terms of these functions the infinitesimal interval becomes [50]

$$ds'^2 = (N^2 + N^iN_i)ds^2 + 2N_i ds d\zeta^i + h_{ij}d\zeta^i d\zeta^j, \tag{4.15}$$

where h_{ij} is the induced metric on the spacelike hypersurface Σ. Note that we assume that all fields $\phi(\zeta)$ have been canonically quantized on the hypersurface Σ. The equations can be brought into a more familiar form upon choosing the coordinates $(s, \zeta) = (t, \mathbf{x})$, such that $\Sigma = \mathbb{R}^d$. For convenience we demand the metric $g_{\mu\nu}$ to be diagonal, such that we may set $N = \sqrt{g_{00}}$ and $N^i = 0$. One can similarly show that this choice leads to $h_{ij} = g_{ij}$. We are now able to rewrite the Schrödinger equation into a more familiar form, by noting that the determinant $|g| = |g_{00}|h_{ij}$, such that Eq.(4.14) becomes

$$i\frac{\partial}{\partial t}\Psi[\phi] = \frac{1}{2}\int \mathrm{d}\mathbf{x}\sqrt{|g|}\{\frac{g_{00}}{g}\frac{\partial^2}{\partial\phi^2} - g^{ij}\partial_i\phi\partial_j\phi + m^2\}\Psi[\phi]. \tag{4.16}$$

As before, we observe that a simple Gaussian *Ansatz* will be sufficient:

$$\Psi_0[\phi, t] = N_0 \exp\{-\frac{1}{2}\int \mathrm{d}\mathbf{x}\sqrt{|h_x|}\int \mathrm{d}\mathbf{x}'\sqrt{|h_{x'}|}\phi(\mathbf{x})G(\mathbf{x}, \mathbf{x}'; t)\phi(\mathbf{x}')\}, \tag{4.17}$$

where $h_x = h(\mathbf{x})$ is a shorthand for the determinant of the induced metric in terms of the coordinate $\mathbf{x}$. The only difference with the Minkowski spacetime, are the measures ensuring that the spatial integrals are invariant d-dimensional volume elements. We insert the *Ansatz* into the Schrödinger equation, for now only studying the left-hand side, which is trivially seen to give

$$i\frac{\partial}{\partial t}\Psi_0 = i\frac{\partial}{\partial t}\log(N_0)\Psi_0 - \frac{i}{2}\int \mathrm{d}\mathbf{x}\sqrt{|h_x|}\int \mathrm{d}\mathbf{x}'\sqrt{|h_{x'}|}\phi(\mathbf{x})(\frac{\partial}{\partial t}G(\mathbf{x}, \mathbf{x}'; t))\phi(\mathbf{x}')\Psi_0. \tag{4.18}$$

Next, we act with the right-hand side of the Schrödinger equation on the vacuum wave functional Eq.(4.17) and collect like terms, such that the time-derivative of N_0 yields

$$i\frac{\partial}{\partial t}\log(N_0) = \frac{1}{2}\int \mathrm{d}\mathbf{x}\sqrt{h_x}\sqrt{|g^x_{00}|}G(\mathbf{x}, \mathbf{x}). \tag{4.19}$$

Similarly, we equate the other terms with the second part of Eq.(4.18), such that we obtain a kernel equation

$$\begin{aligned} -\frac{i}{2}\int \mathrm{d}\mathbf{x}\sqrt{|h_x|}\int \mathrm{d}\mathbf{x}'\sqrt{|h_{x'}|}\phi(\mathbf{x})(\frac{\partial}{\partial t}G(\mathbf{x}, \mathbf{x}'; t))\phi(\mathbf{x}') = \\ \frac{1}{2}\int \mathrm{d}\mathbf{z}\sqrt{|g_z|}\int \mathrm{d}\mathbf{x}\sqrt{|h_x|}\int \mathrm{d}\mathbf{x}'\sqrt{|h_{x'}|}\phi(\mathbf{x})G(\mathbf{x}, \mathbf{z}; t)G(\mathbf{z}, \mathbf{x}'; t)\phi(\mathbf{x}') \\ + \frac{1}{2}\int \mathrm{d}\mathbf{x}\sqrt{|h_x|}(-g^{ij}\partial_i\phi\partial_j\phi + m^2\phi^2). \end{aligned} \tag{4.20}$$

This rather lengthy expression can be simplified considerably by stripping off the integrals over $\mathbf{x}$ and $\mathbf{x}'$. The first term on the right-hand side is already in an appropriate form, yet the other two terms still need some work. We assume vanishing boundary conditions for the fields, such that partial integration over the second term introduces a Laplacian, and

subsequently introduce a delta function:

$$\frac{1}{2}\int \mathrm{d}\mathbf{x}\sqrt{|h_x|}(-g^{ij}\partial_i\phi(\mathbf{x})\partial_j\phi(\mathbf{x})) = \frac{1}{2}\int \mathrm{d}\mathbf{x}\sqrt{|h_x|}\sqrt{|g^x_{00}|}\phi(\mathbf{x})\hat{\Box}_x\phi(\mathbf{x}')\delta(\mathbf{x}-\mathbf{x}'), \tag{4.21}$$

where $\sqrt{|g_x|}\hat{\Box}_x = \partial_i(\sqrt{|g_x|}g^{ij}_x\partial_j)$. Note that the extra factor $\sqrt{|g^x_{00}|}$ stems from using the diagonality of the metric to write $\sqrt{|g|} = \sqrt{|g_{00}|}\sqrt{h_{ij}}$, which yields the full metric instead of the induced metric to support the conventional definition of our Laplacian. We also introduce a delta-function in the mass term, after which we are able to strip away the aforementioned integrals, such that we eventually obtain the kernel equation

$$\begin{aligned} i\frac{\partial}{\partial t}(\sqrt{h_x h_{x'}}G(\mathbf{x},\mathbf{x}';t)) = \int \mathrm{d}\mathbf{z}\sqrt{h_z}\sqrt{h_x h_{x'}}\sqrt{|g^z_{00}|}G(\mathbf{x},\mathbf{z};t)G(\mathbf{z},\mathbf{x}';t) \\ - \sqrt{h_x h_{x'}}\sqrt{|g^x_{00}|}(\hat{\Box}_x + m^2)\delta(\mathbf{x}-\mathbf{x}'), \end{aligned} \tag{4.22}$$

as described in [50]. Since we are ultimately interested in a Schwarzschild-*like* manifold, which is static, we may take the kernel to be time-independent and set the left-hand side to zero. Hence, the kernel equation reduces to the simpler expression

$$\int \mathrm{d}\mathbf{z}\sqrt{|g_z|}G(\mathbf{x},\mathbf{z};t)G(\mathbf{z},\mathbf{x}';t) = \sqrt{|g^x_{00}|}(\hat{\Box}_x + m^2)\delta(\mathbf{x}-\mathbf{x}'). \tag{4.23}$$

Note that we have recombined the determinants, by writing $|g_z| = |g^z_{00}|h_z$, which is allowed for a diagonal metric. Before solving the kernel equation, we observe that the diagonality of the metric allows us to rewrite the d'Alembertian as

$$\hat{\Box} = \hat{\Box}_0 + \hat{\Box}_i = g^{00}\partial_0^2 + \hat{\Box}_i, \tag{4.24}$$

where the second term denotes the Laplacian we introduced earlier. After a Fourier decomposition of the field $\psi(\mathbf{x},t)$ into modes $e^{-i\omega t}\tilde{\psi}(\mathbf{x};\omega)$, the wave equation can be conveniently rewritten as

$$(\hat{\Box}_i + m^2)\tilde{\psi}(\mathbf{x};\omega) = g^{00}\omega^2\tilde{\psi}(\mathbf{x};\omega). \tag{4.25}$$

It therefore becomes clear that the kernel equation Eq.(4.23) can be solved by means of the eigenfunctions of the wave equation, provided they are orthogonal and complete. These two requirements, however intuitive these concepts may be in flat spacetime, require slightly more care when considering non-trivial geometries. Hence, we introduce the orthonormality and completeness on curved spaces in line with [30], where the author demonstrates that the completeness becomes

$$\int \frac{\mathrm{d}\mu(\omega)}{(2\pi)^d}\tilde{\psi}^*(\mathbf{x};\omega)\tilde{\psi}(\mathbf{x}';\omega) = \sqrt{\frac{|g^x_{00}|}{h_x}}\delta(\mathbf{x}-\mathbf{x}') \tag{4.26}$$

and the orthonormality takes the form

$$\int \frac{\mathrm{d}\mathbf{x}}{(2\pi)^d}\sqrt{|g_x|}g_x^{00}\tilde{\psi}^*(\mathbf{x};\omega)\tilde{\psi}(\mathbf{x};\omega') = \delta(\omega,\omega'). \tag{4.27}$$

The measure $\mathrm{d}\mu(\omega)$ and the delta function density $\delta(\omega,\omega')$ are defined such that

$$\int \mathrm{d}\mu\, \delta(\omega,\omega')f(\omega) = f(\omega'), \tag{4.28}$$

for an arbitrary function $f(\omega)$. Considering the Minkowski metric (or variants thereof in different coordinate systems) brings the definitions back in line with our flat-space intuition. An example would be a delta function density of the form $\delta(\omega-\omega')/\omega$, which combined with the measure $\mathrm{d}\mu = \omega\,\mathrm{d}\omega$ is seen to satisfy the definition of the Dirac delta function. Assuming that we have obtained eigenfunctions which obey the orthornormality and completeness requirements for general curved backgrounds, we may write the solution to the kernel equation as

$$G(\mathbf{x},\mathbf{x}') = \sqrt{g_x^{00}g_{x'}^{00}}\int \frac{\mathrm{d}\mu}{(2\pi)^d}\omega\tilde{\psi}(\mathbf{x};\omega)\tilde{\psi}^*(\mathbf{x}';\omega). \tag{4.29}$$

This can rather easily be verified by inserting the above into the kernel equation, which we will leave as an exercise to the reader.[1] Note that we have slightly departed from the notation of [50], where they make explicit that the measure, dispersion and both eigenfunctions share the same quantum numbers (*i.e.* the wave number). In our case this will be left implicit, as none of the examples we consider cause ambiguity on this front. Using this result and $N_0 = \exp(-iE_0t)$, we find the vacuum ground state by simply inserting the kernel into Eq.(4.17):

$$\Psi_0[\phi] = N_0\exp\Big\{-\frac{1}{2}\int\frac{\mathrm{d}\mu}{(2\pi)^d}\,\omega\int\mathrm{d}\mathbf{x}\sqrt{|h_x|}\sqrt{|g_x^{00}|}\tilde{\psi}(\mathbf{x};\omega)\phi(\mathbf{x}) \times\int\mathrm{d}\mathbf{x}'\sqrt{|h_{x'}|}\sqrt{|g_{x'}^{00}|}\phi(\mathbf{x}')\tilde{\psi}^*(\mathbf{x}';\omega)\phi(\mathbf{x}')\Big\}. \tag{4.30}$$

This is the main result of this section, which allows us to write down the vacuum wave functional for a scalar field on a general curved spacetime. As a natural extension, we will use this result to explore the ground state wave function of the analogue black hole. There are a few other relations we develop, as they will proof useful later down the line. We begin with the trivial observation that the inverse of the kernel is given by

$$\Delta(\mathbf{x},\mathbf{x}') = \int\frac{\mathrm{d}\mu}{(2\pi)^d}\frac{1}{\omega}\tilde{\psi}(\mathbf{x};\omega)\tilde{\psi}^*(\mathbf{x}';\omega). \tag{4.31}$$

This result is crucial in finding the expectation value of the energy-component of the stress-energy tensor, which we will only state for brevity, and more details on its derivation can be

[1] I have waited many years to finally use this famous sentence myself.

found in [51]:

$$\langle 0|T_{00}(\mathbf{x},\mathbf{x}'|0\rangle = -\frac{1}{4}g_{00}\Big\{G(\mathbf{x},\mathbf{x}') + g^{ij}\partial_i\partial_j\Delta(\mathbf{x},\mathbf{x}')\Big\}, \tag{4.32}$$

where we assumed the scalar field is massless. This expression only holds if the kernel is real. If the kernel is imaginary, the expectation value contains an extra term, which can be found in [51] (but is unnecessary in our case).

4.3 Two illustrative examples

In this section we shall demonstrate the construction of ground states in the Schrödinger picture by means of two examples: a scalar field on (2+1)-dimensional Minkowski spacetime in polar coordinates, and a scalar field on a (1+1)-dimensional Rindler spacetime. The former also acts as a simple test of our discussion so far, since we can compare the result with the ground state wave functional we obtained earlier through the Jacobi-Anger expansion. The metric of flat spacetime in polar coordinates is given by

$$ds^2 = -dt^2 + dr^2 + r^2 d\theta^2. \tag{4.33}$$

We consider a Fourier decomposition of the field into

$$\psi(t,r,\theta) = \sum_{m=-\infty}^{\infty} e^{-i\omega t}e^{im\theta}\tilde{\psi}_m(r;\omega). \tag{4.34}$$

The wave equation governing the radial Fourier modes is then trivially show to yield

$$(\partial_r^2 + \frac{1}{r}\partial_r + \omega^2 - \frac{m^2}{r^2})\tilde{\psi}_m(r;\omega) = 0, \tag{4.35}$$

which can be rewritten into a Bessel differential equation, as discussed in appendix B, for which the solutions are given by

$$\tilde{\psi}_m(r;\omega) = c_1 J_m(\omega r) + c_2 Y_m(\omega r), \tag{4.36}$$

where $Y_\nu(z)$ denotes a Bessel function of the second type. However, since the latter causes the field to diverge near the origin, we take $c_2 = 0$. The eigenfunctions can be shown to obey the requirement of orthogonality by means of appendix (B.3.5), leading to

$$\int_0^\infty \mathrm{d}r\, r J_m(\omega r)J_m(\omega' r) = \frac{\delta(\omega-\omega')}{\omega} \tag{4.37}$$

Note that this delta function obeys the definition of $\delta(\omega,\omega')$:

$$\int_0^\infty \mathrm{d}\mu(\omega)\frac{\delta(\omega-\omega')}{\omega}f(\omega) = f(\omega'), \tag{4.38}$$

when the measure is chosen as $\mathrm{d}\mu(\omega) = \omega\,\mathrm{d}\omega$. By means of Eq.(4.29), the kernel can then be written as

$$G(r,r';\theta,\theta') = \sum_m \int_{\mathbb{R}^+} \frac{\mathrm{d}\omega}{(2\pi)^2}\,\omega^2 J_m(\omega r) J_m(\omega r') e^{-im(\theta-\theta')}. \tag{4.39}$$

The vacuum wave functional for the scalar field is then seen to become

$$\Psi_0[\phi] \propto \exp\Big\{-\frac{1}{2}\int_0^{2\pi}\mathrm{d}\theta \int_0^{2\pi}\mathrm{d}\theta' \int_{\mathbb{R}^+}\mathrm{d}r\, r \int_{\mathbb{R}^+}\mathrm{d}r'\, r' G(r,r;\theta,\theta')\phi(r,\theta)\phi(r',\theta')\Big\}. \tag{4.40}$$

We then assume the fields $\phi(r,\theta)$ to allow for a decomposition into a radial part and circular harmonics $Y_m(\theta)$, such that $\phi = \sum_m \phi_m(r)Y_m(\theta)/\sqrt{r}$. If we assume that $Y_m(\theta) = e^{\pm im\theta}$ are valid harmonics, we are able to perform a dimensional reduction of the kernel in the angular variable:

$$\Psi_0[\phi] \propto \exp\Big\{-\frac{1}{2}\sum_{m,m',m''}\int_0^{2\pi}\mathrm{d}\theta\int_0^{2\pi}\mathrm{d}\theta'\int_{\mathbb{R}^+}\mathrm{d}r\,\sqrt{r}\int_{\mathbb{R}^+}\mathrm{d}r'\,\sqrt{r'}\int_{\mathbb{R}^+}\frac{\mathrm{d}\omega}{(2\pi)^2}\omega^2 J_m(\omega r)J_m(\omega r') \\ \times e^{-i\theta(m-m')}e^{i\theta'(m-m'')}\phi_{m'}(r)\phi_{m''}(r')\Big\}. \tag{4.41}$$

We perform the integration over $\theta^{(\prime)}$ and sum over m' and m'', after which one obtains the dimensionally reduced ground state

$$\Psi_0[\phi] \propto \exp\Big\{-\frac{1}{2}\sum_m \int_{\mathbb{R}^+}\mathrm{d}r\int_{\mathbb{R}^+}\mathrm{d}r'\,\sqrt{rr'}\int_{\mathbb{R}^+}\mathrm{d}\omega\,\omega^2 J_m(\omega r)J_m(\omega r')\phi_m(r)\phi_m(r')\Big\}. \tag{4.42}$$

This is the same result we obtained in section 4.1, yet with considerably less effort. Upon using the asymptotic expansion of the Bessel functions (appendix B.4), the ground state wave functional is seen to take the asymptotic form

$$\Psi_0[\phi] \sim \exp\Big\{-\frac{1}{2}\sum_m \int_{\mathbb{R}^+}\mathrm{d}r\int_{\mathbb{R}^+}\mathrm{d}r'\int_{\mathbb{R}^+}\mathrm{d}\omega\,\omega(\cos(\omega(r-r')) \\ + \cos(\omega(r+r') - \pi(m-\frac{1}{2})))\phi_m(r)\phi_m(r')\Big\}, \tag{4.43}$$

where we have used the cosine multiplication identity. Despite the phase shift, we observe that the ground state, in the asymptotic region, resembles plane-wave behaviour.

Before we continue with the second (and slightly more challenging) example, we attempt to connect the current mode expansion to the left-moving and right-moving behaviour we observed for a free scalar field on the acoustic geometry of our analogue black hole. This potential connection becomes evident when combining (B.8) and (B.9), leading to the expression

$$J_m(\omega r) = \frac{1}{2}[H_m^{(1)}(\omega r) + H_m^{(2)}(\omega r)]. \tag{4.44}$$

Note that this could also have been observed by comparing the asymptotic expansion of the Bessel function and the Hänkel functions from appendix (B). Since the asymptotic expansion of the Hänkel functions describe right-moving (first type) and left-moving (second type) waves, it might be tempting to consider a mode expansion of the form

$$\tilde{\psi}_m(r;\omega) \propto c_1 H_m^{(1)}(\omega r) + c_2 H_m^{(2)}(\omega r). \tag{4.45}$$

In other words: instead of expanding the field in terms of superpositions of Hänkel functions (the Bessel function of the first type), we explicitly expand in individual Hänkel functions, such that the field is 'decomposed' in (asymptotic) left-moving and right-moving sectors. Note that we preemptively demand $c_1 \neq c_2$, since it would otherwise reduce to the intial Bessel function. However, it can be shown that, with respect to the polar-coordinate Klein-Gordon inner product, the Hänkel functions do not form an orthogonal basis. One possible way to show this, is by writing the inner product as a Sturm-Liouville problem, after which no lower bound appears to exist for the Hänkel functions. One can also follow a more straightforward, yet slightly more tedious, route and provide a counter-proof by means of the Nicholson integral, which we will set forth to show here. For convenience we take $n = m$ and $\omega = \omega'$, such that the Klein-Gordon inner product between $\tilde{\psi}_n(\omega r)$ and $\tilde{\psi}_m(\omega' r)$ must give unity. The inner product can then be written as

$$\langle \tilde{\psi}_n, \tilde{\psi}_n \rangle = \int_0^\infty \mathrm{d}r r(c_1 H_n^{(1)}(\omega r) + c_2 H_n^{(2)}(\omega r))(c_1 H_n^{(1)}(\omega r) + c_2 H_n^{(2)}(\omega r)). \tag{4.46}$$

Let us consider one of the 'cross-terms' between a type 1 and type 2 Hänkel function. Using (B.8) and (B.9) and expanding out the brackets yields

$$c_1 c_2 \int_0^\infty \mathrm{d}r r H_n^{(1)}(\omega r) H_n^{(2)}(\omega r) = c_1 c_2 \int_0^\infty \mathrm{d}r r(J_n^2(\omega r) + Y_n^2(\omega r)). \tag{4.47}$$

We can then use Nicholson's formula (B.25), such that the integral becomes

$$c_1 c_2 \int_0^\infty \mathrm{d}r\, r(J_n^2(\omega r) + Y_n^2(\omega r)) = \frac{8 c_1 c_2}{\pi^2} \int \mathrm{d}r r \int_0^\infty \mathrm{d}\alpha K_0(2\omega r \sinh(\alpha)) \cosh(2n\alpha). \tag{4.48}$$

After changing the order of integration, this integral can be evaluated using analytical integration software, which gives

$$c_1 c_2 \int_0^\infty \mathrm{d}r\, r H_n^{(1)}(\omega r) H_n^{(2)}(\omega r) = \frac{2 c_1 c_2}{\pi^2 \omega^2} \int_0^\infty \mathrm{d}\alpha \cosh(2n\alpha) \mathrm{csch}^2(\alpha), \tag{4.49}$$

where $\mathrm{csch}(x)$ denotes the hyperbolic cosecant. The integrand is strongly divergent around $r = 0$ and does not convergence on the domain of integration $\alpha \in [0, \infty)$. We must therefore either set $c_1 = 0$ or $c_2 = 0$. Let us, without loss of generality, choose the latter. In this

particular case Eq.(4.46) reduces to

$$\langle\tilde{\psi}_n, \tilde{\psi}_n\rangle = c_1^2 \int_0^\infty \mathrm{d}r r(J_n^2(\omega r) - Y_n^2(\omega r) + 2iJ_n(\omega r)Y_n(\omega r)). \tag{4.50}$$

Since the inner product should be real, we must show that the integral over the product of Bessel functions of the first and second kind vanishes. Integrals of this particular type have known solutions for cylindrical functions, which in our case reduces to a non-zero, real solution for $n \in \mathbb{Z}$ and $\omega r \in \mathbb{R}$ (see appendix (B.26) for the evaluation). Hence, for equal order and frequency, the Klein-Gordon inner product of Eq.(4.45) shows that the orthogonality is not respected for the case when $n = m$ and $\omega = \omega'$, and as such Eq.(4.45) does not constitute as a suitable basis. Note that this counter-proof has no discernible consequences for the remainder of the thesis. It was merely an interesting excursion to explore the possibility of a left/right decomposition of our Klein-Gordon scalar field.

This second example aims at finding a Schrödinger picture description of the ground state for a scalar field in Rindler spacetime. Despite the interesting physics hidden in this deceptively simple spacetime, we stay rather close to the derivation in [51], and leave a more in-depth treatment of the physics to the reader. All we need at this point, is that the metric of a (1+1)-dimensional Rindler spacetime, which describes a coordinate system for accelerating observers, is given by

$$ds^2 = -z^2 dt^2 + dz^2, \tag{4.51}$$

where $z \in (0, \infty)$ and $t \in (-\infty, \infty)$. It takes little effort to demonstrate that the equation of motion of the Fourier decomposed field is given by

$$(\partial_z^2 + \frac{1}{z}\partial_z + \frac{\omega^2}{z^2} - m^2)\tilde{\psi}(z;\omega) = 0. \tag{4.52}$$

This equation is nothing but the Bessel differential equation in disguise, for which we obtain the eigenfunctions

$$\tilde{\psi}(z;\omega) = c_1 J_{i\omega}(-imz) + c_2 Y_{i\omega}(-imz), \tag{4.53}$$

where $c_1, c_2 \in \mathbb{C}$. Despite the fact that this expression is perfectly valid, we will follow (and elaborate on) the discussion in [51], where they obtain a more compact expression for the eigenfunctions. In appendix (B.1) we proof the following relation between Bessel functions of the first and second type, and modified Bessel functions of the second type:

$$J_\nu(z) - iY_\nu(z) = \frac{2i}{\pi} e^{\nu\pi i/2} K_\nu(iz). \tag{4.54}$$

Hence, the modes can be written in the form

$$\tilde{\psi}(z;\omega) = c_1(J_{i\omega}(-imz) - iY_{i\omega}(-imz)) = c_1\frac{2i}{\pi}e^{-\omega\pi/2}K_{i\omega}(mz), \tag{4.55}$$

where we have chosen $c_2 = -ic_1$, such that the identity Eq.(4.54) can be applied. According to [51], the completeness and orthogonality of these eigenfunctions, and hence the appropriate choice of c_1, are a result of the Kontorovich-Lebedev transform, which is discussed in appendix (B.2). Using these reciprocal relations allows us to demand

$$f(\omega) = \frac{2}{\pi^2}\int_0^\infty \mathrm{d}\omega \int_0^\infty \mathrm{d}z\frac{\omega}{z}\sinh(\pi\omega)f(\omega)K_{i\omega}(mz)K_{i\omega}(mz), \tag{4.56}$$

for an arbitrary function $f(\omega)$. We note that this relation is only satisfied if the completeness and orthogonality are respected, *i.e.* we must have

$$\frac{2}{\pi^2}\int_0^\infty \frac{\mathrm{d}z}{z}\sinh(\pi\omega)K_{i\omega}(mz)K_{i\omega'}(mz) = \delta(\omega-\omega'), \tag{4.57}$$

and similarly

$$\frac{2}{\pi^2}\int_0^\infty \mathrm{d}\omega\,\omega\sinh(\pi\omega)K_{i\omega}(mz)K_{i\omega}(mz') = z\delta(z-z') \tag{4.58}$$

This is only ensured upon choosing c_1 such that the modes can be written as

$$\tilde{\psi}(z;\omega) = 2\sqrt{\frac{\omega\sinh(\pi\omega)}{\pi}}K_{i\omega}(mz). \tag{4.59}$$

We must therefore take the coefficients to be

$$c_1 = -i\pi e^{\omega\pi/2}\sqrt{\frac{\omega\sinh(\pi\omega)}{\pi}} \quad \text{and} \quad c_2 = \pi e^{\omega\pi/2}\sqrt{\frac{\omega\sinh(\pi\omega)}{\pi}}. \tag{4.60}$$

These Fourier modes then allow us to write down the explicit kernel and ground state wave functional of a scalar field in Rindler spacetime, where the former takes the shape

$$G(z,z') = \frac{2}{zz'}\int_0^\infty \frac{\mathrm{d}\omega}{\pi^2}\omega^2\sinh(\pi\omega)K_{i\omega}(mz)K_{i\omega}(mz'), \tag{4.61}$$

and the ground state wave functional takes the (by now) familiar form

$$\Psi_0[\phi] \propto \exp\Big\{-\frac{1}{2}\int_{\mathbb{R}^+}\mathrm{d}z\int_{\mathbb{R}^+}\mathrm{d}z'\phi(z)G(z,z')\phi(z')\Big\}. \tag{4.62}$$

This relation and its massless equivalent can be used to demonstrate that the Unruh effect, where a uniformly accelerated observer in the Minkowski vacuum observes a thermal spectrum [44], can also be obtained from the Schrödinger representation of Rindler spacetime. However,

since an elaborate discussion of this effect will not aid the goal of this thesis in any way, we refer the interested reader to [29] and [38].

4.4 Acoustic black hole ground state

In this last section we aim to apply the formalism we have discussed, motivated and illustrated to the field expansion used in [48]. In other words, we consider the $m = 0$ modes which we expressed in the in-basis and out-basis (Eq.(3.52) and Eq.(3.53)), and attempt to derive an analogue black hole ground state wave functional containing these expressions. In general, the vacuum state for the in-basis and out-basis fields will be given by

$$\Psi_0[\phi(r)] = \mathcal{N}_0 \exp\{-\frac{1}{2}\int_{\mathbb{R}^+} \mathrm{d}\zeta(r)\sqrt{|g_r^{00}|}\int_{\mathbb{R}^+} \mathrm{d}\zeta(r')\sqrt{|g_{r'}^{00}|} \times \int_{\mathbb{R}^+} \mathrm{d}\mu(\omega)\,\omega\tilde{\psi}_0^{\mathrm{in/out}}(\omega;r)\tilde{\psi}_0^{\mathrm{in/out}}(\omega;r')^*\phi(r)\phi(r')\}, \quad (4.63)$$

where we have made the assumption that the angular dependence of $\phi(r,\theta)$ also vanishes upon choosing $m = 0$. We have subsequently performed the integration over the angular variables, such that the factor $(2\pi)^2$ in the measure $\mathrm{d}\mu(\omega)$ is canceled. Note that the integral Eq.(3.50), which appeared in determining the commutation relation between the phase fluctuation operators and density operators, leads us to choose the metric $\mathrm{d}\mu(\omega) = \omega\,\mathrm{d}\omega$ (modulus a factor of 2π, canceled by the angular integration). Furthermore, the spatial measure $\mathrm{d}\zeta(x) = \sqrt{|h_x|}\Theta(x)\mathrm{d}x$ contains the determinant of the induced metric. The step function $\Theta(x)$ is defined as $[r < c_0]$ for the supersonic region and $[r > c_0]$ for the subsonic region, where $[x]$ denotes the Iverson bracket. For the remainder of this discussion we restrict our focus to the subsonic region, and the step function will therefore be omitted for brevity, but must be assumed present in any wave functional containing the measure $\mathrm{d}\zeta(x)$. The Fourier modes $\tilde{\psi}_0^{\mathrm{in/out}}(\omega;r)$ are eigenfunctions of the d'Alembertian operator, satisfying

$$\hat{\Box}\tilde{\psi}_0^{\mathrm{in/out}}(\omega;r) = \omega^2 g^{00}\tilde{\psi}_0^{\mathrm{in/out}}(\omega;r), \quad (4.64)$$

which correspond to the in-basis and out-basis solutions presented in the previous chapter. Adopting the Schwarzschild-*like* geometry for the analogue black hole, one finds the determinant of the induced metric for constant timelike hypersurfaces to be $h_x = x^2 f(x)^{-1}$. We assume that the radial modes found in [48] and discussed in the previous chapter form an orthonormal and complete basis. [2] Hence, the vacuum wave functional for the in-basis can

[2] Sadly, we have not succeeded in showing this explicitly due to time constraints. It should be clear that a verification of the orthogonality and completeness must be performed before the resulting wave functional can be used in determining the entanglement entropy of the acoustic black hole.

be written as

$$\Psi_0^{\text{in}}[\phi(r)] \propto \exp\Big\{-\frac{1}{2}\mathcal{N}^2 \int_0^\infty \mathrm{d}\omega \int_0^\infty dr\, r \underbrace{\sqrt{h_{00}^r g_r^{00}}}_{=f(r)^{-1}} \int_0^\infty dr'\, r' \omega^2 \underbrace{\sqrt{h_{00}^{r'} g_{r'}^{00}}}_{=f(r')^{-1}} e^{2\pi c_0 \omega}(e^{2\pi c_0\omega} - 1) \\ \times I_{ic_0\omega}(i\omega\sqrt{r^2 - c_0^2}) I_{-ic_0\omega}(-i\omega\sqrt{r'^2 - c_0^2})\phi(r)\phi(r')\Big\}, \quad (4.65)$$

which simplifies to

$$\Psi_0^{\text{in}}[\phi(r)] \propto \exp\Big\{-\frac{1}{2}\mathcal{N}^2 \int_0^\infty \mathrm{d}\omega\, \omega^2 e^{\pi c_0\omega}(e^{2\pi c_0\omega} - 1) \int_0^\infty dr\, r f(r)^{-1} I_{ic_0\omega}(i\omega\sqrt{r^2 - c_0^2}) \\ \times \int_0^\infty dr'\, r' f(r')^{-1} I_{-ic_0\omega}(i\omega\sqrt{r'^2 - c_0^2})\phi(r)\phi(r')\Big\}, \quad (4.66)$$

where we have used identity (B.14) to change the sign in the argument of the second Bessel function. Similarly, the out-basis wave functional is given by the expression

$$\Psi^{\text{out}}[\phi(r)] \propto \exp\{-\frac{1}{2}\mathcal{N}^2 \int_0^\infty \mathrm{d}\omega\, \omega e^{\pi c_0\omega} \int_0^\infty dr\, r f(r)^{-1}[e^{2\pi c_0\omega} I_{ic_0\omega}(i\omega\sqrt{r^2 - c_0^2}) - I_{-ic_0\omega}(i\omega\sqrt{r^2 - c_0^2})] \\ \times \int_0^\infty dr'\, r' f(r')^{-1}[e^{2\pi c_0\omega} I_{-ic_0\omega}(i\omega\sqrt{r'^2 - c_0^2}) - I_{ic_0\omega}(i\omega\sqrt{r'^2 - c_0^2})]\phi(r)\phi(r')\}, \quad (4.67)$$

where for the last equality we have rewritten the modified Bessel functions in terms of positive argument and subsequently collected like powers. Next, we will consider the behaviour of the wave functional in the asymptotic region specified by $r \to \infty$. Note that in this limit we need not consider the warping factor $f(r)$ in the wave functional, as $f(r) \to 1$ in the limit of large r. We recall that the Poincaré expansion for large argument of the out-basis Fourier modes was given by

$$\begin{aligned} \tilde{\psi}_0^{\text{out}}(\omega; r) &\underset{r\to\infty}{\sim} \mathcal{N}(\omega)\sqrt{\frac{1}{\omega r}}\{e^{2\pi c_0\omega}(e^{i\omega r} + ie^{-\pi c_0\omega}e^{-i\omega r}) - (e^{i\omega r} + ie^{-\pi c_0\omega}e^{-i\omega r})\} \\ &= \mathcal{N}(\omega)\sqrt{\frac{1}{\omega r}}(e^{2\pi c_0\omega} - 1)e^{i\omega r}, \end{aligned} \quad (4.68)$$

such that the kernel contains an asymptotic term

$$\begin{aligned} \tilde{\psi}_0^{\text{out}}(\omega; r)\tilde{\psi}_0^{\text{out}}(\omega; r')^* &\underset{r\to\infty}{\sim} \mathcal{N}(\omega)^2 \frac{1}{\omega\sqrt{rr'}}(e^{2\pi c_0\omega} - 1)^2 e^{i\omega(r-r')} \\ &\propto \frac{1}{\omega\sqrt{rr'}} e^{i\omega(r-r')}. \end{aligned} \quad (4.69)$$

Substituting this relation into the wave functional and using the one-dimensional inverse Fourier transform $\phi(\omega) = \int_{\mathbb{R}^+} \frac{\mathrm{d}r}{2\pi}\phi(r)e^{i\omega r}$, together with the shift $\phi(r) \to \Phi(r) = \sqrt{r}\phi(r)$, one

observes that asymptotically

$$\Psi^{\text{out}}[\Phi] \propto \exp\{-\frac{1}{2}\int_0^\infty \mathrm{d}\omega\, \omega|\Phi(\omega)|^2\}, \tag{4.70}$$

where $\Phi(-\omega) = \Phi(\omega)^*$ to preserve reality of the field. Note that the wave functional is Minkowski-like, with frequency ω. Similarly, we considered the asymptotic expansion of the in-basis Fourier modes, which were given by

$$\tilde{\psi}_0^{\text{in}}(\omega; r) \underset{r\to\infty}{\sim} \mathcal{N}(\omega)\sqrt{\frac{1}{\omega r}}e^{\pi c_0\omega}\sqrt{e^{2\pi c_0\omega}-1}(e^{i\omega r} + ie^{-\pi c_0\omega}e^{-i\omega r}). \tag{4.71}$$

We recall that the quantum description of the phase fluctuations is only valid in the hydrodynamic regime, and therefore $c_0\omega \ll 1$ [48]. Hence, we may safely assume that the moduli adhere to $|e^{\pi c_0\omega}\mathcal{N}| > |\mathcal{N}|$, which allows us to approximately neglect the second term in the in-basis asymptotic expansion. This argument is strengthened even further if the frequency is allowed to be large, which is seen instantly. As a result, the product of the Fourier modes in the kernel may be written as

$$\begin{aligned}\tilde{\psi}_0^{\text{in}}(\omega; r)\tilde{\psi}_0^{\text{in}}(\omega; r')^* &\underset{r\to\infty}{\sim} \mathcal{N}(\omega)^2\frac{1}{\omega\sqrt{rr'}}e^{2\pi c_0\omega}(e^{2\pi c_0\omega}-1)e^{i\omega(r-r')} \\ &\propto \frac{1}{\omega\sqrt{rr'}}(1-e^{-2\pi c_0\omega})^{-1}e^{i\omega(r-r')},\end{aligned} \tag{4.72}$$

where we recognize the Bogoliubov coefficient $|u_0|^2 = 1/(1-e^{-2\pi c_0\omega})$. Substituting these into the wave functional and using the same arguments as above, one finds

$$\Psi^{\text{in}}(\Phi) \propto \exp\{-\frac{1}{2}\int_0^\infty \mathrm{d}\omega\, \omega(1-e^{-2\pi c_0\omega})^{-1}|\Phi(\omega)|^2\}. \tag{4.73}$$

As for the out-basis functional, we observe a Minkowksi-like behaviour in the asymptotic region with frequency $\omega|u_0|^2$.

We have managed to show that, asymptotically, the ground state wave functional of the acoustic black hole shows Minkowski-like behaviour, as required for a scalar field on a Schwarzschild spacetime. However, an important last test would be to demonstrate the existence of acoustic Hawking radiation using the expressions Eq.(4.66) and Eq.(4.67). We recall from Eq.(4.32) that the expectation value of the $(0,0)$-component of the energy-momentum tensor is given by

$$\langle 0|T_{00}(\mathbf{x},\mathbf{y};t)|0\rangle = -\frac{g^{00}}{4}\{G(\mathbf{x},\mathbf{y};t) + g^{ij}\frac{\partial^2}{\partial x^i\partial y^j}\Delta(\mathbf{x},\mathbf{y};t)\}, \tag{4.74}$$

For the Schwarzschild-*like* geometry, this simplifies to

$$\langle 0|T_{00}(\mathbf{x},\mathbf{y};t)|0\rangle = \frac{1}{4}f(r)^{-1}\{G(r,r') + f(r)\frac{\partial^2}{\partial r\partial r'}\Delta(r,r')\}. \tag{4.75}$$

Since $f(r) \to 1$ when $r \to \infty$, the expectation value may be determined rather easily by substituting our kernels and the inverse kernels into the expression. We recall from the 'Minkowski test' that

$$\text{(In-vacuum)} \begin{cases} G(r,r') \underset{r\to\infty}{\sim} \int_0^\infty \frac{\mathrm{d}\omega}{2\pi}\, \omega |u_0|^2 e^{i\omega(r-r')} \\ \Delta(r,r') \underset{r\to\infty}{\sim} \int_0^\infty \frac{\mathrm{d}\omega}{2\pi}\, \frac{1}{\omega} |u_0|^2 e^{i\omega(r-r')} \end{cases}$$

for the in-basis vacuum, whereas for the out-basis vacuum we obtained

$$\text{(Out-vacuum)} \begin{cases} G(r,r') \underset{r\to\infty}{\sim} \int_0^\infty \frac{\mathrm{d}\omega}{2\pi}\, \omega e^{i\omega(r-r')} \\ \Delta(r,r') \underset{r\to\infty}{\sim} \int_0^\infty \frac{\mathrm{d}\omega}{2\pi}\, \frac{1}{\omega} e^{i\omega(r-r')}. \end{cases}$$

Since the energy-density is defined as [50, 51]

$$\langle 0|T_{00}(r)|0\rangle = \lim_{r\to r'} \langle 0|T_{00}(r,r')|0\rangle\,, \tag{4.76}$$

we are at last able to write the difference between the energy-density of the two vacua as

$$\begin{aligned} \langle 0|T_{00}(r)|0\rangle_{\text{in}} - \langle 0|T_{00}(r)|0\rangle_{\text{out}} &= \frac{1}{2}\int_0^\infty \frac{\mathrm{d}\omega}{2\pi}\, \omega(|u_0|^2 - 1) \\ &= \frac{1}{2}\int_0^\infty \frac{\mathrm{d}\omega}{2\pi}\, \omega |v_0|^2 = \frac{1}{2}\int_0^\infty \frac{\mathrm{d}\omega}{2\pi} \frac{\omega}{(e^{2\pi c_0 \omega} - 1)}. \end{aligned} \tag{4.77}$$

Thus, an in-mode phonon observers the out-mode phonons to be thermalized in accordance with the Hawking spectrum. This expression is line with our expectation from Ch.3. However, we have not yet reduced this expression to Eq.(3.88), which describes the total number of emitted particles from the acoustic horizon. This might serve as an interesting additional verification of the obtained ground state wave functional. After the orthogonality and completeness of the in-basis and out-basis Fourier modes have been properly studied and confirmed, one can discretize the kernel from Eq.(4.66) in line with the formalism sketched in the next two chapters to obtain a numerical estimate for the entanglement entropy of the acoustic black hole.

Chapter 5

Full-lattice dependent entanglement entropy

"If people do not believe that mathematics is simple, it is only because they do not realize how complicated life is."
John von Neumann

5.1 Entanglement entropy and harmonic oscillators

The previous chapter presented the theory necessary for writing down vacuum wave functionals for scalar fields on curved backgrounds. Yet the question remains how the associated kernels can ultimately be used to (numerically) determine the entanglement entropy of subregions of these spacetimes. The aim of this chapter is to introduce the ideas, formalism and algorithm proposed in [69], which together with [11] count as some of the earliest attempts to calculate the entanglement entropy. Collectively, this approach is known as the real-time formalism of entanglement entropy, and provides the basis for our approach. The general idea behind this formalism, which we will elaborate on later in this chapter, hides in breaking down, or discretizing, the degrees of freedom of a massless scalar field theory on a finite (or countably infinite) lattice of spherical shells [45] (or 1-spheres for a (2+1)-dimensional theory). In practice, this entails representing the scalar field by a finite/countably infinite one-dimensional lattice of harmonic oscillators, where the coupling constants are chosen such that, in the continuum limit, the system retrieves the original field theory. After a general description of the formalism and its distillation to an algorithm (in the most abstract terms), we will subject it to various flat-spacetime examples, and discuss its connection with the aforementioned kernels.

5.1.1 Properties of the harmonic oscillator

As the remainder of this chapter will lean heavily on the 'deconstruction' of scalar fields into lattices of harmonic oscillators, we will commence our discussion with a concise review of the main properties of a single harmonic oscillator. Since the reader is expected to have encountered these concepts a plethora of times, we will confine ourselves to a set of brief statements, and further information can be found in any respectable book on introductory quantum mechanics, see *e.g.* [65, 47, 34]. In the remainder of this section we take $\hbar = 1$ and consider ω to be (angular) frequency of the oscillator, unless explicitly stated otherwise. The Hamiltonian for the (single) harmonic oscillator is given by

$$H = \frac{\hat{p}^2}{2m} + \frac{1}{2}m\omega^2\hat{x}^2, \tag{5.1}$$

where m denotes the mass of the oscillator. Solving the time-independent Schrödinger equation $H\,|\psi_n\rangle = E_n\,|\psi_n\rangle$ via the reader's favourite method, allows one to obtain the eigenstates and the eigenenergies of the single harmonic oscillator. The wave function of the linear oscillator is obtained by writing the eigenstates in the positional basis, leading to the well-known expression [47, 34]

$$\psi_n(x) = (\frac{m\omega}{\pi})^{1/4}\frac{1}{\sqrt{2^n n!}}e^{-\frac{m\omega}{2}x^2}H_n(\sqrt{m\omega}x), \tag{5.2}$$

with $H_n(x) \equiv \mathrm{Herm}_n(x)$ denoting the physicist's Hermite polynomials [4]

$$H_n(x) = (-1)^n e^{x^2}\frac{d^n}{dx^n}e^{-x^2}. \tag{5.3}$$

For the ground state, *i.e.* $n = 0$, the Hermite polynomial reduces to unity, such that the ground state wave function is given by the simple Gaussian distribution

$$\psi_0(x) = (\frac{m\omega}{\pi})^{1/4}e^{-\frac{m\omega}{2}x^2}. \tag{5.4}$$

Note that the prefactor has been chosen such that wave function is properly normalized. Similarly, the Hermite polynomials with $n \geq 1$ enter when expressing the wave function for excited states, the first of which will reappear later in this chapter. In a sense, Eq.(5.2) and Eq.(5.4) capture all the prerequisites one needs to grasp the derivations presented in [69], and we will refer to Eq.(5.2) on a frequent basis.

5.2 A simple system: two coupled harmonic oscillators

The next section's final aim is to determine the reduced density matrix of a chain of arbitrarily many harmonic oscillators, and its eigenvalues. Finding the reduced density matrix for a

mere two coupled oscillators is, as we shall later observe, more than just an easy 'toy model'. It turns out, as we shall proof soon, that the reduced density matrix of N oscillators is nothing but the tensor product of the reduced density matrices for pairs of oscillators, thereby reducing the entire problem to the results discussed below. There are many excellent reviews on this topic, and we have been greatly inspired by [58, 24].

Consider a system of two harmonic oscillators centered at x_A and x_B, respectively, both experiencing an identical self-coupling k_0 and quadratically coupled with coupling constant k_1. The Hamiltonian in position space is given by

$$H = \frac{1}{2}[p_A^2 + p_B^2 + k_0(x_A^2 + x_B^2) + k_1(x_A - x_B)^2]. \tag{5.5}$$

Note that in order to determine the ground state wave function of the system, it is convenient to first decouple the oscillators, find the wave function in these new coordinates, and then transform back to the initial coordinates. Specifically, we define

$$x_\pm = \frac{1}{\sqrt{2}}(x_A \pm x_B), \tag{5.6}$$

such that the Hamiltonian describing the uncoupled oscillators, centered at x_+ and x_-, is given by

$$H = \frac{1}{2}[p_+^2 + p_-^2 + k_0 x_+^2 + (k_0 + 2k_1)x_-^2]. \tag{5.7}$$

From the Hamiltonian we infer that the joint wave function of the uncoupled oscillators is separable, *i.e.* $\psi(x_+, x_-) = \psi(x_+)\psi(x_-)$, such that determining the aforementioned boils down to solving the two Schrödinger equations

$$\begin{cases} \frac{1}{2}(p_+^2 + \omega_+^2 x_+^2)\psi(x_+) = E_+\psi(x_+) \\ \frac{1}{2}(p_-^2 + \omega_-^2 x_-^2)\psi(x_-) = E_-\psi(x_-) \end{cases} \tag{5.8}$$

where we have defined the frequencies $\omega_+ = {k_0}^{1/2}$ and $\omega_- = (k_0 + 2k_1)^{1/2}$, and $E = E_+ + E_-$. In light of Eq.(5.2), we find that the joint ground state for the uncoupled oscillators is

$$\psi(x_+, x_-) = \frac{(\omega_+\omega_-)^{1/4}}{\sqrt{\pi}} e^{-\frac{1}{2}(\omega_+ x_+^2 + \omega_- x_-^2)}. \tag{5.9}$$

As explained before, for the sake of further analysis we rewrite the joint ground state in terms of the initial variables Eq.(5.6), such that

$$\psi(x_A, x_B) = \frac{(\omega_+\omega_-)^{1/4}}{\sqrt{\pi}} e^{-\frac{1}{4}((\omega_+ + \omega_-)(x_A^2 + x_B^2) + 2(\omega_+ - \omega_-)x_A x_B)}. \tag{5.10}$$

Next, recall from Ch.2 that the reduced density matrix for the second oscillator (or: region B) is given by

$$\rho_B(x_B, x'_B) = \langle x'_B| \operatorname{Tr}_{\mathrm{A}}(\rho) |x_B\rangle , \tag{5.11}$$

where in the position basis the density matrix in terms of the ground state wave functions is

$$\rho(x_A, x'_A, x_B, x'_B) = \psi_0(x_A, x_B)\psi_0^*(x'_A, x'_B). \tag{5.12}$$

Hence, the reduced density matrix of region B can be shown to reduce to

$$\begin{aligned}\rho_B(x_B, x'_B) &= \int_{-\infty}^{\infty} \mathrm{d}x_A \psi_0(x_A, x_B)\psi_0(x'_B, x_A) \\ &= \frac{\sqrt{\omega_+\omega_-}}{\pi} \int_{-\infty}^{\infty} \mathrm{d}x_A e^{-\frac{1}{4}((\omega_+ + \omega_-)(2x_A^2 + x_B^2 + x'^2_B) + 2(\omega_+ - \omega_-)(x_B + x'_B)x_A)}.\end{aligned} \tag{5.13}$$

Completing the square of the exponential of Eq.(5.13) allows us to write

$$\begin{aligned}\rho_B(x_B, x'_B) = \frac{\sqrt{\omega_+\omega_-}}{\pi} e^{-\frac{\omega_+ + \omega_-}{4}(x_B^2 + x'^2_B) + \frac{(\omega_+ - \omega_-)^2}{8(\omega_+ + \omega_-)}(x_B + x'_B)^2} \\ \times \int_{-\infty}^{\infty} \mathrm{d}x_A e^{-\frac{(\omega_+ + \omega_-)}{2}(x_A + \frac{\omega_+ - \omega_-}{2(\omega_+ + \omega_-)} x_B)^2},\end{aligned} \tag{5.14}$$

after which we observe that the integrand is simply a shifted Gaussian distribution, and can therefore be performed after defining

$$x_A \to \tilde{x_A} = x_A - \frac{\omega_+ - \omega_-}{2(\omega_+ + \omega_-)}. \tag{5.15}$$

Since the transformation carries a unity Jacobian, the integral amounts to a standard Gaussian integral, which evaluates to

$$\rho_B(x_B, x'_B) = \sqrt{\frac{2\omega_+\omega_-}{\pi(\omega_+ - \omega_-)}} e^{-\frac{\omega_+ + \omega_-}{4}(x_B^2 + x'^2_B) + \frac{(\omega_+ - \omega_-)^2}{8(\omega_+ + \omega_-)}(x_B + x'_B)^2}. \tag{5.16}$$

Since we have integrated out the x_A-dependence and there is only a single oscillator left, we will from now on denote $x_B = x$ for convenience. The expression simplifies considerably by introducing the constants

$$\begin{cases} \beta = \frac{(\omega_+ - \omega_-)^2}{4(\omega_+ + \omega_-)} \\ \gamma + \beta = \frac{\omega_+ + \omega_-}{2}, \end{cases} \tag{5.17}$$

where the latter is equivalent to writing $\gamma = \omega_+\omega_-/4(\omega_+ + \omega_-)$. Hence, we at last obtain a simple, intuitive form for the reduced density matrix of the outer oscillator:

$$\rho_B(x, x') = \sqrt{\frac{\gamma - \beta}{\pi}} \exp\left(-\frac{1}{2}\gamma(x^2 + x'^2) + \beta x x'\right). \tag{5.18}$$

In order to determine the entanglement entropy by means of Eq.(2.6), we must obtain the spectrum of the matrix ρ_B. First, we aim to derive the eigenvalue equation stated in [69]. Then, contrary to Srednicki's approach, we will determine the eigenvalues and eigenfunctions explicitly, instead of merely using an *Ansatz*. Consider the eigenvalue equation $\hat{\rho}_B \left|f_n\right\rangle = p_n \left|f_n\right\rangle$. This can rather easily be rewritten into the form of [69] by simply contracting with $\langle x|$ and inserting unity:

$$\begin{aligned} \langle x| \hat{\rho}_B \left|f_n\right\rangle = \langle x| \hat{\rho}_B \underbrace{\left(\int_{-\infty}^{\infty} \mathrm{d}x' \left|x'\right\rangle \langle x'|\right)}_{=\mathbb{1}} \left|f_n\right\rangle = \langle x| p_n \left|f_n\right\rangle \\ \hat{\rho}_B \left|f_n\right\rangle = p_n \left|f_n\right\rangle \quad \Rightarrow \quad \int_{-\infty}^{\infty} \mathrm{d}x' \rho_B(x,x') f_n(x') = p_n f_n(x) \end{aligned} \tag{5.19}$$

where the last equality follows directly by noting that p_n is a scalar. In [69] the authors consider an *Ansatz* for the eigenfunctions and eigenvalues, the latter claimed to be $p_n = (1-\zeta)\zeta^n$, with ζ a particular constant, without explicit proof of this relation. We accept this invitation and will explicitly derive a form of ρ_B which allows us to evaluate Eq.(5.19). Our derivation begins by noting that the exponential in the reduced density matrix can be expanded in terms of a product of Hermite poynomials, as we will demonstrate shortly, by means of Mehler's formula [65, 27]:

$$\sum_{n=0}^{\infty} \frac{\zeta^n}{2^n n!} H_n(x) H_n(x') e^{-\frac{1}{2}(x^2+x'^2)} = \frac{1}{\sqrt{1-\zeta^2}} \exp\{-\frac{(1+\zeta^2)(x^2+x'^2) - 4\zeta x x'}{2(1-\zeta^2)}\}. \tag{5.20}$$

Upon comparing Eq.(5.20) with the reduced density matrix Eq.(5.18), we observe that the expansion requires enforcing the relations

$$\frac{(1+\zeta^2)}{(1-\zeta^2)}(\tilde{x}^2 + \tilde{x}'^2) \stackrel{!}{=} \gamma(x^2 + x'^2) \quad \text{and} \quad \frac{2\zeta}{(1-\zeta^2)} \tilde{x}\tilde{x}' \stackrel{!}{=} \beta x x', \tag{5.21}$$

which are only satisfied when $\tilde{x} = \alpha^{1/2} x$ and $\tilde{x'} = \alpha^{1/2} x'_2$. Furthermore, we are led to identify

$$\zeta = \frac{\beta}{\gamma + \alpha} \quad \text{and} \quad \alpha = \sqrt{\gamma^2 - \beta^2}. \tag{5.22}$$

Substituting these constants into Mehler's formula allows the reduced density matrix to be written as

$$\rho_B(x,x') = (1-\zeta) \sum_{n=0}^{\infty} \frac{\alpha^{1/2} \zeta^n}{\pi 2^n n!} H_n(\alpha^{1/2} x) H_n(\alpha^{1/2} x') e^{-\frac{\alpha}{2}(x^2+x'^2)}. \tag{5.23}$$

Using the expression Eq.(5.2), the reduced density matrix for the outer oscillator can be rewritten as

$$\rho_B(x,x') = \sqrt{\frac{\alpha}{\pi}}(1-\zeta)\sum_{n=0}^{\infty}\zeta^n\psi_n(\alpha^{1/2}x)\psi_n(\alpha^{1/2}x'), \tag{5.24}$$

with $\alpha = \omega_+\omega_-$ as the effective eigenfrequency of the oscillators. The eigenvalue equation can be efficiently solved by exploiting the orthogonality relation for Hermite polynomials [4]

$$\int_{-\infty}^{\infty}\mathrm{d}x e^{-x^2}H_n(x)H_m(x) = \sqrt{\pi}2^n n!\delta_{n,m}. \tag{5.25}$$

Inserting Eq.(5.23) in Eq.(5.19), allows the eigenvalue problem to be written as

$$\sqrt{\frac{\alpha}{\pi}}(1-\zeta)\sum_{r=0}^{\infty}\frac{\zeta^r}{2^r r!}e^{-\frac{\alpha}{2}x^2}\int_{\infty}^{\infty}\mathrm{d}x' e^{-\alpha x'^2}H_r(\alpha^{1/2}x)H_r(\alpha^{1/2}x')f_n(x') = p_n f_n(x), \tag{5.26}$$

where $r,n \in \mathbb{Z}^+$. We consider an *Ansatz* for f_n which allows us to exploit the orthogonality, which in this particular case is chosen in line with [69]:

$$f_n(x) = H_n(\alpha^{1/2}x)e^{-\frac{\alpha}{2}x^2}. \tag{5.27}$$

Substitution of this equation in Eq.(5.26) yields the relation

$$\begin{aligned}\sqrt{\frac{\alpha}{\pi}}(1-\zeta)\sum_{r=0}^{\infty}\frac{\zeta^r}{2^r r!}e^{-\frac{\alpha}{2}x^2}H_r(\alpha^{1/2}x)\int_{-\infty}^{\infty}\mathrm{d}x' e^{-\alpha x'^2}H_r(\alpha^{1/2}x')H_n(\alpha^{1/2}x')& \\ = (1-\zeta)\sum_{r=0}^{\infty}\zeta^r e^{-\frac{\alpha}{2}x^2}H_r(\alpha^{1/2}x)\delta_{r,n} = (1-\zeta)\zeta^n f_n(x),&\end{aligned} \tag{5.28}$$

where from the first to the second line we have used the orthogonality relation Eq.(5.25) and for the last equality we have simply summed over all r. The eigenvalues can therefore be identified as

$$p_n = (1-\zeta)\zeta^n, \tag{5.29}$$

with ζ defined as in Eq.(5.22). From the normalization of ρ_B, Eq.(5.19) infers that $0 < p_n < 1$ and equivalently $0 < \zeta < 1$. The von Neumann entropy for this system can now be determined by means of Eq.(2.6), which can be rewritten in terms of the eigenvalues of the reduced density matrix, *i.e.* we recall that $S_A = S_B$ and hence

$$S_A = -\mathrm{Tr}(\rho_B\log\rho_B) = -\sum_{n=0}^{\infty}p_n\log p_n. \tag{5.30}$$

The entanglement entropy in its current form cannot be efficiently computed due to the infinite sum over n. However, the expression can be shown to simplify considerably upon

inserting the eigenvalues Eq.(5.29), giving

$$\begin{aligned} S_A &= -(1-\zeta)\sum_{n=0}^{\infty}\zeta^n \log((1-\zeta)\zeta^n) \\ &= -(1-\zeta)\log(1-\zeta)\sum_{n=0}^{\infty}\zeta^n - (1-\zeta)\log(\zeta)\sum_{n=0}^{\infty} n\zeta^n. \end{aligned} \tag{5.31}$$

We recall that the geometric series and the simplest form of the arithmetico-geometric sequence are given by [4]

$$\begin{cases} \sum_{n\geq 0} r^n = \frac{1}{1-r} & \text{if} \quad |r|<1 \\ \sum_{n\geq 1} nr^n = \frac{r}{(1-r)^2} & \text{if} \quad |r|<1 \end{cases}, \tag{5.32}$$

where for the latter we note that one may extend the index to zero. Applying these relations to Eq.(5.31) allows the von Neumann entropy for region A to be rewritten in the more convenient shape

$$S_A = -\log(1-\zeta) - \frac{1}{1-\zeta}\log\zeta. \tag{5.33}$$

Hence, all one needs to determine the entanglement entropy of the individual oscillators, are the values of ζ, or indirectly the values of α, β and γ, which are obtained from the reduced density matrix. Since Eq.(5.18) can be determined exactly and only depends on the choice of k_0 and k_1, one could in principle perform this computation without any difficulties. In the next section we will expand our system to contain N coupled harmonic oscillators. The aim is to reproduce the derivation performed above, albeit in a slightly more abstract manner, and to arrive at an expression for the von Neumann entropy for a finite region of a chain of arbitrary length similar to Eq.(5.33).

5.3 Extension to larger lattices

We extend our simple system of two coupled harmonic oscillators to a lattice of size $N \in \mathbb{N} \cap (2,\infty)$, where each site contains an harmonic oscillator. As shown in fig.(5.1), we divide the chain of oscillators into two finite regions: region A of n_b lattice sites, and region B of $N-n_b$ sites. We will interchangeably refer to these regions as 'inner' and 'outer', respectively. The addition of a constant $\epsilon \in (0,1)$ to the boundary point will be explained in a later section, yet is shown nonetheless to illustrate that the entangling boundary of the subsystems can be shifted to non-integer values. The lattice spacing a acts as a UV-regulator, whereas the finite lattice size IR-regulates the system (we effectively place it in a 'box' of length $N+1$). Our discussion is similar to the previous case, since we aim to derive a reduced density matrix for the outer region, then find its eigenvalues, and finally compute the entanglement entropy of the inner region.

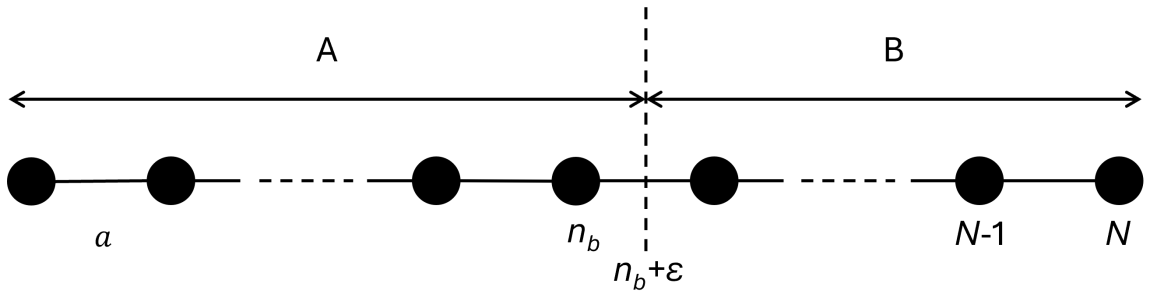

Fig. 5.1 A chain of N harmonic oscillators divided into two subsystems A and B. The boundary point of subsystem A is denoted by n_b.

5.3.1 Ground state

We start our derivation by defining the vector $\mathbf{x} = (\mathbf{x}_A, \mathbf{x}_B)^T$, where $\mathbf{x}_A$ is an n_b-dimensional vector containing the lattice sites of the inner region, and $\mathbf{x}_B$ an $(N - n_b)$-dimensional vector describing the coordinates of the B-region oscillators. The joint ground state of these N oscillators can be specified by assuming that we have performed some transformation to uncouple the oscillators, and then transform them back to their original coordinates:

$$\Psi_0(\mathbf{x}, \mathbf{x}') = (\frac{\det(\Omega)}{\pi^N})^{1/4} \exp\{-\frac{1}{2}\mathbf{x}^T\Omega\mathbf{x}\}. \tag{5.34}$$

Note that the matrix Ω contains entries which are remnants from undoing the decoupling transformation, as well as the original coupling terms. The kernel can be partitioned into 4 submatrices, such that

$$\Omega = \begin{pmatrix} A & B \\ B^T & C \end{pmatrix} \tag{5.35}$$

where submatrix A is of size $n_b \times n_b$, B is a $n_b \times (N - n_b)$ matrix and C is $(N - n_b) \times (N - n_b)$. Multiplying out the vectors and Ω gives an expression we recognize from the previous discussion:

$$\Psi_0(\mathbf{x}, \mathbf{x}') = (\frac{\det(\Omega)}{\pi^N})^{1/4} \exp\{-\frac{1}{2}(\mathbf{x}_A^T A\mathbf{x}_A + \mathbf{x}_A^T B\mathbf{x}_B + \mathbf{x}_B^T B^T\mathbf{x}_A + \mathbf{x}_B^T C\mathbf{x}_B)\} \tag{5.36}$$

The reduced density matrix is found in a similar fashion as before, where we use Eq.(5.36) to construct the density matrix and integrate out the coordinates in the inner region:

$$\rho_B(\mathbf{x}_B, \mathbf{x}_B') = \int_{-\infty}^{\infty} \mathrm{d}\mathbf{x}_A \Psi_0^*(\mathbf{x}_A, \mathbf{x}_B)\Psi_0(\mathbf{x}_A, \mathbf{x}_B'), \tag{5.37}$$

where $\mathrm{d}\mathbf{x}_A = \prod_{i=1}^{n_b} \mathrm{d}x_i$ is a measure over the internal oscillators. Inserting Eq.(5.36) is then trivially seen to give

$$\begin{aligned}\rho_B(\mathbf{x}_B, \mathbf{x}'_B) = (\frac{\det(\Omega)}{\pi^N})^{1/2} \exp\{-\frac{1}{2}(\mathbf{x}_B^T C \mathbf{x}_B + \mathbf{x}_B'^T C \mathbf{x}'_B\} \\ \times \int_{-\infty}^{\infty} \mathrm{d}\mathbf{x}_A \exp\{-\frac{1}{2}(2\mathbf{x}_A^T A \mathbf{x}_A + 2\mathbf{x}_A^T B(\mathbf{x}_B + \mathbf{x}'_B))\}\end{aligned} \tag{5.38}$$

We can evaluate this integral by completing the square. First, we define a matrix

$$Q = A^{-1} B(\mathbf{x}_B + \mathbf{x}'_B), \tag{5.39}$$

such that the second exponential contains

$$\mathbf{x}_A^T A \mathbf{x}_A + \mathbf{x}_A^T A Q = (\mathbf{x}_A^T + \frac{1}{2} Q^T) A (\mathbf{x}_A + \frac{1}{2} Q) - \frac{1}{4} Q^T A Q. \tag{5.40}$$

The reduced density matrix is therefore seen to become

$$\begin{aligned}\rho_B(\mathbf{x}_B, \mathbf{x}'_B) = (\frac{\det(\Omega)}{\pi^N})^{1/2} \exp\{-\frac{1}{2}(\mathbf{x}_B^T C \mathbf{x}_B + \mathbf{x}_B'^T C \mathbf{x}'_B\} \exp\{\frac{1}{4} Q^T A Q\} \\ \times \int_{-\infty}^{\infty} \mathrm{d}\mathbf{x}_A \exp\{-(\mathbf{x}_A^T + \frac{1}{2} Q^T) A (\mathbf{x}_A + \frac{1}{2} Q)\}\end{aligned} \tag{5.41}$$

As before, we shift the coordinates to a uniform multivariate Gaussian distribution:

$$\mathbf{x}_A \to \tilde{\mathbf{x}}_A = \mathbf{x}_A - \frac{1}{2} Q, \tag{5.42}$$

after which the integral is seen to give

$$\exp\{\frac{1}{4} Q^T A Q\} \int_{-\infty}^{\infty} \mathrm{d}\mathbf{x}_A \exp\{-\tilde{\mathbf{x}}_A^T A \tilde{\mathbf{x}}_A\} = (\frac{\pi^{n_b}}{\det(A)})^{1/2} \exp\{\frac{1}{4} Q^T A Q\}. \tag{5.43}$$

The reduced density matrix then takes a form similar to Eq.(5.16), leading to

$$\rho_B(\mathbf{x}_B, \mathbf{x}'_B) = \pi^{(n-N)/2} (\frac{\det(\Omega)}{\det(A)})^{1/2} \exp\{-\frac{1}{2}(\mathbf{x}_B^T C \mathbf{x}_B + \mathbf{x}_B'^T C \mathbf{x}'_B) + \frac{1}{4} Q^T A Q\}. \tag{5.44}$$

Before, we defined the constants β and γ. This time around, we opt for matrices instead, and define

$$\begin{cases} \beta = \frac{1}{2} B^T A^{-1} B \\ \gamma = C - \beta \end{cases}. \tag{5.45}$$

We will later see that, as with the constants in the dual oscillator system, finding these matrices will play a crucial role in evaluating the von Neumann entropy. For completeness, note that both β and γ are $(N - n_b) \times (N - n_b)$ matrices. As before, we drop the subscript

of $\mathbf{x}_B$, since it is apparent that these belong to the outer region. The reduced density matrix then becomes

$$\rho_B(\mathbf{x},\mathbf{x}') = \pi^{(n-N)/2}(\frac{\det(\Omega)}{\det(A)})^{1/2}\exp\{-\frac{1}{2}(\mathbf{x}^T\gamma\mathbf{x}+\mathbf{x}'^T\gamma\mathbf{x}')+\mathbf{x}^T\beta\mathbf{x}'\}. \tag{5.46}$$

Note that we are not yet in a position to (easily) find the eigenvalues of the reduced density matrix, since it is non-diagonal. We remedy this by first diagonalizing $\gamma = V^T\gamma_D V$, and through defining a vector $\mathbf{y}$ such that $\mathbf{x} = V^T\gamma_D^{-1/2}\mathbf{y}$. Eq.(5.46) then takes the simplified form

$$\rho_B(\mathbf{y},\mathbf{y}') = \pi^{(n-N)/2}\left(\frac{\det(\Omega)}{\det(A)}\right)^{1/2}\exp\{-\frac{1}{2}(\mathbf{y}^T\gamma_D^{-1/2}\underbrace{VV^T}_{=\mathbb{1}}\gamma_D\underbrace{VV^T}_{=\mathbb{1}}\gamma_D^{-1/2}\mathbf{y}+\mathbf{y}'^T\mathbf{y}') + \mathbf{y}^T\gamma_D^{-1/2}V\beta V^T\gamma_D^{-1/2}\mathbf{y}'\}. \tag{5.47}$$

We have only written out the matrix structure of the first term to give an impression of what the cancellations look like. It can instantly be seen that the same holds for the second term. We require a few more auxiliary matrices before the reduced density matrix is diagonal. We define the matrix

$$\beta' = \gamma_D^{-1/2}V\beta V^T\gamma_D^{-1/2}, \tag{5.48}$$

which is of the shape $(N-n_b)\times(N-n_b)$. Subsequently, we diagonalize $\beta' = W^T\beta'_D W$, and use the orthogonal matrix W to define a new variable $\mathbf{z}$, such that $\mathbf{y} = W\mathbf{z}$. At last, we are able to write

$$\rho_B(\mathbf{z},\mathbf{z}') = \pi^{(n-N)/2}(\frac{\det(\Omega)}{\det(A)})^{1/2}\exp\{-\frac{1}{2}(\mathbf{z}^T\mathbf{z}+\mathbf{z}'^T\mathbf{z}')+\mathbf{z}^T\beta'_D\mathbf{z}'\}. \tag{5.49}$$

Since all involved matrices are now diagonal, we note that this is equivalent to replacing these by their eigenvalues, and instead write

$$\rho_B(\mathbf{z},\mathbf{z}') = \pi^{(n-N)/2}(\frac{\det(\Omega)}{\det(A)})^{1/2}\prod_{i=n_b+1}^{N}\exp\{-\frac{1}{2}(z_i^2+z'^2_i)+\beta'_i z_i z'_i\}, \tag{5.50}$$

with β'_i the eigenvalues of β'. The tensor product above shows that, as previously mentioned, the reduced density matrix for a chain of harmonic oscillators with $N>2$ reduced to a product of reduced density matrices for pairs of oscillators in the region $(N-n_b)$, in the spirit of Eq.(5.46). The only discernible difference hides in the identification $\gamma\to 1$ and $\beta\to\beta'_i$. The eigenvalue equation we solved in the previous chapter can, given Eq.(5.50), be seen to reduce to the by now trivial problem

$$\int_{-\infty}^{\infty}\mathrm{d}x_i\rho_B(x_i,x'_i)f_n(x'_i) = p_n f_n(x_i), \tag{5.51}$$

for each $i \in \{n_b + 1, ..., N\}$. The solution to this equation is the same as before (Eq.(5.29)), provided we take into account the aforementioned new identifications for γ and β, leading to

$$p_n = (1 - \frac{\beta_i'}{1 - (1 - \beta_i'^2)^{1/2}})(\underbrace{\frac{\beta_i'}{1 - (1 - \beta_i'^2)^{1/2}}}_{=\zeta_i})^n. \tag{5.52}$$

Inserting these eigenvalues in Eq.(5.31) leads to the von Neumann entropy for the inner region:

$$S_A = \sum_{i=n_b+1}^{N} S_i, \tag{5.53}$$

where S_i is given by the expression from before per $i \in \{n_b + 1, ..., N\}$, namely

$$S_i = -\log(1 - \zeta_i) - \frac{1}{1 - \zeta_i} \log \zeta_i. \tag{5.54}$$

As before, we observe that the expression above only requires the values for ζ_i, or indirectly $\beta_i{}'$ through Eq.(5.52). This, in turn, is fully fixed by the matrix Ω and the submatrices depending on the 'boundary lattice point' n_b. The covariance matrix Ω can in principle be obtained in various different ways, yet we will highlight the two most convenient ones. A vast majority of the literature uses a 'discrete Hamiltonian' to obtain the joint wave function, which can easily be illustrated in the following way. Consider a Hamiltonian of the general form

$$H = \frac{1}{2} \sum_{i,j=1}^{N} [p_i p_j \delta_{ij} + x_i K_{ij} x_j], \tag{5.55}$$

where we choose the elements of K such that the Hamiltonian reproduces a specific scalar field theory in the limit of zero lattice spacing (examples will follow soon). Upon diagonalizing the matrix $K = O^T K_D O$ and taking $\mathbf{y} = O\mathbf{x}$, one can show that the joint ground state is given by

$$\Psi_0(\mathbf{y}) \propto \exp\{-\frac{1}{2}\mathbf{y}^T K_D^{1/2} \mathbf{y}\}. \tag{5.56}$$

We define the covariance matrix as $\Omega = O^T K_D^{1/2} O$, after which we obtain

$$\Psi_0(\mathbf{x}) \propto \exp\{-\frac{1}{2}\mathbf{x}^T \Omega \mathbf{x}\}. \tag{5.57}$$

At this point it only remains to normalize the wave function, after which we return to our original expression Eq.(5.34). Clearly, since 'all' we need to determine the von Neumann entropy is the matrix $\Omega = K^{1/2}$, the problem reduces to choosing a proper discretization scheme and finding K. The idea behind the second approach, which is centered around the kernel of a continuum-spacetime vacuum wave functional, should be apparent at this point. Note that one could obtain Eq.(5.34) by discretizing the Hamiltonian, finding K and then

constructing the joint wave function of coupled oscillators (the previous approach), but one could equally well find the kernel of a scalar field theory in line with Ch.4, and then perform a series of discretization steps on the kernel directly, which bypasses the need to envision our system as a lattice of interacting oscillators. There exists, as we will show later, a strong connection between this method and a more recent approach taken in the literature (the topic of discussion of the next chapter), and hence we will postpone its explicit evaluation till then.

The pseudocode provided below gives an overview of the required auxiliary matrices for a (3+1)-dimensional example and their order, their dependence on l, and the structure of the algorithm. The multiplicity $(2l + 1)$ will be explained in a later section. Note that the pseudocode can easily be adapted to a (2+1)-dimensional example by replacing the multiplicity $(2l + 1)$ by 2 for each $m \neq 0$, and by 1 for $m = 0$, as will become clear later. For a (1+1)-dimensional theory it simplifies even further, since in this case one can remove all loops.

Algorithm 1 GS Von Neumann entropy: $d = 3 \oplus 1$

for $i \in$ inner region **do**
  Initialize S
  for $l \in \{0, l_{max}\}$ **do** ▷ Loop depends on d; see below
    Determine K
    Calculate $\Omega = UK_D^{1/2}U^T$
    Decompose Ω into A, B and C
    Construct $\beta = \frac{1}{2}B^T A^{-1}B$ and $\gamma = \beta - C$
    Diagonalize $\gamma_D = V\gamma V^T$
    Construct $\beta' = \gamma_D^{-1/2} V\beta V^T \gamma_D^{-1/2}$ and find eigenvalues ${\beta'}_i$
    Determine S_i
    Calculate $(2l + 1)S_i$ ▷ Choose multiplicity based on d
  end for
  Update S
end for

5.4 Free scalar fields on a lattice

Srednicki's seminal paper [69] did not only discuss the construction of the algorithms we derived so far, but also used these to numerically demonstrate the existence of an area law for a (3+1)-dimensional massless, free scalar field in Minkowski spacetime. It is only natural that this famous result constitutes one of the main tests we subject our algorithm to. However, our first example will be a simple (1+1)-dimensional massless, free scalar in Minkowski spacetime, and ultimately the (2+1)-dimensional case, which is our main point of focus, since it is associated with the extension to our analogue black hole geometry. Lastly,

we remark that connecting the numerical results to the literature is largely postponed to the next chapter, where we study the same examples with a slightly more sophisticated method.

5.4.1 $D = 1 \oplus 1$

As stated in the previous section, we will (for now) only concern ourselves with the discrete-Hamiltonian approach. The natural starting point for the (1+1)-dimensional example is therefore the Hamiltonian

$$H = \frac{1}{2}\int dx[\pi^2(x) + |\nabla\phi(x)|^2], \tag{5.58}$$

with $\phi(x)$ is a real scalar field. This theory can be discretized rather easily by simply transforming to the discrete variables

$$r \to ja \tag{5.59}$$

$$\partial_r\phi(r) \to (\phi_{j+1} - \phi_j)/a \tag{5.60}$$

$$\int \mathrm{d}x \to a\sum_{j=0}^{N+1}, \tag{5.61}$$

where $j \in \mathbb{N}$ and we used a finite-difference approach for the derivative. The discrete Hamiltonian can then be written as

$$H = \frac{1}{2a}\sum_{j=1}^{N}[\pi_j^2 + (\phi_{j+1} - \phi_j)], \tag{5.62}$$

where we considered Dirichlet boundary conditions for $j = 0$ and $j = N + 1$, *i.e.* we enforced $\phi_0 = 0$ and $\phi_{N+1} = 0$. Note that we have effectively reduced our scalar field to the lattice of fig.(5.1). This allows us to write the Hamiltonian as

$$H = \frac{1}{2a}\sum_{i,j=1}^{N}[\pi_i\pi_j\delta_{ij} + \phi_i K_{i,j}\phi_j], \tag{5.63}$$

with the coupling matrix given by

$$K = \begin{pmatrix} 2 & -1 & 0 & \dots & 0 \\ -1 & 2 & -1 & & \vdots \\ 0 & -1 & 2 & \ddots & 0 \\ \vdots & & \ddots & \ddots & -1 \\ 0 & \dots & 0 & -1 & 2 \end{pmatrix} \tag{5.64}$$

Note that, using the techniques discussed before, this matrix immediately allows us to compute the entanglement entropy of a small subregion of a finite chain, where n_b is gradually extended to $n_b = N$, *i.e.* the complement of region A becomes zero. This simulation has been performed for a small lattice of size $N = 50$, with $n_b \in \{1, ..., 50\}$, and lattice parameter $a = 1$, as shown in fig.(5.3). The von Neumann entropy is maximal for $n_b = N/2$ and minimal when n_b comprises one of the boundary points, as expected. However, the situation we are particularly interested in, is the one where $N \to \infty$. Since this is not computationally achievable, we consider a small subregion A and choose the lattice large enough to minize the boundary effects from lattice point $N + 1$. Fig.(5.2a) shows a convergence analysis for the von Neumann entropy as a function of the lattice size for five distinct values of n_b. It is shown that, for a subregion with a boundary $n_b = 25$, approximate convergence in N is achieved for a lattice of 300 sites, and hence can be used for the entropy of a subregion A of the semi-line $l \in [0, \infty)$. We performed a similar analysis for a sublattice with $n_b = 100$, and found that a lattice size of $N = 500$ is suitable for convergence of the entropy. Using these parameters to determine the entanglement entropy of the semi-line, we find the result shown in fig.(5.2b).

It is known [13] that the von Neumann entropy for a finite interval $[0, l)$ of a semi-line $[0, \infty)$, which is subjected to boundary conditions at l, is given by

$$S_A = \frac{c}{6} \log(\frac{\beta}{\pi a} \sinh(\frac{2\pi l}{\beta})) + d, \tag{5.65}$$

where in our case $l = n_b$. When $l \ll \beta$, which we assume for our system, the authors argue that the entropy of the subregion can be written as

$$S_A = \frac{c}{6} \log(\frac{2l}{a}) + d \tag{5.66}$$

where c is the conformal parameter, which for a scalar field is $c = 1$. The constant d is dependent on the particular theory. We performed a numerical fit to the curve in fig.(5.2b) and obtained a function

$$S_A = \frac{\tilde{c}}{6} \log(\frac{2l_b}{a}) + \tilde{d}, \tag{5.67}$$

where $l_b = n_b a$. The coefficients are given by $\tilde{c} = 0.917$ and $\tilde{d} = 0.024$. We note that this relation is approximately equivalent to Eq.(5.66), which is further supported by our retrieval of the conformal weight $\tilde{c} \approx 1$, suggesting that the numerical simulation correctly approximates the entanglement entropy of the (1+1)-dimensional scalar field.

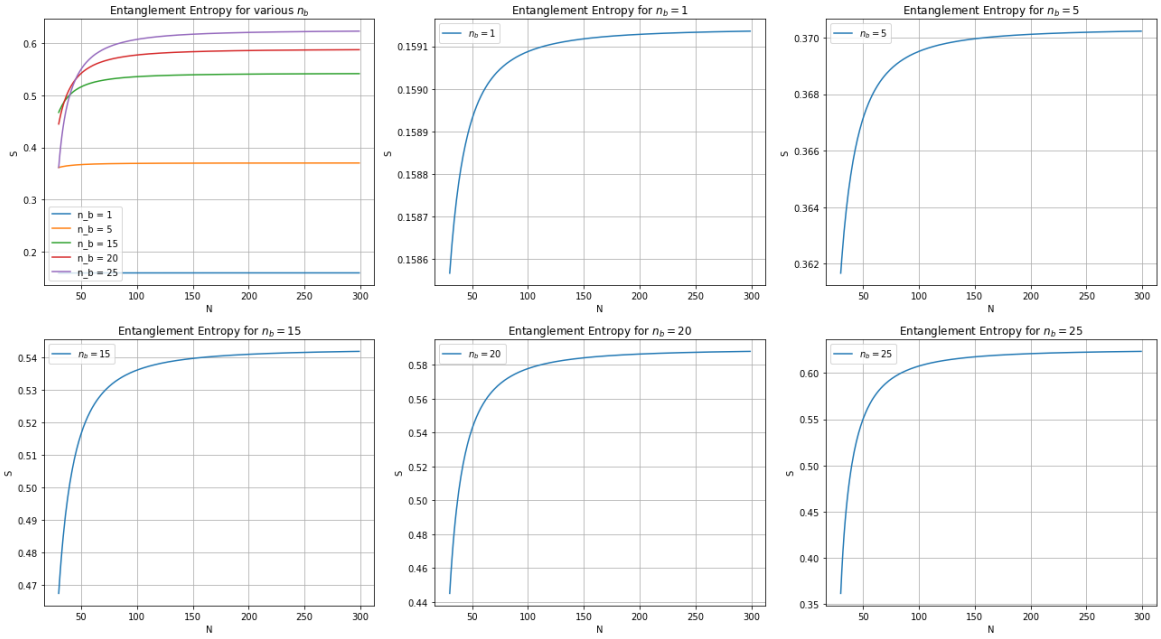

Fig. 5.2 The figure in the upper left corner shows the entanglement entropy for various n_b as a function of the lattice size $N \in [30, 300]$. The remaining figures display the entanglement entropy for each n_b versus the lattice size. It is shown that S converges for large N for these particular boundary points.

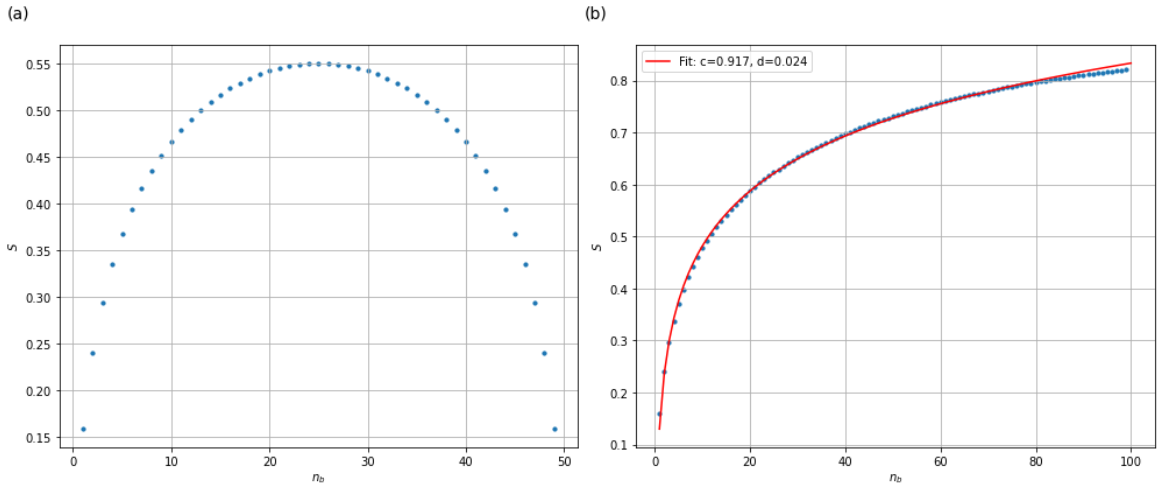

Fig. 5.3 Figure (a) shows the von Neumann entropy for the subregion of a finite chain, with $N = 50$. Figure (b) displays the entanglement entropy of a subregion with $n_b \in \{1, ..., 100\}$ on a lattice with $N = 500$ sites. A fitted function is shown by means of a red line.

5.4.2 $D = 3 \oplus 1$

Before we consider the case of a two-dimensional spacetime, we study the case of a free, massless scalar field on a (3+1)-dimensional spacetime. In this section we reproduce the derivation from [69], but with some slight differences. We primarily choose this rather unnatural order as to verify our algorithm for more complicated systems, where a comparison with Srednicki's coefficient for the area law is decisive. Consider the Hamiltonian for the Klein-Gordon field:

$$H = \frac{1}{2}\int \mathrm{d}^3x[\pi^2(\mathbf{x}) + |\nabla\phi(\mathbf{x})|^2], \tag{5.68}$$

where, with a slight abuse of notation, we write $|\pi_{lm}|^2 = \pi_{lm}\pi_{l'm'}$. We assume that the fields admit a mode-decomposition using spherical harmonics, leading to

$$\begin{cases} \phi(\mathbf{x}) = \sum_{l=0}^{\infty}\sum_{m=-l}^{l} \frac{\phi_{lm}(r)}{r} Y_{lm}(\theta,\alpha) \\ \pi(\mathbf{x}) = \sum_{l=0}^{\infty}\sum_{m=-l}^{l} \frac{\pi_{lm}(r)}{r} Y_{lm}(\theta,\alpha) \end{cases} \tag{5.69}$$

Furthermore, we recall that the derivatives of the fields in these coordinates are given by

$$|\nabla\phi|^2 = (\frac{\partial\phi}{\partial r})^2 + \frac{1}{r^2}(\frac{\partial\phi}{\partial\theta})^2 + \frac{1}{r^2\sin^2(\theta)}(\frac{\partial\phi}{\partial\alpha})^2. \tag{5.70}$$

As remarked in [69], we use real spherical harmonics, as to ensure the reality of the field. We adopt Srednicki's notation and write Z_{lm} such that

$$\begin{cases} m = 0: & Z_{l0} = Y_{l0} \\ m > 0: & Z_{lm} = \sqrt{2}\mathfrak{Re}(Y_{lm}) \\ m < 0: & Z_{lm} = \sqrt{2}\mathfrak{Im}(Y_{lm}) \end{cases} \tag{5.71}$$

which can be shown to obey the typical orthonormality relation for spherical harmonics [69]. Let us, for clarity, consider the Laplace operator and conjugate momentum separately. Starting with the easiest term (the conjugate momentum), we have:

$$\sum_{l,m}\sum_{l',m'}\int \mathrm{d}r \int \mathrm{d}\Omega\, Z_{lm}(\theta,\varphi)Z_{l'm'}(\theta,\varphi)\pi_{lm}(r)\pi_{l'm'}(r) = \sum_{lm}\int \mathrm{d}r\, \pi_{lm}^2(r). \tag{5.72}$$

The measure is given by $\mathrm{d}\Omega = \sin^2(\theta)\mathrm{d}\theta\,\mathrm{d}\varphi$, where the sine is a remnant from the volume, after which we used the relation [4]

$$\int_0^{\pi}\int_0^{2\pi} \mathrm{d}\Omega Z_{lm}(\theta,\varphi)Z_{l'm'}(\theta,\varphi) = \delta_{ll'}\delta_{mm'}, \tag{5.73}$$

and summed over the indices l', m'. The derivative term can be written as

$$|\nabla\phi(\mathbf{x})|^2 = \sum_{l,m}\sum_{l',m'}[(\frac{\partial}{\partial r}\frac{\phi_{lm}(r)}{r})^2|\mathrm{Y}_{lm}(\theta,\alpha)|^2 + |\phi_{lm}(r)|^2|\nabla Z_{lm}(\theta,\varphi)|^2], \tag{5.74}$$

where ∇ denotes the gradient. Substituting this result into the Hamiltonian and integrating out all angular dependence (apart from the ∇ term) leads to the simple relation

$$H = \frac{1}{2}\sum_{lm}\sum_{l'm'}\int \mathrm{d}r\,[\pi^2_{lm}(r)\delta_{ll'}\delta_{mm'} + r^2(\frac{\partial}{\partial r}\frac{\phi_{lm}(r)}{r})^2\delta_{ll'}\delta_{mm'} + |\phi_{lm}(r)|^2\int \mathrm{d}\Omega\,|\nabla Z_{lm}(\theta,\varphi)|^2], \tag{5.75}$$

with $\mathrm{d}\Omega$ the measure from before. The last term simplifies considerably by taking the partial derivative and discarding all boundary terms, such that the last contribution becomes

$$\int \mathrm{d}\Omega\,|\nabla Z_{lm}(\theta,\varphi)|^2 = -\int \mathrm{d}\Omega\, Z_{lm}(\theta,\varphi)\triangle Z_{l'm'}(\theta,\varphi) = \frac{l'(l'+1)}{r^2}\int \mathrm{d}\Omega\, Z_{lm}(\theta,\varphi)Z_{l'm'}(\theta,\varphi), \tag{5.76}$$

where $\triangle$ is the Beltrami-Laplace operator, for which we know that [4] $\triangle\mathrm{Y}_{lm} = -l(l+1)\mathrm{Y}_{lm}/r^2$. Inserting this result back into Eq.(5.75), taking the last integral over the measure $\mathrm{d}\Omega$ and summing over l', m' leads to the Hamiltonian of a one-dimensional chain, given by

$$H = \frac{1}{2}\sum_{lm}\int \mathrm{d}r\,\underbrace{[\pi^2_{lm}(r) + r^2(\frac{\partial}{\partial r}\frac{\phi_{lm}(r)}{r})^2 + \frac{l(l+1)(\phi_{lm}(r))^2}{r^2}]}_{=2H_{lm}} \tag{5.77}$$

This particular expression can be discretized rather easily, where, as before, we consider $r \to (j+\epsilon)a$, with a the lattice spacing and $j \in \mathbb{N}/\{0\}$. The only difference is the addition of the term $\epsilon \in [0,1]$, which reflects the possibility to shift the boundary away from its original lattice site. In [69] this simple trick is used to mimic the geometry of a static black hole, in the sense that in integrating over the inner region one should take care with the horizon, which is singular. By taking $\epsilon = 1/2$ and $a = 1$, the authors chose the lattice such that the event horizon is in between two lattice points n_b and $n_b + 1$, and then integrated out the region $[1, ..., n_b]$, therefore capturing the entire inner region without running into singular behaviour. However, this event horizon was 'fictional'; they chose to restrict a subregion of Minkowski spacetime to a sphere, but did not use the actual geometry appropriate for a Schwarzschild black hole. This will not be of great concern to us in this chapter, but it is important to realize the restrictions to their result. In our case we will take $\epsilon = 0$, yet for completeness the finite-difference term is shown for arbitrary ϵ, and the reader is free to shift

the boundary in all further terms. The finite-difference becomes

$$\frac{\partial}{\partial r}\frac{\phi_{lm}(r)}{r} \to \frac{1}{a^2}\left(\frac{\phi_{lm,j+1}}{j+1+\epsilon} - \frac{\phi_{lm,j}}{j+\epsilon}\right). \tag{5.78}$$

Taking all these terms into account, we obtain the Hamiltonian for a chain of harmonic oscillators of the form

$$H = \frac{1}{2a}\sum_{l,m}\sum_{j=1}^{N}\left(\pi_{lm,j}^2 + (j+1/2)^2\left(\frac{\phi_{lm,j+1}}{j+1} - \frac{\phi_{lm,j}}{j}\right)^2 + \frac{l(l+1)}{j^2}\phi_{lmj}^2\right), \tag{5.79}$$

which corresponds to the Hamiltonian found in [49]. We have furthermore written $\phi_{lm}(ja) \to \phi_{lmj}$ and $\pi_{lm}(ja) \to \pi_{lmj}$. This result shows the essence of fig.(5.4); since each lattice point captures the contribution of a 'shell' of oscillators (*i.e.* for the j-th lattice point all oscillators on the 2-sphere with radius $r = j + \epsilon$), we have discretized the system to a lattice of spherical shells. Taking the limit $a \to 0$, undoing the finite difference term, writing the Riemann sum as an integral and re-inserting the spherical harmonics retrieves the continuum theory. Let us now return to the discrete Hamiltonian and start our search for the coupling matrix K. For each pair (l, m) the expression reduces to

$$H_{lm} = \frac{1}{2a}\sum_{i,j=0}^{N}\left(\pi_{lm,i}\pi_{lm,j}\delta_{ij} + \phi_{lm,i}K_{ij}\phi_{lm,j}\right), \tag{5.80}$$

where the coupling matrix K can be found by comparing this expression with the Hamiltonian Eq.(5.79). As before, we consider boundary conditions $\phi_{lm,0} = \phi_{lm,N+1} = 0$. The coupling matrix can then be shown to correspond to the one described in [49], where the real, symmetric, semipostive, tridiagonal matrix contains elements

$$\begin{cases} K_{11} = \frac{9}{4} + l(l+1) \\ K_{jj} = 2 + \frac{1}{j^2}\left(\frac{1}{2} + l(l+1)\right) \quad \text{for} \quad j \in [2, ..., N] \\ K_{j,j+1} = K_{j+1,j} = -\frac{(j+\frac{1}{2})^2}{j(j+1)} \quad \text{for} \quad j \in [1, ..., N-1] \end{cases} \tag{5.81}$$

We note that the coupling matrix is not explicitly dependent on m. Since $m \in [-l, l]$ for each l, we may write the entanglement entropy (including correct multiplicity) as

$$S_A = \sum_{l=0}^{\infty}\sum_{i=n_b+1}^{N}(2l+1)S_i, \tag{5.82}$$

where S_i is given by Eq.(5.54). Before performing the entropy simulations, we select a maximal $l_{\max}$ which ensures convergence in the angular parameter, as we will discuss shortly. The (numerical) convergence of the entanglement entropy as a function of N is demonstrated in fig.(5.5). We have first selected an arbitrarily large l and manually showed that $\Delta S(l) \ll 1$

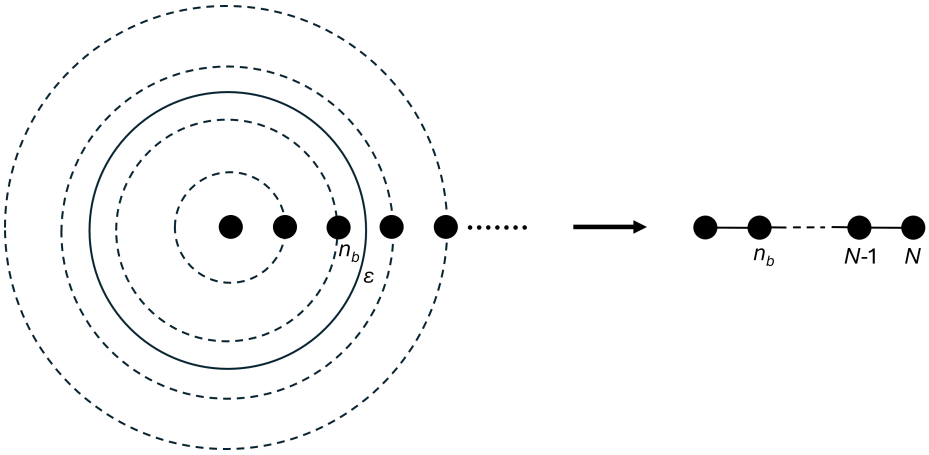

Fig. 5.4 Impression of a scalar field with a discretized radial coordinate, which reduces to a chain of N oscillators after the angular degrees of freedom are integrated out. The dotted circles either represent spherical shells or circular shells, depending on the spatial dimension of the field.

for a sample of the values $n_b \in [0, 100]$, including the maximum surface position $n_b = 100$. Note, however, that this approach leads to exceedingly large CPU times and greatly improves when eventually taking the two convergence results together. It is shown that a lattice size of $N = 300$, with large enough l, leads to approximate convergence to the maximum entanglement entropy for all considered n_b. Subsequently, we have considered the same procedure for S as a function of l, where we have first considered an arbitrarily large N to ensure (approximate) convergence in this parameter, *i.e.* $\Delta S(N) \ll 1$ for each n_b, and then determined the contribution of each angular momentum mode to the entanglement entropy. It can be seen in fig.(5.6) that, for entangling surfaces up to $n_b = 100$, the entropy receives ample contribution from the angular momentum modes from $l \approx 700$ onwards for the larger values of n_b, whereas the lower values are hardly affected by greater l at all. In the following simulations we shall therefore enforce convergence by taking $N = 300$ and $l = 800$ for all surface positions $n_b \in [0, 100]$.

We determine the entanglement entropy of a subregion with an entangling surface up to $\mathcal{A}/4\pi = 1600$, where $\mathcal{A} = 4\pi R_b^2$ and $R_b = n_b a$, which correspond to a maximal boundary point $n_b = 40$. The optimal parameters $N = 300$ and $l = 800$ were used for each simulation. Fig.(5.7) shows the resulting von Neumann entropy, including a numerical fit, which is given by the expression

$$S_A = s(\frac{R_b}{a})^2 + c\log(\frac{R_b}{a})^2 + d, \tag{5.83}$$

where the numerical coefficients were found to be $s = 0.29805$, $c = 1.65674$ and $d = -0.67725$. In [69] the authors found a coefficient $s = 0.30$, serving as numerical confirmation of the area law. However, they were not yet able to determine logarithmic corrections. More recent

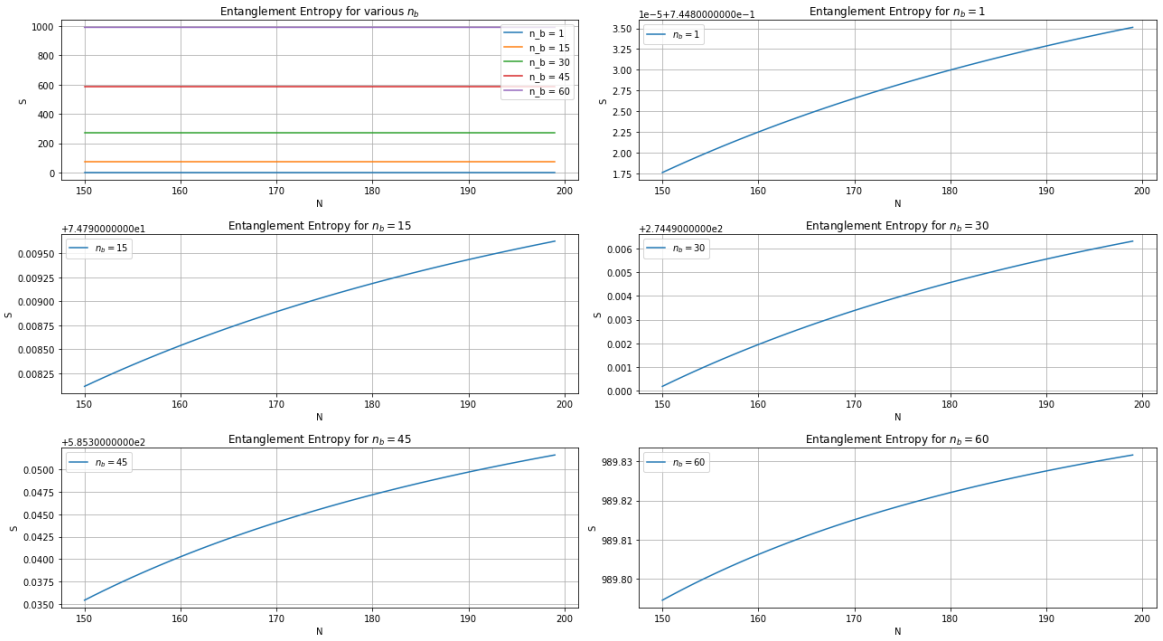

Fig. 5.5 The entanglement entropy of various n_b is shown as a function of the lattice size N. The first plot considers 5 particular values of n_b, which are shown individually in the remaining subfigures.

numerical work [49] has found coefficients $s = 0.295431$, $c = -0.005545$ and $d = -0.03537$. The coefficient s is seen to correspond to our result, yet the coefficients of the corrections are not compatible. In particular the difference between the values of c are striking, as this is known to be $c = -1/90$ analytically [15], which is indeed found by [49] when absorbing the square of the logarithmic term into the coefficient. This difference lies in the fact the authors of [49] used a significantly larger lattice and larger entangling surface, and fitted the curve only to the predicted entanglement entropy for the last 20 lattice sites $[n_b - 20, n_b]$. Hence, they minimized the influence of the boundary at $j = 0$, which causes a slightly curved offset in our plot, and therefore overestimates the magnitude of our estimate of the logarithmic coefficient c. Reproducing the approach by Lohmayer *et al.* yielded coefficients close to those found in [49], yet as we did not manage to achieve numerical convergence in l, we will depart the topic for now and proceed to study the (2+1)-dimensional case.

5.4.3 $D = 2 \oplus 1$

Despite the greater importance of the (2+1)-dimensional scalar field in light of our analogue black hole, we decided to present the (3+1)-dimensional case first, as it not only provides a road map for the discretization of the current system, but in fact simplifies it considerably. We start from the 2-dimensional equivalent of the Hamiltonian Eq.(5.68) and write the scalar

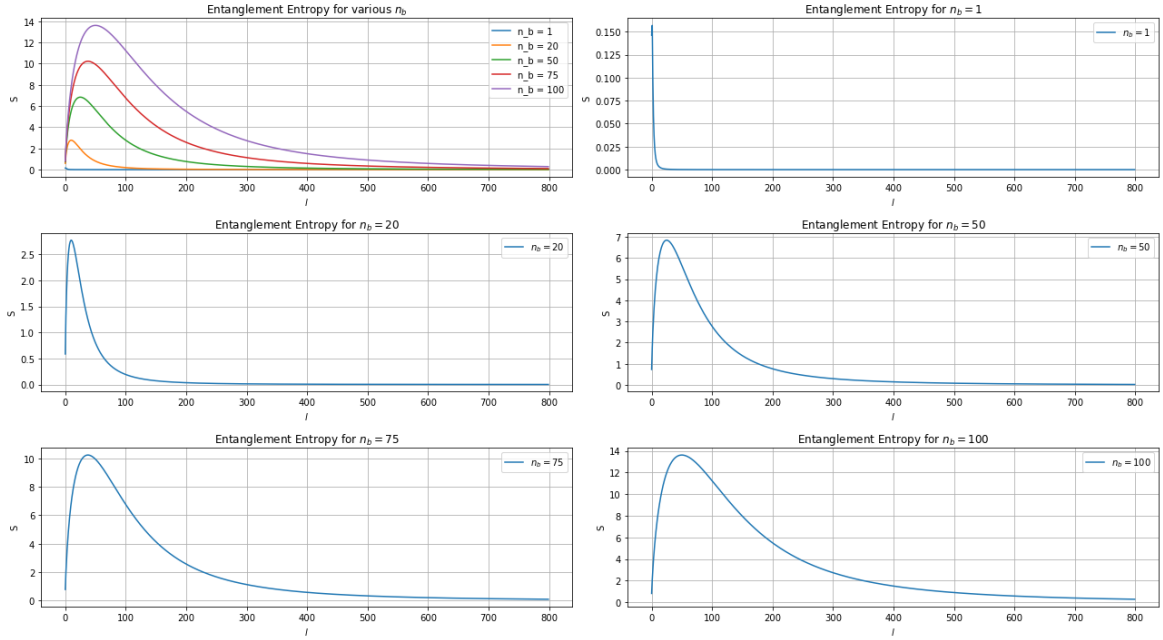

Fig. 5.6 The contribution of each angular momentum mode l to the entanglement entropy of a specific surface n_b is displayed. The first figure considers 5 particular values of n_b. Consecutive figures consider each of the n_b individually to show more properly the behaviour of the tail.

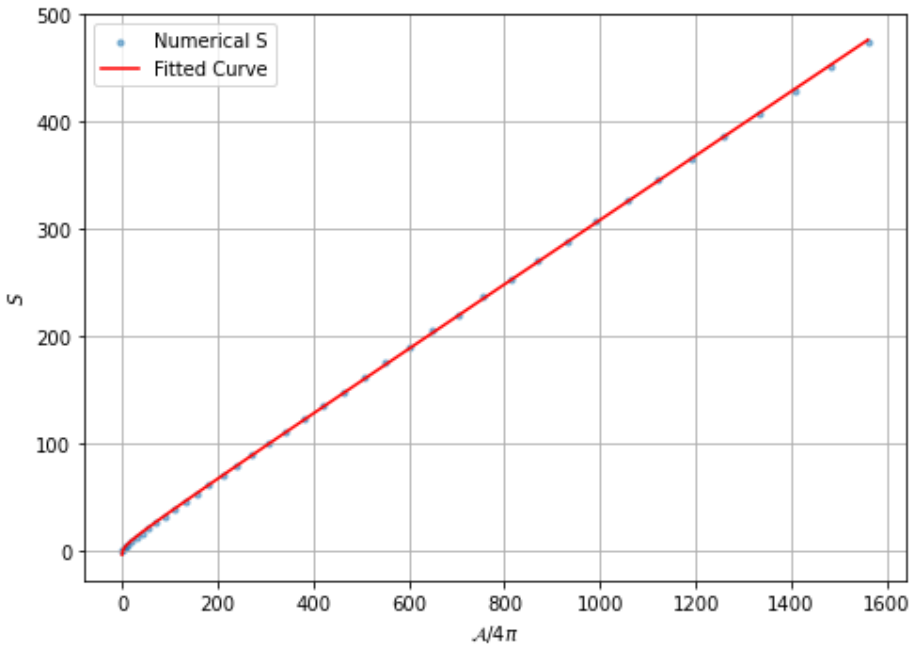

Fig. 5.7 The figure shows the numerical predictions for the entanglement entropy of the scalar field. The red-line corresponds to the function fitted to the curve. The small 'kink' near the origin is an artifact of the boundary conditions.

field and its conjugate momentum as a mode-decomposition

$$\begin{cases} \phi(r,\theta) = \sum_m \frac{\phi_m(r)}{\sqrt{r}} Z_m(\theta) \\ \pi(r,\theta) = \sum_m \frac{\pi_m(r)}{\sqrt{r}} Z_m(\theta) \end{cases} \tag{5.84}$$

where we denote $Z_m = \mathfrak{Re}\{Y_m\}$ for $m > 0$, $Z_m = \mathfrak{Im}\{Y_m\}$ for $m < 0$, and $Z_0 = 1$, where $Y_m(\theta)$ are the circular harmonics [28], which are chosen such that they form an orthonormal basis:

$$\int_0^{2\pi} \mathrm{d}\theta \, Y_m(\theta) Y_{m'}(\theta) = \delta_{mm'}. \tag{5.85}$$

Upon writing the Hamiltonian in polar coordinates and inserting the aforementioned mode-expansion, we obtain the expression

$$H = \frac{1}{2} \sum_{m,m'} \int \mathrm{d}r \mathrm{d}\theta \, [|\pi_m(r)|^2 |Y_m(\theta)|^2 + r(\frac{\partial}{\partial r} \frac{\phi_m(r)}{\sqrt{r}})^2 |Y_m|^2 + \frac{|\phi_m|^2}{r^2} (\frac{\partial Y_m}{\partial \theta})^2], \tag{5.86}$$

where we use the same shorthand as before. We consider a partial integration of the last term and identify the Laplace-Beltrami operator with fixed radius such that

$$\int \mathrm{d}\theta \, (\frac{\partial Y_m}{\partial \theta})^2 = -\int \mathrm{d}\theta \, Y_m \triangle^* Y_{m'}, \tag{5.87}$$

which in this case is merely the second-order derivative with respect to θ. We note from [28] that $\triangle^* Y_m(\theta) = -m^2 Y_m(\theta)$ for all circular harmonics Y_m. Inserting this result into the Hamiltonian and using Eq.(5.85) yields

$$H = \frac{1}{2} \sum_m \int \mathrm{d}r \, [(\pi_m(r))^2 + r(\frac{\partial}{\partial r} \frac{\phi_m}{\sqrt{r}})^2 + \frac{m^2}{r^2} \phi_m(r)^2], \tag{5.88}$$

where we have integrated over θ and subsequently summed over m'. Choosing the discretization scheme from before, *i.e.* $\phi_m(ja) \to \phi_{mj}$ and $\pi_m(ja) \to \pi_{mj}$, we obtain the dimensionally reduced Hamiltonian

$$H = \frac{1}{2a} \sum_m \sum_{j=1}^{N} [\pi_{m,j}^2 + (j + 1/2)(\frac{\phi_{m,j+1}}{\sqrt{j+1}} - \frac{\phi_{m,j}}{\sqrt{j}}) + \frac{m^2}{j^2} \phi_{m,j}^2] \tag{5.89}$$

This expression resembles the result from the (3+1)-dimensional scalar field. The Hamiltonian describes a chain of oscillators where the i-th site contains the contributions from the 1-sphere of harmonic oscillators of radius $r = ia + \epsilon$, corresponding to fig.(5.4). Performing the sum over j in Eq.(5.89) and collecting like-terms gives the m-mode Hamiltonian

$$H_m = \frac{1}{2a} \sum_{i,j=1}^{N} [\pi_{mi} \pi_{mj} \delta_{ij} + \phi_{mi} K_{ij} \phi_{mj}]. \tag{5.90}$$

The coupling matrix is identical to the one found in [39, 40], where the author studies scalar fields and Maxwell fields confined to cylinders and disks, and are found to be

$$\begin{cases} K_{11} = \frac{3}{2} + m^2 \\ K_{jj} = 2 + \frac{m^2}{j^2} \quad \text{for} \quad j \in [2, N] \\ K_{j,j+1} = K_{j+1,j} = -\frac{j+1/2}{\sqrt{j(j+1)}} \quad \text{for} \quad j \in [1, N-1] \end{cases} \tag{5.91}$$

Since the elements of the coupling matrix only contain even powers of m, we observe that each $S_{i,m}$ carries a multiplicity of $(1 + [m \neq 0])$, where $[x]$ is the Iverson bracket (*i.e.* 0 if $m = 0$ and 1 if $m \neq 0$). We can therefore write the entanglement entropy of the subregion A as

$$S_A = \sum_{i=n_b+1}^{N} \sum_{m=0}^{\infty} (1 + [m \neq 0]) S_i, \tag{5.92}$$

where S_i is given by Eq.(5.54). Determining the entanglement entropy proceeds along the same lines as before, and as such we start with the convergence analysis for the entropy in m and N, shown in fig.(5.8). Subplot fig.(5.8a) shows the von Neumann entropy as a function of N, where we have taken the entangling surface $n_b \in [1, 60]$, of which a subset is explicitly shown. The azimuthal mode m was chosen large and manually varied until $\Delta S(m) \ll 1$. After selecting an appropriate $m_{\max}$, the interval $N \in [65, 150]$ was considered, which shows approximate convergence in N for lattice sizes of $N \geq 120$. Fig.(5.8b) shows a similar analysis for m, where the contribution of each m to the total entanglement entropy is shown. We first selected an arbitrarily large N, such that $\Delta S(m) \ll 1$, after which we used this parameter to determine $S(m)$ for $m \in [0, 150]$. It shown that the von Neumann entropy approximately convergences in m for $m > 140$.

Subsequently, we consider a lattice of size $N = 150$ and an entangling surface $n_b \in [1, 60]$. The maximal azimuthal mode $m_{\max} = 150$ is chosen in line with the convergence analysis. The result of this simulation is shown in fig.(5.9). We fitted a function [1]

$$S_A = s(\frac{L_b}{a}) + c \log(\frac{L_b}{a}) + d, \tag{5.93}$$

where $L_b = n_b a$, to our data and determined the coefficients s, c and d. The reader should note that the terminology 'area law' for the entangling surface is slightly misleading, since in the (2+1)-dimensional case it is expected to scale with the perimeter, not the area. Hence,

[1] It was pointed out to us shortly before finishing this dissertation that a (2+1)-dimensional scalar field with a smooth boundary should not contain a subleading logarithmic term. Time-constraints have prevented us from researching this statement further and, if needed, performing new fits. Anyone who feels tempted to continue this inquiry should therefore take the fits for $d = 2$ with a grain of salt, yet pay close attention to the predictive power for the polynomial coefficients. However, our successors can take comfort in the fact that the results for the $d = 1$ and $d = 3$ scalar fields are in line with relevant literature.

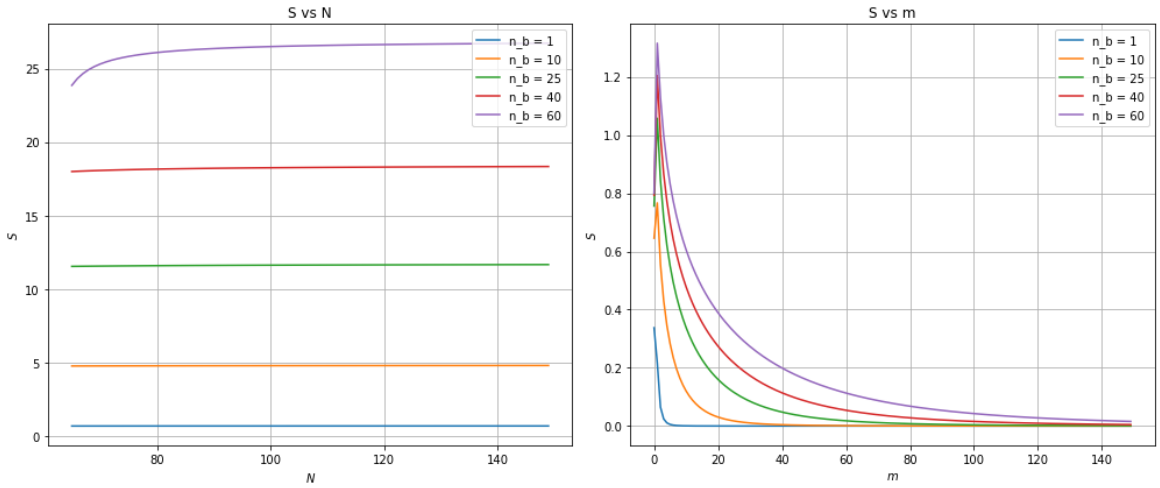

Fig. 5.8 The first subfigure shows the entanglement entropy for various entangling boundary points n_b as a function of the lattice size N. The second figure shows the contribution of each azimuthal mode m to the entanglement entropy of a specific surface n_b.

we adopt the somewhat confusion notation $\mathcal{A} = 2\pi L_b \equiv 2\pi n_b a$. The coefficients are found to be $s = 0.432$, $c = 0.267$ and $d = -0.033$, confirming the that the entanglement entropy of the scalar field scales with its perimeter.

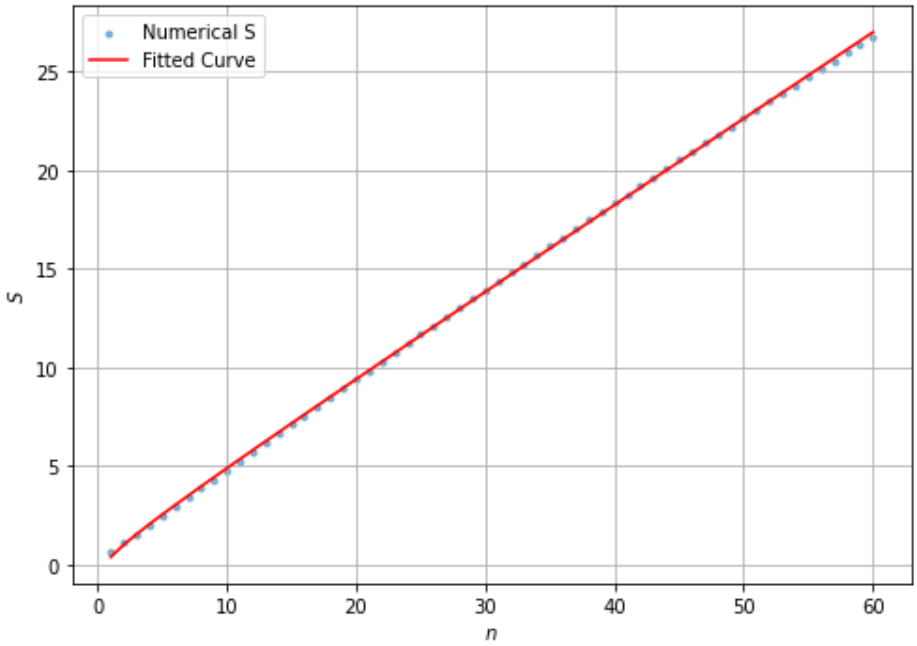

Fig. 5.9 The entanglement entropy of a free, massless (2+1)-dimensional scalar field as a function of the boundary points $n_b \in [1, 60]$. The fitted curve is seen to be almost linear.

Chapter 6

Sublattice-dependent entanglement entropy

"Joy in looking and comprehending is Nature's most beautiful gift."
Albert Einstein

In the previous chapter we 'decomposed' free scalar fields into chains of N-coupled harmonic oscillators by integrating out the angular degrees of freedom contained by the Hamiltonian, followed by subsequent discretization of its radial coordinate. The resulting ground state wave functions were then used to determine the reduced density matrix of the complement of some predefined sublattice $A \subset \mathcal{M}$, after which the introduction of several auxiliary structures resulted in an algorithm for the estimation of its entanglement entropy. Although the efficiency of the approach is apparent, the requirement of the coupling matrix to be calculated for the full lattice $\mathcal{M}$ may lead to significant computational times and, when one is not careful, inconspicuous convergence issues. This chapter attempts to arrive at a similar algorithm, yet approached from a different angle. Contrary to *ab initio* considering a chain of harmonic oscillators and computing their joint wave function, we will follow the approach of [15], where they exploit the fact that the reduced density matrix of a subregion A can be constructed solely from the knowledge of the correlators in A. We will then proceed by expressing both the von Neumann *and* Rényi entropy in terms of the position and conjugate momentum correlators. Lastly, we will discuss an explicit connection between the correlators and the coupling matrix of the discrete-system Hamiltonian, which allows us to create an algorithm which only requires knowledge of the correlators (and no auxiliary structures) constrained to region A.

6.1 Entropy and correlators

We base our discussion on the original work by Cassini *et al.* [15] and their excellent review [17]. Since the accompanying discussion of their derivation in these publications is on the frugal side, and stands quite far from the aim of this dissertation, we shall state the most important results while briefly motivating their origin, after which we join in on the derivation at a point suitable for our purposes; finding a more efficient algorithm to compute the entanglement entropy. As before, we consider the bosonic fields ϕ_i and its conjugation momentum π_i, for which the standard commutation relations are assumed. For the sake of brevity, we will furthermore introduce the notation for the correlators

$$X_{ij} = \langle \phi_i \phi_j \rangle \quad \text{and} \quad P_{ij} = \langle \pi_i \pi_j \rangle. \tag{6.1}$$

Using the commutation relations, one can also demonstrate that [15]

$$\langle \phi_i \pi_j \rangle = \langle \pi_j \phi_i \rangle = \frac{i}{2} \delta_{ij}. \tag{6.2}$$

The authors assume that subsystem A can be described by the modular Hamiltonian $H_A = \sum_\kappa \epsilon_\kappa a_\kappa^\dagger a_\kappa \equiv \sum_\kappa \epsilon_\kappa n_\kappa$, as in [58], which is defined as the logarithm of the normalized reduced density matrix of region A [64, 22]. In this terminology, the reduced density matrix for a chain of oscillators is given by [61, 60, 19]

$$\rho_A = C e^{-\sum_\kappa \epsilon_\kappa a_\kappa^\dagger a_\kappa} \equiv C e^{-H_A}, \tag{6.3}$$

where C is the normalization constant $C = \prod_l (1 - e^{-\epsilon_l})$, which can be obtained by enforcing the condition $\mathrm{Tr}(\rho) = 1$. The authors proceed to show that, by means of this reduced density matrix for subregion A, one can obtain the correlator matrices

$$X = \alpha(2n+1)\alpha^T, \tag{6.4}$$

$$P = \beta(2n+1)\beta^T, \tag{6.5}$$

with α and β real matrices, and n a diagonal matrix containing the expectation values of the occupation numbers, which according to [15] are given by $\langle n_k \rangle = (e^{-\epsilon_k} - 1)^{-1}$. Furthermore, one can demonstrate that $\alpha = -(\beta^T)^{-1}/2$. More details on the derivation of the correlator matrices can be found in [24]. The relation between matrices α and β can be exploited to dissect the correlator matrix products XP and PX, which are non-commutative, but can be shown to have the same spectrum. The former can be demonstrated to give

$$XP = \alpha(2n+1)\underbrace{\alpha^T\beta}_{=-\frac{1}{2}}(2n+1)\beta^T = \frac{1}{4}\alpha(2n+1)^2\alpha^{-1}. \tag{6.6}$$

In the same manner, one can show that

$$PX = \beta(2n+1)\underbrace{\beta^T\alpha}_{=-\frac{1}{2}}(2n+1)\alpha^T = \frac{1}{4}\beta(2n+1)^2\beta^{-1}, \tag{6.7}$$

where we have rewritten β in terms of α. Since n is a diagonal matrix, both products are seen to have eigenvalues $(n+1/2)^2$. As they are not orthogonally diagonalizable, the matrix products are not identical, yet they are similar. The spectrum of the correlator products is therefore given by

$$\nu_\kappa^2 \equiv (n_\kappa + \frac{1}{2})^2 = (\frac{1}{e^{\epsilon_\kappa}-1} + \frac{1}{2})^2. \tag{6.8}$$

Using some basic trigonometry, the eigenvalues can be shown to reduce to the simple expression $\nu_\kappa = \frac{1}{2}\coth(\epsilon_\kappa/2)$, which describe the eigenvalues of the matrix $C = \sqrt{XP}$, where, as shown before, the order of the correlators is irrelevant. Since $\nu_\kappa \geq \frac{1}{2}$, we find the additional constraint $C \geq \frac{1}{2}\mathbb{1}$, or $XP \geq \frac{1}{4}\mathbb{1}$. By using analytical evaluation software, we then inverted the eigenvalues to obtain

$$\epsilon_\kappa = \log(\frac{\nu_\kappa + \frac{1}{2}}{\nu_\kappa - \frac{1}{2}}). \tag{6.9}$$

At this point it is possible to take two distinct routes. One could either decide to follow [15] and derive the entanglement entropy in terms of ν_κ directly from the reduced density matrix, or one could take the $r \to 1$ limit of the Rényi entropy Eq.(2.8) as a starting point, as discussed in [67, 24]. We will follow the latter and stay rather close to their derivation. Before considering the full Rényi entropy, we shall demonstrate that Eq.(6.9) causes the trace-term to simplify considerably, therefore rendering the Rényi entropy (and consequently the von Neumann entropy) relatively easy to compute. We note that

$$\mathrm{Tr}[\rho^q] = \mathrm{Tr}[K^q \prod_{\kappa=1}^{N} e^{-q\epsilon_\kappa n_\kappa}] = K^q \prod_{\kappa=1}^{N}\sum_{n_\kappa}(\frac{\nu_\kappa - \frac{1}{2}}{\nu_\kappa + \frac{1}{2}})^{qn_\kappa}. \tag{6.10}$$

Since the fraction in the summation is always smaller than one, we may use the geometric series, such that the trace becomes

$$\mathrm{Tr}[\rho^q] = \prod_{\kappa=1}^{N}(1 - \frac{\nu_\kappa - \frac{1}{2}}{\nu_\kappa + \frac{1}{2}})^q[1 - (\frac{\nu_\kappa - \frac{1}{2}}{\nu_\kappa + \frac{1}{2}})^q]^{-1}, \tag{6.11}$$

where in the last line we have inserted the definition of the normalization constant K. This expression can be rewritten to

$$\mathrm{Tr}[\rho^q] = \prod_{\kappa=1}^{N}[(\nu_\kappa + \frac{1}{2})^q - (\nu_\kappa - \frac{1}{2})^q]^{-1} \tag{6.12}$$

which we then substitute into the definition of the Rényi entropy Eq.(2.8) with $q \to 1$:

$$\begin{aligned} S &= \lim_{q\to 1} \frac{1}{1-q} \log \big(\prod_{\kappa} [(\nu_\kappa + \frac{1}{2})^q - (\nu_\kappa - \frac{1}{2})^q]^{-1}\big) \\ &= \lim_{q\to 1} \sum_{\kappa} \frac{-1}{1-q} \log \big[(\nu_\kappa + \frac{1}{2})^q - (\nu_\kappa - \frac{1}{2})^q\big]. \end{aligned} \tag{6.13}$$

Note that this expression, without the limit, is in fact sufficient to evaluate the Rényi entropy for any order $q \in \mathbb{Z}^+ \backslash \{1\}$. The limit can be evaluated by using l'Hôpital's rule, after which one finds

$$\begin{aligned} S &= \lim_{q\to 1} \sum_{\kappa} \frac{(\nu_\kappa + \frac{1}{2})^q \log(\nu_\kappa + \frac{1}{2}) - (\nu_\kappa - \frac{1}{2})^q \log(\nu_\kappa - \frac{1}{2})}{(\nu_\kappa + \frac{1}{2})^q - (\nu_\kappa - \frac{1}{2})^q} \\ &= \sum_{\kappa} [(\nu_\kappa + \frac{1}{2}) \log(\nu_\kappa + \frac{1}{2}) - (\nu_\kappa - \frac{1}{2}) \log(\nu_\kappa - \frac{1}{2})]. \end{aligned} \tag{6.14}$$

This last expression provides the von Neumann entropy for our scalar field, which in terms of the matrix C becomes

$$S = \mathrm{Tr}[(C + \frac{1}{2}) \log(C + \frac{1}{2}) - (C - \frac{1}{2}) \log(C - \frac{1}{2})]. \tag{6.15}$$

We note that this expression is valid provided $\nu_\kappa \geq 1/2$, for each $\kappa \in A$. Recalling that the eigenvalues of the product $XP > 1/4$, we conclude that the eigenvalues of $C = \sqrt{XP}$ must necessarily obey the lower bound $C > 1/2$, hence fulfilling the requirement posed on ν_κ.

Up to this point, the calculation of X and P itself has received little attention. In [15] it is only stated that the matrices are given by the simple relation

$$P_{ij} = \frac{1}{2}(K^{1/2})_{ij} \quad \text{and} \quad X_{ij} = \frac{1}{2}(K^{-1/2})_{ij} \tag{6.16}$$

where we note the explicit connection between P and the kernel as defined in the previous chapter: $\Omega = K^{1/2}$. We proceed to demonstrate these relations explicitly by writing the reduced density matrix in the Schrödinger representation. This derivation is inspired by [67], and we retrace their work in slightly more detail. We note that, as in Ch.5, we may write

$$\rho(\Phi, \Phi') = \pi^{-N/2} \sqrt{\det(\Omega)} e^{-\frac{1}{2}\Phi'^T \Omega \Phi'} e^{-\frac{1}{2}\Phi^T \Omega \Phi}, \tag{6.17}$$

where $\Phi = (\phi_1, ..., \phi_N)^T$. Using the definition of the position correlator, we can now write

$$\langle \phi_i \phi_j \rangle = \mathrm{Tr}[\rho \phi_i \phi_j] = \pi^{-N/2} \sqrt{\det(\Omega)} \int \Big(\prod_{n=1}^{N} \mathrm{d}\phi_n \Big) \phi_i \phi_j e^{-\Phi^T \Omega \Phi}, \tag{6.18}$$

where one must take care to use the density matrix, and not the reduced density matrix corresponding to A with B integrated out. This is integral is nothing but a simple multivariate Gaussian, for which solutions are known to be [67]

$$\int \mathrm{d}\mathbf{x} f(\mathbf{x}) e^{-\frac{1}{2}\mathbf{x}^T A \mathbf{x}} = \sqrt{\frac{(2\pi)^N}{\det(A)}} \exp\left(-\frac{1}{2}\sum_{n,m=1}^{N} (A^{-1})_{nm} \frac{\partial}{\partial_n}\frac{\partial}{\partial_m}\right) f(\mathbf{x})|_{\mathbf{x}=0}. \tag{6.19}$$

Given $f(\mathbf{x}) = x_i x_j$, we observe that in Taylor expanding the exponential, all terms but the first-order contribution vanish. Hence, the correlator $\langle \phi_i \phi_j \rangle$ evaluates to

$$\begin{aligned} X_{ij} = \langle \phi_i \phi_j \rangle &= \frac{1}{4}\pi^{-N/2}\sqrt{\det(\Omega)}\sqrt{\frac{(2\pi)^N}{\det(2\Omega)}}\sum_{n,m}\delta_{n,i}\delta_{m,j}(\Omega^{-1})_{nm} \\ &= \frac{1}{2}(\Omega^{-1})_{ij} = \frac{1}{2}(K^{-1/2})_{ij}. \end{aligned} \tag{6.20}$$

Despite the fact that we could have expressed the result in terms of K from the start, we have explicitly chosen to elucidate its connection with the kernels from Ch.4. Similarly, the other correlator can be written as

$$\langle \pi_i \pi_j \rangle = \mathrm{Tr}[\rho \pi_i \pi_j] = -\pi^{-N/2}\sqrt{\det(\Omega)} \int \Big(\prod_{n=1}^{N} \mathrm{d}\phi_n\Big) e^{-\frac{1}{2}\Phi^T K^{1/2}\Phi} \frac{\partial}{\partial\phi_i}\frac{\partial}{\partial\phi_j} e^{-\frac{1}{2}\Phi^T K^{1/2}\Phi}. \tag{6.21}$$

We can easily evaluate the integral by taking the derivatives and applying the general solution Eq.(6.19), which gives

$$\begin{aligned} \langle \pi_i \pi_j \rangle &= \pi^{-N/2}\sqrt{\det(\Omega)} \int \Big(\prod_{n=1}^{N} \mathrm{d}\phi_n\Big)(K_{ij}^{1/2} - \sum_{r,m}\sum_{k,l}\delta_{kj}\delta_{ri}K_{kl}K_{rm}\phi_l\phi_m) e^{-\Phi^T K^{1/2}\Phi} \\ &= \pi^{-N/2}\sqrt{\det(\Omega)} \int \Big(\prod_{n=1}^{N} \mathrm{d}\phi_n\Big)(K_{ij}^{1/2} - K_{jl}K_{im}\phi_l\phi_m) e^{-\Phi^T K^{1/2}\Phi}, \end{aligned} \tag{6.22}$$

where the first part of the integral is immediately seen to cancel the prefactor of Eq.(6.22) upon evaluation. The second part requires more care, as only the first-order expansion of Eq.(6.19) is non-vanishing. After acting with the derivatives $\partial_a \partial_{a'}$ on the fields and summing over the resulting delta-functions, we obtain

$$P_{ij} = \langle \pi_i \pi_j \rangle = K_{ij}^{1/2} - \frac{1}{2}K_{ia}^{1/2}K_{aa'}^{-1/2}K_{a'j}^{1/2} = \frac{1}{2}K_{ij}^{1/2}, \tag{6.23}$$

which confirms the vacuum correlators postulated in [15], in line with the derivation from [67].

As can rather easily be deduced from our discussion up to this point, the crux of our numerical scheme hides in determining the matrix $C = \sqrt{XP}$, for which no auxiliary matrices

had to be defined. The most straightforward and perhaps also most obvious route one can take, is marked by identifying the coupling matrix K from the previous chapter for a particular theory and using the relations specified in Eq.(6.20) and Eq.(6.23) to construct the matrix C. While this is a perfectly acceptable approach which leads to a small correction compared to Srednicki's scheme, as the algorithm is significantly shorter and more efficient, there are several less obvious routes which one may explore. We will list the three options explored in this chapter below, yet the reader is of course free to identify more paths leading to the matrix C.

1. This first route has a strong resemblance to Srednicki's paper, where one positions the scalar field on a finite lattice and then traces over the lattice sites of the pre-specified subregion A. After identification of K on the *full lattice* $\mathcal{M} = A \cup B$, one is able to compute C and determine Eq.(6.15). The advantage is its relative computational ease (the algorithm is much shorter than the previous one), yet, as before, one requires information of the full lattice $\mathcal{M}$, whereas the aim is to construct C from knowledge of A alone. A schematic approach to the calculation and algorithm is shown below.

$$\begin{array}{ccccc} K\big|_{\mathcal{M}} & \longrightarrow & X\big|_{\mathcal{M}} & \longrightarrow & X\big|_{A} \\ \downarrow & & & & \downarrow \\ P\big|_{\mathcal{M}} & \longrightarrow & P\big|_{A} & \longrightarrow & C\big|_{A} \end{array}$$

2. A second approach aims at finding a 'bypass' around K in the sense of the second approach discussed in Ch.5. Writing down the ground state wave functional for a simple, free scalar field theory (most of which have been extensively described in the literature), one is able to discretize (and if necessary decompose) the kernel $\Omega = K^{1/2} \sim P$ directly, therefore avoiding explicitly constructing K from the Hamiltonian. However, this approach tends to be more intensive from a computational perspective, which can easily be inferred from the schematic depiction below. Furthermore, as with route 1, we require the scalar to be placed on a *finite* lattice, where the calculation of C depends on $\mathcal{M}$ instead of solely on A, as argued below.

$$\begin{array}{ccccc} P\big|_{\mathcal{M}} & \longrightarrow & P\big|_{A} & \longrightarrow & C\big|_{A} \\ \downarrow & & & \nearrow & \\ X\big|_{\mathcal{M}} & \longrightarrow & X\big|_{A} & & \end{array}$$

3. The third, and potentially most interesting, route to Eq.(6.15) follows from finding the correlators $X\big|_{A}$ and $P\big|_{A}$ explicitly, such that $C\big|_{A}$ can be constructed *solely based* on knowledge of the region A. It is trivial to note that, in this case, one may consider $N \to \infty$, *i.e.* the full lattice can be taken to be infinitely large and no boundary

conditions for ϕ_{N+1}, $N \in \mathbb{Z}^+$, are required. The only disadvantage to this approach is the requirement that X and P must be evaluated, either numerically or (partially) analytically, without resorting explicitly to K. This may, as we will encounter later, lead to significant computational restraints.

$$\begin{array}{ccc} P\big|_A & \longrightarrow & C\big|_A \\ & \nearrow & \\ X\big|_A & & \end{array}$$

It should be noted that, in route 2, proceeding from $P\big|_A \sim K^{1/2}\big|_A$ to $X\big|_A \sim K^{-1/2}\big|_A$ directly, strictly requires computing $K^{1/2}$ on the full lattice $\mathcal{M}$. This can be understood rather easily by considering the decomposition of K in submatrices A, B and C, and partitioning K^{-1} into submatrices M, N and O, with the same dimensions as A, B and C, respectively. Since all submatrices are invertible, the submatrix $M = K^{-1}\big|_A$ is given by the Schur complement, *i.e.* finding $X\big|_A$ from $P\big|_A$ (or vice versa) requires us to find $M = (A - BC^{-1}B^T)$. We must therefore perform a partition of the full matrix P, instead of just considering its restriction to A. As such, despite the fact that one can use the kernel from a vacuum wave functional, we are still restricted to finite lattices. The advantage of the third route resides in the fact that this particular problem does not occur, provided both X and P can be evaluated explicitly.

6.2 Free scalar fields

The entanglement entropy of a scalar field theory, as demonstrated in the previous section, can be determined numerically through the knowledge of the correlators X and P, given by Eq.(6.20) and Eq.(6.23), respectively. Contrary to before, we will not provide an explicit pseudo-code, since the algorithm is a few lines at most. We will consider the numerical predictions for the three cases from Ch.5, specifically elucidating the third route when possible. In lieu of this approach, we shall consider the remaining routes.

6.2.1 $D = 1 \oplus 1$

Instead of deriving the matrix K again, we simply recall that we previously found

$$H = \frac{1}{2a} \sum_{i,j=1}^{N} [\pi_i \pi_j \delta_{ij} + \phi_i K_{ij} \phi_j], \tag{6.24}$$

where the interaction matrix was found to be

$$K_{ij} = 2\delta_{ij} - \delta_{i,j+1} - \delta_{i+1,j}. \tag{6.25}$$

As before, we impose the Dirichlet boundary conditions $\phi_0 = 0$ and $\phi_{N+1} = 0$. We are now able to consider the three different scenarios we explained earlier. Let us start with route 3, where the correlators are determined exactly. This particular example has been studied in [16], and we review it here. From the continuum theory, one is able to show that

$$\frac{\partial^2}{\partial r^2}\psi_k(r) = -k^2\psi_k(r), \tag{6.26}$$

which has the trivial solutions $\psi_k(r) = c_1 \sin(kr) + c_2 \cos(kr)$. In order to respect the boundary conditions, we must take $c_2 = 0$. Next, we discretize the radial coordinate and set $a = 1$, after which one can Fourier transform K_{ij} and derive the normalization constant $c_1 = 1/\sqrt{2\pi}$. Note that $k \in [-\pi, \pi]$ is restricted to the first Brioullin zone. According to [16], the correlators can therefore be written as

$$X_{ij} = \frac{1}{4\sqrt{2}\pi}\int_{-\pi}^{\pi} \mathrm{d}k \frac{\sin(ki)\sin(kj)}{|\sin(k/2)|} \tag{6.27}$$

and similarly

$$P_{ij} = \frac{1}{4\sqrt{2}\pi}\int_{-\pi}^{\pi} \mathrm{d}k |\sin(k/2)| \sin(ki)\sin(kj). \tag{6.28}$$

Both of these integrals can be evaluated using analytical evaluation software, which for the momentum correlator gives

$$P_{ij} = -\frac{4ij}{\pi(2(i^4+j^4) - (i^2+j^2) - 4i^2j^2 + \frac{1}{8})}. \tag{6.29}$$

For the position correlator, we introduce the digamma function $\psi(x)$, which is defined as $\psi(x) = \mathrm{d}\log\Gamma(x)/\mathrm{d}x$, with $\Gamma(x)$ the gamma function. Its solution can be shown to be

$$X_{ij} = \frac{1}{4\pi}(\psi[\frac{1}{2} - i - j] + \psi[\frac{1}{2} + i + j] - \psi[\frac{1}{2} + i - j] - \psi[\frac{1}{2} - i + j]). \tag{6.30}$$

We use these relations to construct the matrix $C = \sqrt{XP}$, after which Eq.(6.15) can be evaluated. Since the (discrete) correlators can be determined exactly for the region A, we take $N \to \infty$ and hence forsake the introduction of an IR-regulator. The von Neumann entropy is shown in fig.(6.2c). Note that the countably infinite lattice renders a convergence analysis moot, as the latter is assured. We note that this approach is similar to the formalism we discussed earlier, since $P = \frac{1}{2}K^{1/2} \equiv \frac{1}{2}\Omega$. Naively using the general kernels defined in [50] directly and employing the symmetry of the integral gives the incorrect result

$$\Omega \sim \int_{-\pi}^{\pi} \mathrm{d}k |\sin(k/2)| \cos(ik(n-n')), \tag{6.31}$$

as it does not take into account the appropriate boundary conditions. We recall from Ch.4 that the ground state wave functional for a (1+1)-dimensional free scalar theory has a kernel

given by

$$\Omega = \int_{-\pi}^{\pi} \frac{\mathrm{d}k}{2\pi} \omega(k) \tilde{\psi}(k;r) \tilde{\psi}^*(k;r'), \tag{6.32}$$

where ω is the solution to the eigenvalue equation $\hat{\Box}\tilde{\psi}(k;r) = -\omega^2\tilde{\psi}(k;r)$. The Fourier decomposed wave function $\tilde{\psi}$ has already been determined in Eq.(6.26). We express the d'Alembertian operator, which in this particular spacetime simply reduced to a 1-dimensional Laplacian, as a finite-difference scheme, such that one obtains

$$\begin{aligned}
\hat{\Box}\tilde{\psi}_n &= \frac{1}{a^2}[\tilde{\psi}_{n+1} + \tilde{\psi}_{n-1} - 2\tilde{\psi}_n] \\
&= \frac{1}{2ia^2}\sqrt{\frac{2}{\pi}}[e^{ik}(e^{ikn} - e^{-ikn}) + e^{-ik}(e^{ikn} - e^{-ikn}) - 2(e^{ikn} - e^{-ikn})] \\
&= \frac{1}{a^2}[e^{ik} + e^{-ik} - 2]\tilde{\psi}_n = -\frac{4}{a^2}\sin^2(\frac{k}{2})\tilde{\psi}_n,
\end{aligned} \tag{6.33}$$

where in the second line we have re-ordered the discrete derivative such that the sine-terms can be isolated, and the last line follows after application of some basic trigonometric identities. For the remainder of our discussion, we shall take $a = 1$, in line with before. Hence, the eigenvalues are found to be $\omega(k) = 2|\sin(k/2)|$, such that the kernel becomes

$$\Omega_{n,n'} = \frac{1}{\sqrt{2}\pi}\int_{-\pi}^{\pi} \mathrm{d}k |\sin(\frac{k}{2})| \sin(kn)\sin(kn'). \tag{6.34}$$

Hence, the method discussed in Ch.4 is equivalent to the exact route discussed in [16], and can equally well be used. From this point onwards one can either use the kernel as $P\big|_A$, invert this relation to obtain $X\big|_A$ and replicate the approach from the exact correlators, or one may decide to follow route 2 by using P to compute K on a finite lattice, compute its inverse and proceed with the steps outlined in route 1. Since we have not examined route 2 explicitly as of yet, we briefly compare its prediction with the exact kernel. The lattice was kept particularly small ($N = 60$), as the calculation is CPU intensive and the numerical integration is prone to convergence issues. Furthermore, we compare route 1 with the result from the previous chapter, which is shown in fig.(6.2a), together with the von Neumann entropy of the exact route. A convergence analysis is shown in fig.(5.5). We find that the entropy of Srednicki's algorithm and route 3 coincides on a lattice with $N = 500$ and a boundary value of $n_b \in [1, 100]$.

Similar to the previous chapter, we fit a function

$$S_A = \frac{c}{6}\log(\frac{2l_b}{a}) + d, \tag{6.35}$$

where $l_b = n_b a$, to the predictions of all three routes. The results for the fits are summarized in table 6.1. It can be seen that route 1 and route 3 produce relatively similar results, with the exact route indeed approximating $c = 1$ best.

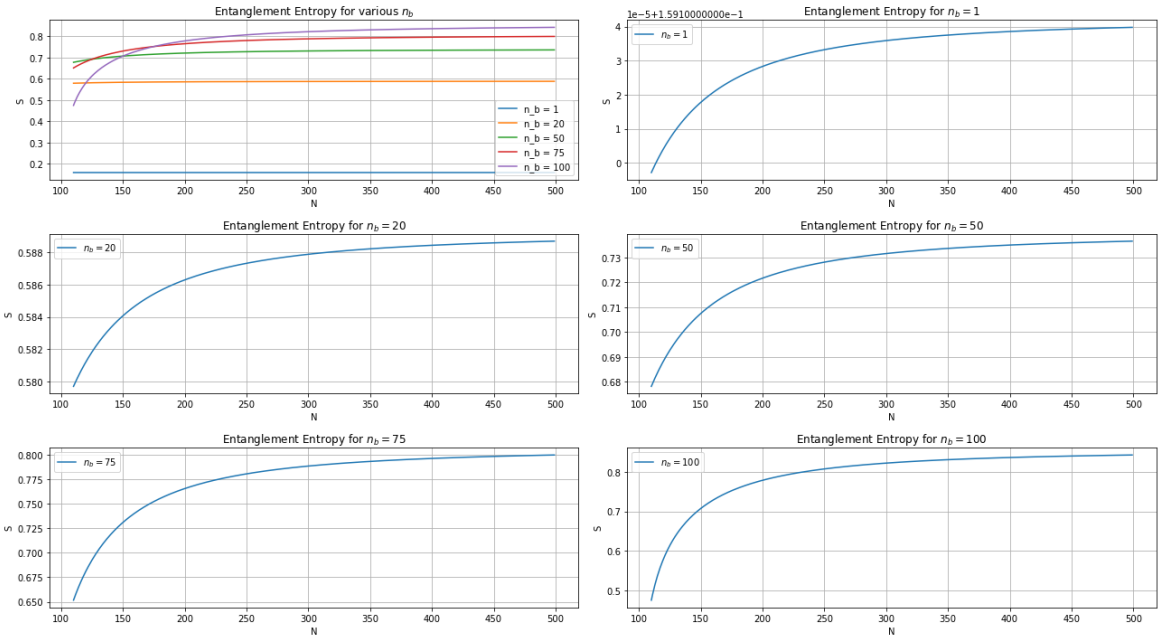

Fig. 6.1 A convergence analysis for the values $n_b \in \{1, 20, 50, 75, 100\}$ with a variable lattice size $N \in [110, 500]$.

	Route 1 ($N = 500$)	Route 2 ($N = 60$)	Route 3
c	0.937	0.849	0.953
d	0.048	0.015	0.006

Table 6.1 The obtained logarithmic coefficients and constants for the three described routes.

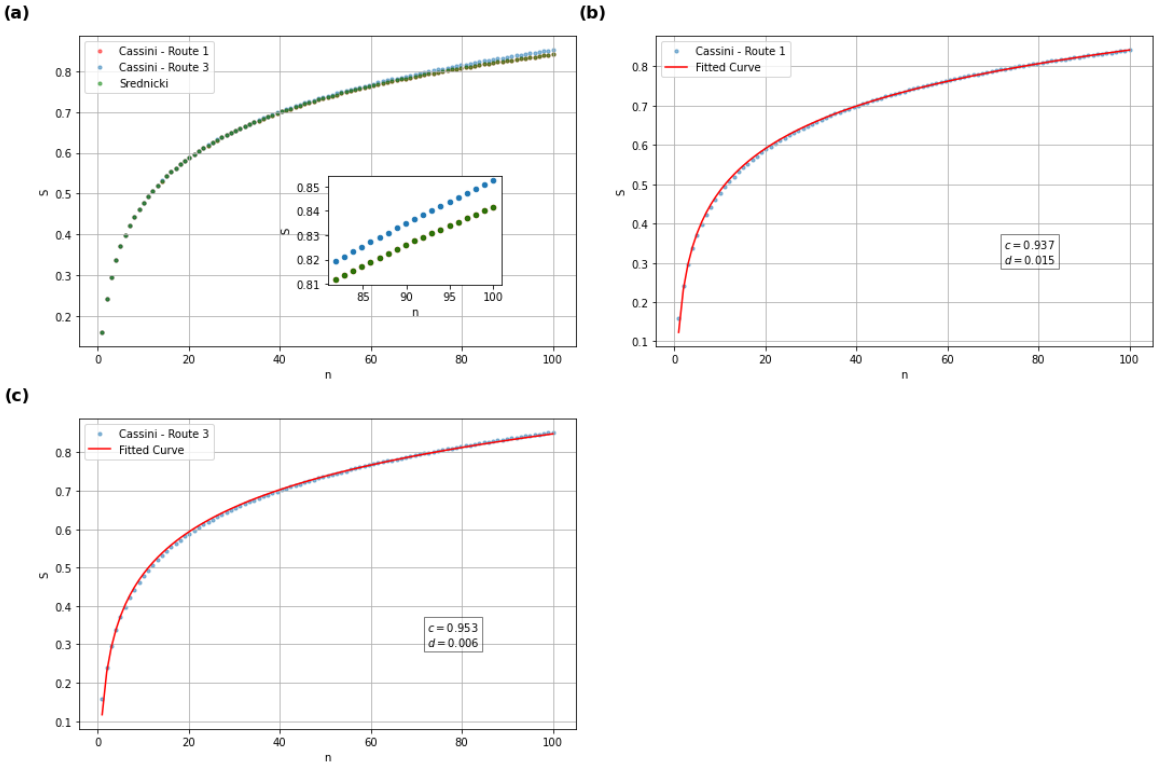

Fig. 6.2 Entanglement entropy of a (1+1)-dimensional scalar field via route 1 and 3 of Cassini's formalism, and Srednicki's formalism. The values of route 1 and Srednicki's approach are coincident for all values of n_b.

6.2.2 $D = 2 \oplus 1$

In previous we chapter we demonstrated that

$$K_{ij} = (\frac{3}{2} + m^2)\delta_{1,1} + (2 + \frac{m^2}{i^2})\delta_{i,j} - \frac{i+1/2}{\sqrt{i(i+1)}}\delta_{i,j+1} - \frac{i+1/2}{\sqrt{i(i+1)}}\delta_{i+1,j}. \tag{6.36}$$

We will rather quickly discuss the results from route 1, and then continue with the more direct kernel-based methods. Fig.(6.3a) demonstrates that convergence in N is reached rather quickly for a surface up to $n_b = 60$, where $N \geq 120$ already leads to approximate convergence of $S(N)$. In fig.(6.3b) we consider the contribution of each m to the von Neumann entropy to fixed, large N. It is apparent that $m_{\max} = 200$ causes convergence for the smaller values of n_b, whereas the contribution for $n_b > 30$ because negligibly small. The entanglement entropy for a region with $n_b \in [1, 30]$ with $N = 120$ and $m_{\max} = 200$ is shown in fig.(6.4a), which is shown to scale with its perimeter, as confirmed by the previous chapter's method. We demonstrate the existence of a decreasing logarithmic term in fig.(6.4b).[1] Fitting a function of the form

$$S_A = s\frac{L_b}{a} + c\log(\frac{L_b}{a}) + d, \tag{6.37}$$

where $L_b = n_b a$, to the curve yields coefficients $s = 0.468$, $c = -0.137$ and $d = 0.056$. We note that the term proportional to the perimeter is consistent with the value $s = 0.432$ from the previous chapter, yet the other coefficients are not identical. In order to confirm the possibility of the logarithmic term being negative, we attempted to compute the entanglement entropy through Eq.(4.42), while discretizing the radial coordinate of the Bessel function by $J_m(kr) \to J_m(kja)$, $j \in \mathbb{N}$. The entanglement entropy diverged for large m, despite the continuum kernel being apparently well defined. We considered various experiments with products of Bessel function of the first type and modified Bessel function of the first type, for which the issue kept repeating itself, despite the choice of dispersion (even when it was chosen to suppress the fast-growing contribution from the product). A specific cause for this problem has currently not been identified. However, it is possible that our straightforward method of discretizing the Bessel function accidentally contains zeros due to the oscillatory nature of the product, or does not accurately capture the features and properties of a Bessel function. In fact, discrete Bessel functions are typically obtained in a more involved manner, through defining $J_m(x) \to B_m(x_i)$, with $B_m(x_i)$ a non-trivial function reproducing all properties of the Bessel function [9, 77]. Hence, we turn our attention to a more tractable problem, where we position our scalar on a square lattice.

[1] However, in light the fact that subleading logarithmic terms may not exist for (2+1)-dimensional scalar fields, as mentioned in Ch.5, we could in fact be dealing with an artifact from the boundary. Luckily, these subleading terms are expected for square lattices, which will play an important part in this chapter.

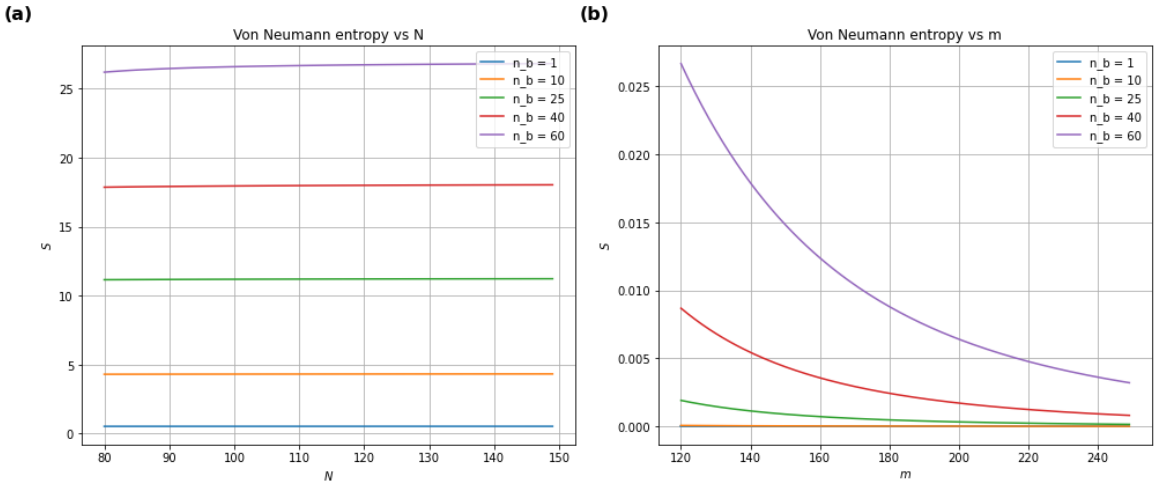

Fig. 6.3 Figure (a) shows the entanglement entropy for various n_b as a function of $N \in [80, 150]$. In subfigure (b) the contribution of each m to the total entropy for various n_b is shown.

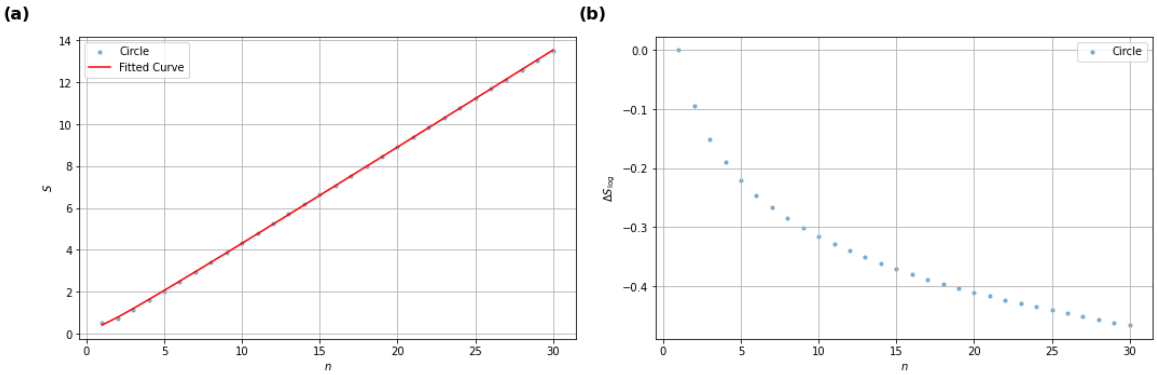

Fig. 6.4 In figure (a) we show the entanglement entropy for a subregion $n \in [1, 30]$ for a (2+1)-dimensional scalar field. Figure (b) displays the subleading term of the fit.

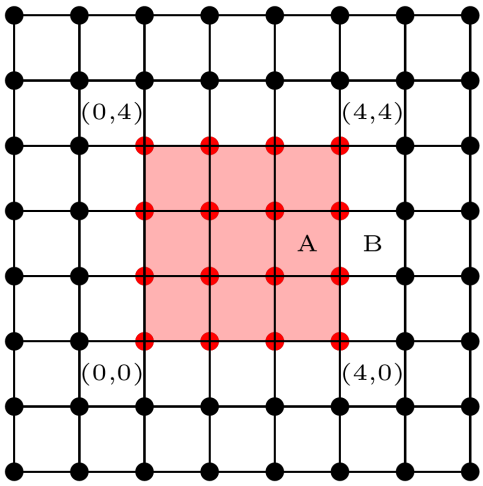

(a) Square subregion

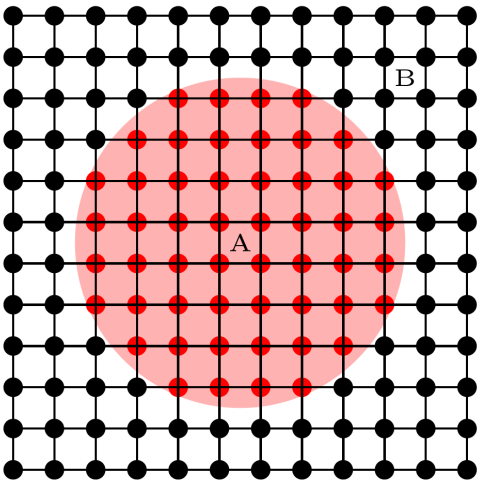

(b) Near-circular subregion

Fig. 6.5 The first figure is divided into a square sublattice A of size 4×4 and its complement B. In figure (b) sublattice A, consisting of the red lattice sites, is chosen such that it approximately describes the circle shown by the red shaded region.

Square lattice

We have seen that the proposed route via the discrete kernel, as well as route three from Cassini's formalism, fails when subjected to the algorithm. A possible solution to this problem is to 'coarse grain' our lattice, *i.e.* instead of integrating out the angular degrees of freedom, we eliminate their influence by considering a scalar on a square lattice. In this section our aim is to construct the kernel and correlators for such a lattice and experiment with various geometries for the region A. Their von Neumann entropy is calculated and (if applicable) compared to the approach through dimensional reduction. Fig(6.5) shows such a lattice, where the shaded area represents subregion A. We consider the Hamiltonian for a free, massless scalar field in $d = 2$, and $\mathbf{r} = (x, y)$. After Fourier transforming the coupling matrix, it can easily be shown that [15, 2]

$$\begin{aligned} K &= \frac{1}{(2\pi)^2} \int_{-\pi}^{\pi} \mathrm{d}k \int_{-\pi}^{\pi} \mathrm{d}k' \sqrt{2(1-\cos(k)) + 2(1-\cos(k'))} e^{i\mathbf{k}\cdot\mathbf{r}} \\ &= \frac{1}{2\pi^2} \int_{-\pi}^{\pi} \mathrm{d}k \int_{-\pi}^{\pi} \mathrm{d}k' \sqrt{\sin^2(k/2) + \sin^2(k'/2)} \cos(ki) \cos(k'j), \end{aligned} \tag{6.38}$$

where in the last line we have used Euler's identity and the symmetry of the integral on the first Brioullin zone. For convenience we have taken $x = ia$ with $a = 1$. The dispersion is a well-known relation for a square lattice, yet we will also derive it later, in a different context.

The propagators can therefore be written as

$$P_{(0,0),(i,j)} = \frac{1}{4\pi^2}\int_{-\pi}^{\pi}\int_{-\pi}^{\pi} \mathrm{d}k\mathrm{d}k' \sqrt{\sin^2(ki)+\sin^2(k'j)}\cos(ki)\cos(k'j), \tag{6.39}$$

$$X_{(0,0),(i,j)} = \frac{1}{16\pi^2}\int_{-\pi}^{\pi}\int_{-\pi}^{\pi} \mathrm{d}k\mathrm{d}k' \frac{\cos(ki)\cos(k'j)}{\sqrt{\sin^2(k/2)+\sin^2(k'/2)}}. \tag{6.40}$$

The integrand of Eq.(6.40) is divergent around $k, k' = 0$. By a Taylor expansion of the integrand around the origin, we identify the divergent part to be of the form $1/\sqrt{k^2+k'^2}$. This term can be evaluated analytically, *i.e.* one can show that

$$\frac{1}{16\pi^2}\int_{-\pi}^{\pi}\int_{-\pi}^{\pi} \mathrm{d}k\mathrm{d}k' \frac{1}{\sqrt{k^2+k'^2}} = \frac{1}{8\pi}\cosh^{-1}(17). \tag{6.41}$$

We subtract the non-evaluated part from the integrand of Eq.(6.40) and add the analytical result of Eq.(6.41). The correlator then becomes

$$X_{(0,0),(i,j)} = \Big(\frac{1}{8\pi^2}\int_{-\pi}^{\pi}\int_{-\pi}^{\pi} \mathrm{d}k\mathrm{d}k' \frac{\cos(ki)\cos(k'j) - \sqrt{4\sin^2(k/2)+4\sin^2(k'j)}/\sqrt{k^2+k'^2}}{\sqrt{4\sin^2(k/2)+4\sin^2(k'j)}}\Big) + \frac{1}{4\pi}\cosh^{-1}(17). \tag{6.42}$$

The part in between brackets can be determined numerically, since it is no longer troubled by singularities. However, since the integration is highly time-intensive (even for small lattices), it may benefit to evaluate one of the integrals analytically, which we performed using analytical evaluation software. This results in expressions for the correlators involving regularized hypergeometric functions:

$$P_{(0,0),(i,j)} = \frac{1}{2\sqrt{2}\pi}\int_{-\pi}^{\pi} \mathrm{d}k \frac{\sqrt{3-\cos(k)}\cos(ki)}{\Gamma(1-j)\Gamma(1+j)} {}_3F_2[\{-\frac{1}{2},\frac{1}{2},1\},\{1-j,1+j\},\frac{2}{3-\cos(k)}], \tag{6.43}$$

$$X_{(0,0),(i,j)} = \frac{1}{8\pi^2}\int_{-\pi}^{\pi} \mathrm{d}k \{\frac{\cos(ki)}{\sqrt{3-\cos(k)}\Gamma(1-j)\Gamma(1+j)} {}_3F_2[\{-\frac{1}{2},\frac{1}{2},1\},\{1-j,1+j\},\frac{2}{3-\cos(k)}] + \log(1+\frac{2\pi}{k^2}(\pi-\sqrt{\pi^2+k^2}))\} + \frac{1}{2}\cosh^{-1}(17), \tag{6.44}$$

where $\Gamma(x)$ is the Euler gamma function. For smaller lattices the expressions above only yield a small difference in terms of computation time, yet for large lattices they bring about a large improvement. The discrete-kernel method can be shown to reduce to Eq.(6.43) and Eq.(6.44) as well by considering Eq.(4.8) and taking the Fourier transform of the fields after

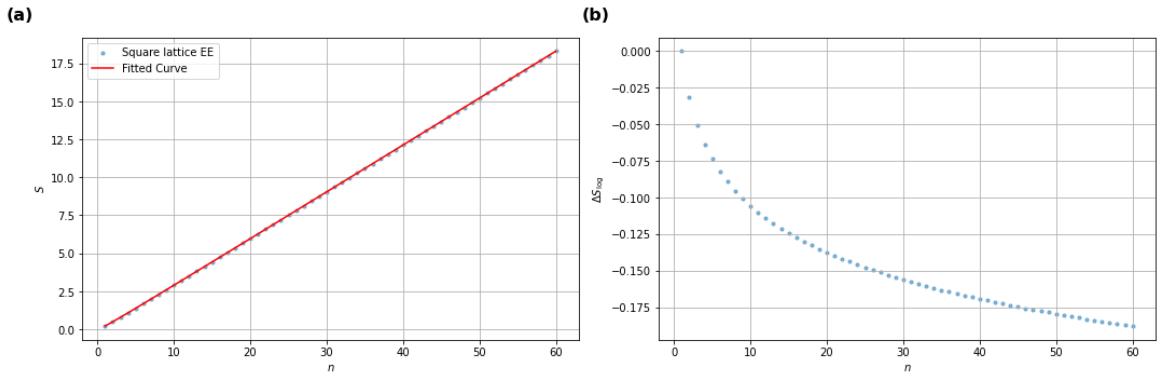

Fig. 6.6 Subplot (a) shows the entanglement entropy of a square lattice with sides $n \in [1, 60]$. In (b) we demonstrate the logarithmic correction to each of these squares.

discretizing $\mathbf{r}$ according to fig.(6.5). Hence, we find

$$\Omega = \int_{-\pi}^{\pi} \frac{\mathrm{d}\mathbf{k}}{(2\pi)^2} \omega(k) e^{i\mathbf{k}\cdot(\mathbf{r}-\mathbf{r}')} \to \sum_{n,n'} \frac{1}{a^2} \int_{-\pi}^{\pi} \frac{\mathrm{d}\mathbf{k}}{(2\pi)^2} \omega(k) \cos(k_x(n_x - n'_x)) \cos(k_y(n_y - n'_y)). \tag{6.45}$$

where we have taken $\tilde{\psi}(\mathbf{k};\mathbf{r}) = e^{i\mathbf{k}\cdot\mathbf{r}}$. Note that, contrary to before, we need not concern ourselves with imposing boundary conditions. We denote the difference between the lattice points as $n = n_x - n'_x$ and $n' = n_y - n'_y$, such that the equation reduces to Eq.(6.39), yet currently without a concrete relation for the dispersion. As in the one-dimensional case, we set forth to solve the eigenvalue problem $\hat{\Box}\tilde{\psi} = -\omega^2\tilde{\psi}$, which for the coordinates describing the square lattice takes the form

$$\begin{aligned} \hat{\Box}\tilde{\psi}(\mathbf{k};\mathbf{r}) &= \sum_{j\in\{1,2\}} \frac{\partial^2}{\partial r_j^2} \tilde{\psi}(\mathbf{k};\mathbf{r}) \to \frac{1}{a^2} \sum_{j\in\{1,2\}} (\tilde{\psi}_{n_j+1} + \tilde{\psi}_{n_j-1} - 2\tilde{\psi}_{n_j}) \\ &= \frac{4}{a^2} \sum_{j\in\{1,2\}} [(e^{ik_j} + e^{-ik_j} - 2)e^{ik_j n_j}] = \frac{1}{a^2} \sum_{j\in\{1,2\}} \sin^2(\frac{k_j}{2})\tilde{\psi}_{n_j}. \end{aligned} \tag{6.46}$$

In the first line we have used the stencil for the Laplacian from the one-dimensional case, after which the discussion is identical. Hence, the eigenvalues become $\omega(\mathbf{k}) = 2\sum_{j\in\{1,2\}} |\sin(\frac{k_j}{2})|$, such that the discrete kernel is seen to reduce to the correlator P given by Eq.(6.39). Now that we are able to build the X and P matrices for the shaded region of fig.(6.5), or for that matter of any subregion A of the lattice, we will examine its entanglement entropy as a function of the size of A. Or more accurately put: as a function of its perimeter. First, we shall consider the von Neumann entropy of a square. After obtaining the leading terms for the square lattice we aim to approximate circular lattices through the discrete circle shown in fig.(6.5b). The latter will subsequently be compared to the 2-dimensional lattice predictions using dimensional reduction, as to gauge whether the discrete circles could be

used to accurately predict the entanglement entropy of a circular subregion. We keep the analysis of the square lattice rather brief, as the results have been at length discussed in [17]. A numerical simulation determining the entanglement entropy as a function of the length n of the square's sides and its logarithmic contribution is shown in fig.(6.6). Upon denoting the sides of the square as $L = na$, we may fit a function

$$S_A = s\frac{L}{a} + c\log(\frac{L}{a}) + d \tag{6.47}$$

to the curve, which yields the coefficients $s = 0.310$, $c = -0.046$ and $d = -0.091$. Hence, we are allowed to write the von Neumann entropy of the square as

$$S_A = 0.077\frac{P(n)}{a} - 0.046\log(\frac{n}{a}) - 0.091, \tag{6.48}$$

where $P(n) = 4na$ denotes the perimeter of the square. This indeed demonstrates that the entanglement entropy scales with the perimeter of the geometry when considering a scalar field on a square lattice. Note that the constant $a/4 = 0.077$ does not match the result from [17], where the authors seem to have missed a factor 10^{-1} and wrote $a = 0.75$, yet show figures where the correct constant has been used.

The discrete circle drawn in fig.(6.5b) is not necessarily more difficult to build, as we simply restrict the tuples (i, j) of the correlators to a region $|i - j| \leq n$, where n denotes the radius of the discrete circle. The discrete radius is defined as $n = \lfloor r \rfloor$, where r is the actual radius of the circle. We determined the entanglement entropy for a discrete circle with radius $n \in [1, 30]$, as shown in fig.(6.7a). We subtracted the linear terms and constant from the entropy to elucidate its logarithmic contribution, which is shown in fig.(6.7b). We fitted the function Eq.(6.37) to the curve, after which we found the coefficients $s = 0.528$, $c = -0.033$ and $d = -0.081$. Fig.(6.7) also contains our earlier results for the entropy of a circle obtained by dimensional reduction. We observe that the linear contribution to the entropy as a function of the radius is overestimated by the discrete circle ($s = 0.538$ vs $s = 0.468$). The logarithmic coefficient is of the right sign, but smaller ($c = -0.033$ vs $c = -0.137$), such that it is underestimated. The constant is of the same order and sign ($d = 0.081$ vs $d = 0.056$). However, since the entanglement entropy is expected to scale with the perimeter of the geometry, selecting the discrete radius n for comparing a discrete circle and actual circle could possibly lead to a distorted picture, as their perimeter is different. In fig.(6.8) we compare the von Neumann entropy of the discrete circle and actual circle as a function of their perimeter. The perimeter of the discrete circle is found by means of the Manhattan geometry and calculated for each n. A fit of Eq.(6.37) to the curve of the discrete circle, while substituting the perimeter for the radius in the linear term, gives the coefficient $s = 0.06725$. The associated coefficient for the actual circle is easily obtained

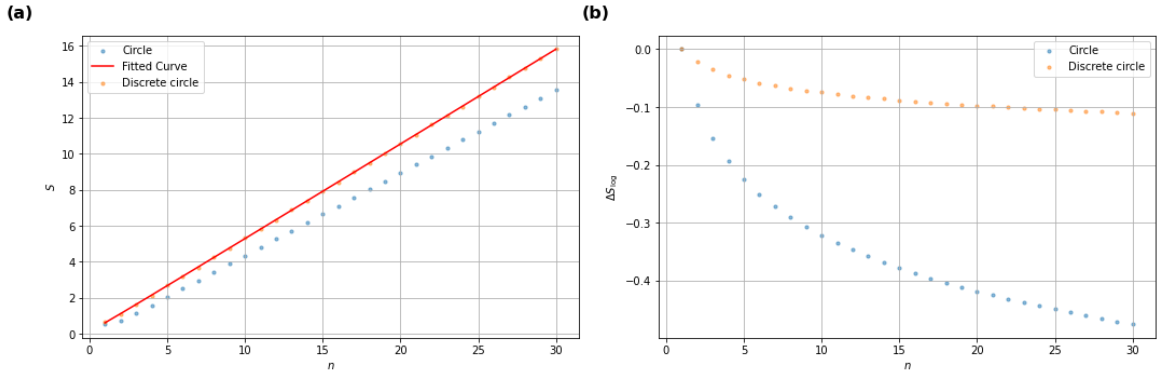

Fig. 6.7 The circle versus the discrete circle as a function of the length $n \in [1, 30]$. The area-law is shown in subplot (a), while the logarithmic correction is shown in (b).

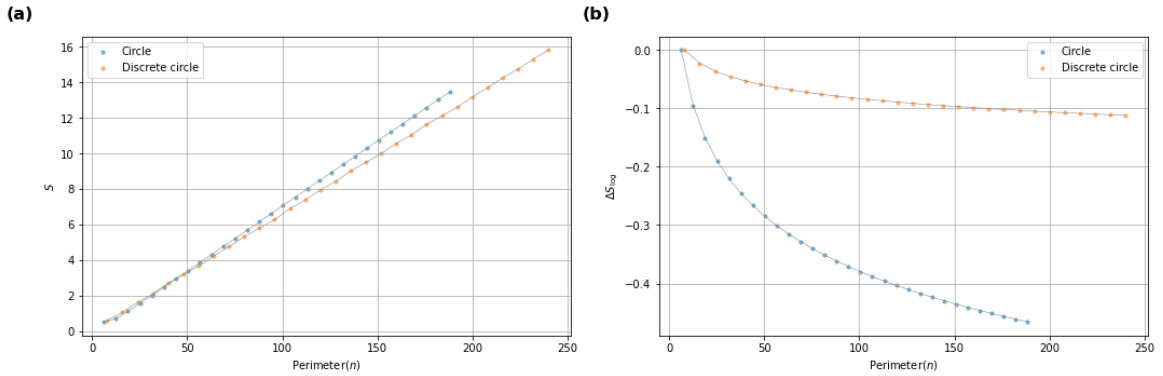

Fig. 6.8 The circle versus the discrete circle in terms of the perimeter. The predicted entanglement entropies approximately coincide for small values of the perimeter. Subplot (b) show the rescaled logarithmic correction.

through $\tilde{s} = s/2\pi \approx 0.0744$. It is shown that the entropies approximately coincide for small perimeters ($P(n) < 75$), corresponding to $r \approx 11.9$ for an actual circle. The logarithmic contributions are still both decreasing and of the same sign, yet is underestimated by the discrete circle. Since this contribution is small with respect to the total $S(n)$ for $P(n) < 25$, corresponding to $r \approx 4$, the discrete circle can potentially be used to approximate circular regions of (2+1)-dimensional scalars on non-square lattices, especially when one is only interested in the contributions scaling with the perimeter. The systematic under-fitting for larger, equal perimeters by the discrete circle can be understood by the density of oscillators in equal-perimeter systems. We recall that the dimensionally reduced circular region of radius r_b contains r_b 1-spheres S^1 of the scalar field condensed into single harmonic oscillators. In a sense, we can think of these as circular shells of 'smeared out' harmonic oscillators. A circle with an area equal to the discrete circle will therefore have a larger density of oscillators, and hence consistently results in a larger entanglement entropy

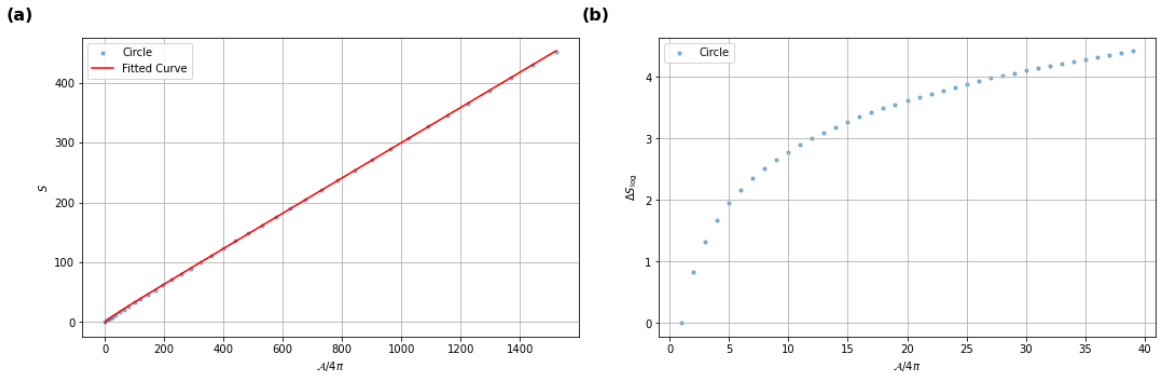

Fig. 6.9 The entanglement entropy for a (3+1)-dimensional scalar field as a function of $n_b \in [1, 40]$. The increasing logarithmic correction is shown in subplot (b).

6.2.3 $D = 3 \oplus 1$

We will keep this last section brief, since the discussion is very similar to the one from Ch.5. The entanglement entropy can be shown to convergence for $N = 200$ and $m = 500$, using a convergence analysis of the type we performed before. Fig.(6.9a) shows the entanglement entropy of the (3+1)-dimensional scalar, to which a function of the type Eq.(5.83) has been fitted. The resulting coefficients are $s = 0.293$, $c = 1.207$ and $d = 1.616$. Both the s-coefficient and the logarithmic coefficient are of the same order of magnitude as the ones from Ch.5, where the logarithmic correction is increasing with n_b, as shown in fig.(6.9b), for which the presence can be explained by means of the same argument we used in Ch.5.

Chapter 7

Conclusion and Outlook

This thesis set about to investigate the entanglement entropy of the analogue black hole proposed in [48]. Despite not being able to achieve this particular goal, we managed to describe and build the necessary ingredients for a successor to approach the aforementioned target through a more well-rounded approach. We have conducted a review of analogue black holes, which we extended to describing (in detail) the analogue proposed in [48], followed by an extensive description of various numerical methods to determine the entanglement entropy of free, massless scalar fields in the ground state. We build the associated algorithms and tested them for multiple scalar fields on flat backgrounds, after which we suggested improvements for greater accuracy.

In Chapter 3, we commenced by studying a classical, water-based analogue black hole, first suggested by [75]. Through using the hydrodynamic equations we demonstrated that, while the background fluid couples to the Minkowski metric, the acoustic perturbations are in fact described by the equation of motion of a free, massless scalar field coupled to a non-trivial acoustic metric. Under an appropriately chosen coordinate transformation this metric was seen to reduce to a Schwarzschild-*like* form, including the presence of an acoustic horizon. Subsequently, we extended our discussion to Bose-Einstein condensates in the hydrodynamic regime. We found the same trend as for the classical case, where the superfluid coupled to the Minkowski metric, while the phonons are governed by the equation of motion for a free, massless scalar field coupled to a Schwarzschild-*like* metric. We elaborated on the latter through a review of [48], which explores an analogue black hole in a Bose-Einstein condensate of light. It was demonstrated that the horizon of this analogue is able to emit acoustic radiation, while an effective potential arose by the propagation of the phonons on a non-trivial background. A possible correlation between phonons in the supersonic and subsonic region was mentioned, and we stipulated the need to compute the entanglement entropy of the acoustic radiation.

The beginning of Chapter 4 temporarily removed our focus from the analogue black hole, as we attempted to derive the ground state wave functional of a (2+1)-dimensional scalar field on a flat background. We extended this analysis by reviewing [50, 51], where the authors derived the expressions to obtain the Schrödinger wave functional for scalar fields on curved spacetimes, in such a way that only the Fourier modes of the field and the metric of the spacetime are required. We considered two examples; one related to our previous derivation of the (2+1)-dimensional vacuum wave functional, and one suggested in [51], which both confirmed the reviewed formalism. We reconciled with our analogue black hole by attempting to write down a vacuum wave functional by means of the Schwarzschild-*like* metric and the radial modes from [48]. However, before we may adopt this expression as the ground state wave functional of our system, and potentially subject it to the algorithms built in Chapter 5 and Chapter 6, we must perform further verification by deriving the expectation value of the total number of emitted particles, and confirm that the radial modes indeed meet the requirements set in [50, 51].

Our discussion of the entanglement entropy followed two numerical schemes, first described in [69] and [15]. Chapter 5 aimed at the former, where we performed a radial discretization of free, massless scalar fields and 'mapped' these regularized fields onto finite one-dimensional chains of harmonic oscillators. The ground state wave function of the chain and the reduced density matrix of an arbitrary subregion could be determined exactly, after which we were able to numerically compute the entanglement entropy by means of the coupling matrix. This matrix was solely dependent on (ratios of) the dispersions and coupling constants of the oscillators, and hence could simply be read off from the Hamiltonian of the discrete system. We reproduced the area-law found in [69] for a (3+1)-dimensional scalar field, yet encountered a discrepancy for the logarithmic coefficient from [49]. However, it seems likely that the 'overfitting' of the logarithmic term is a remnant from the influence of the boundary of the chain at the origin. In fact, in [49] the authors did not fit the expected relation for the entanglement entropy to all possible entangling surfaces contained by the subregion in question, as we did, but instead only fitted the function to those entangling surfaces contained by the subset which were sufficiently far removed from the origin, such that the influence of the boundary on the fit was minimized. Adopting this approach in our methodology will likely result in the correct logarithmic coefficient $c = -1/90$. Subjecting our approach to a (1+1)-dimensional free, massless scalar yielded the correct behaviour of the entanglement entropy when compared to the CFT results from [13]. The fitted function was shown to capture the correct logarithmic behaviour of the entanglement entropy, while reproducing a coefficient $c/6 \approx 1/6$, as predicted in [13]. For the (2+1)-dimensional scalar, the entanglement entropy appeared to scale with the perimeter of the subregion, yet care is required with respect to the subleading terms we included in our fit. There exists the distinct possibility that they arose from the boundary at the origin, and should not be present at all. Contrary

to the (1+1)-dimensional and (3+1)-dimensional scalars, the present case requires more care before being extrapolated to our analogue black hole.

The last chapter was based on [15], which extends the method of Chapter 5 to one where only the position and momentum correlators restricted to a subregion of the chain are required to compute the entanglement entropy. Apart from optimizing the algorithm suggested in Chapter 5, the route taken in Chapter 6 offers the option of analytically determining the correlators on the subregion, after which one may take the chain length $N \to \infty$. The latter proved possible for a (1+1)-dimensional free, massless scalar field, which resulted in an improvement of the obtained coefficient compared with the methods requiring knowledge of the full (finite) chain. Furthermore, we demonstrated that discretizing the continuum-spacetime kernel from Chapter 4 could be reduced to the method described above, and hence could potentially be used for more complicated spacetimes. However, when the method was extended to (2+1)-dimensional scalar fields, we found that both the exact-corrrelator route and the discretized continuum-kernel approach were unable to capture the entanglement entropy. This could potentially be resolved by means of a more accurate discretization scheme for Bessel functions, as suggested in [9, 77]. Subsequently, we attempted to simplify the simulations by removing the angular dependence of the system altogether, and as such considered scalar fields on square lattices. We determined the entanglement entropy of both square sublattices and discrete-circular sublattices. The entanglement entropy of the former was shown to scale with its perimeter, including a negative logarithmic coefficient. The latter was shown to obey a similar relation, and can be used to approximate the entropy of circular subregions of small radius.

The extension of [69] to the outer region of Schwarzschild black holes has already been achieved in [53], where the authors discretize the proper length from the horizon and compute the entanglement entropy of shells enclosing the horizon. However, extending the method from [69] to both the supersonic and subsonic region of the analogue black hole is slightly more problematic, since in the supersonic region the warping factor, which is included in the Hamiltonian and the continuum-kernel, becomes negative. As such, the coupling matrix is no longer semi-positive, and implementation of the algorithm fails. The method described in Chapter 6 might therefore prove more useful, as one could envision computing the correlators on the subsonic region, and using the algorithm from [15] to predict its entanglement entropy with respect to the supersonic region. Yet at the moment this is mere wishful thinking, as the technical obstacles are still great. On this note, hoping to have provided all that is needed to solve the original aim of this thesis, we pass the baton to our successors, and hope they learn as much about the wonders of analogue black holes and entanglement entropy as we have.

References

[1] Abramowitz, M. and Stegun, I. A. (1948). *Handbook of mathematical functions with formulas, graphs, and mathematical tables*, volume 55. US Government printing office.

[2] Agón, C., Bueno, P., and Casini, H. (2022). Tripartite information at long distances. *SciPost Physics*, 12(5):153.

[3] Almeida, C. R. and Jacquet, M. J. (2023). Analogue gravity and the hawking effect: historical perspective and literature review. *The European Physical Journal H*, 48(1):15.

[4] Arfken, G. B. and Weber, H.-J. (1972). Mathematical methods for physicists.

[5] Barcelo, C., Liberati, S., and Visser, M. (2001). Analogue gravity from bose-einstein condensates. *Classical and Quantum Gravity*, 18(6):1137.

[6] Barcelo, C., Liberati, S., and Visser, M. (2011). Analogue gravity. *Living reviews in relativity*, 14:1–159.

[7] Basak, S. and Majumdar, P. (2003). Reflection coefficient for superresonant scattering. *Classical and Quantum Gravity*, 20(13):2929.

[8] Berti, E., Cardoso, V., and Lemos, J. P. (2004). Quasinormal modes and classical wave propagation in analogue black holes. *Physical Review D*, 70(12):124006.

[9] Biagetti, G., Crippa, P., Falaschetti, L., and Turchetti, C. (2016). Discrete bessel functions for representing the class of finite duration decaying sequences. In *2016 24th European Signal Processing Conference (EUSIPCO)*, pages 2126–2130. IEEE.

[10] Birrell, N. D. and Davies, P. C. W. (1984). Quantum fields in curved space.

[11] Bombelli, L., Koul, R. K., Lee, J., and Sorkin, R. D. (1986). Quantum source of entropy for black holes. *Physical Review D*, 34(2):373.

[12] Braunstein, S. L., Faizal, M., Krauss, L. M., Marino, F., and Shah, N. A. (2023). Analogue simulations of quantum gravity with fluids. *Nature Reviews Physics*, 5(10):612–622.

[13] Calabrese, P. and Cardy, J. (2009). Entanglement entropy and conformal field theory. *Journal of physics a: mathematical and theoretical*, 42(50):504005.

[14] Carroll, S. M. (2019). *Spacetime and geometry*. Cambridge University Press.

[15] Casini, H. and Huerta, M. (2009). Entanglement entropy in free quantum field theory. *Journal of Physics A: Mathematical and Theoretical*, 42(50):504007.

[16] Casini, H. and Huerta, M. (2016). Entanglement entropy of a maxwell field on the sphere. *Physical Review D*, 93(10):105031.

[17] Casini, H. and Huerta, M. (2022). Lectures on entanglement in quantum field theory. *arXiv preprint arXiv:2201.13310*.

[18] Castin, Y. (2002). Bose-einstein condensates in atomic gases: simple theoretical results. In *Coherent atomic matter waves: 27 July–27 August 1999*, pages 1–136. Springer.

[19] Chung, M.-C. and Peschel, I. (2000). Density-matrix spectra for two-dimensional quantum systems. *Physical Review B*, 62(7):4191.

[20] Človečko, M., Gažo, E., Kupka, M., and Skyba, P. (2019). Magnonic analog of black-and white-hole horizons in superfluid he 3-b. *Physical Review Letters*, 123(16):161302.

[21] Cover, T. M. (2006). *Elements of information theory*. John Wiley & Sons.

[22] Dalmonte, M., Eisler, V., Falconi, M., and Vermersch, B. (2022). Entanglement hamiltonians: from field theory to lattice models and experiments. *Annalen der Physik*, 534(11):2200064.

[23] de Nova, J. R. M., Golubkov, K., Kolobov, V. I., and Steinhauer, J. (2018). Observation of thermal hawking radiation at the hawking temperature in an analogue black hole. *arXiv preprint arXiv:1809.00913*.

[24] de Souza Menicucci, L. (2022). Entanglement entropy of free scalar fields, a numerical study. Master's thesis.

[25] De Wolf, R. (2019). Quantum computing: Lecture notes. *arXiv preprint arXiv:1907.09415*.

[26] Eisert, J., Cramer, M., and Plenio, M. B. (2010). Colloquium: Area laws for the entanglement entropy. *Reviews of modern physics*, 82(1):277–306.

[27] Erdélyi, A. (1953). Higher transcendental functions. *Higher transcendental functions*, page 59.

[28] Freeden, W. and Schreiner, M. (2022). *Spherical functions of mathematical geosciences: a scalar, vectorial, and tensorial setup*. Springer Nature.

[29] Freese, K., Hill, C. T., and Mueller, M. (1985). Covariant functional schrödinger formalism and application to the hawking effect. *Nuclear Physics B*, 255:693–716.

[30] Fulling, S. A. (1973). Nonuniqueness of canonical field quantization in riemannian space-time. *Physical Review D*, 7(10):2850.

[31] Fulling, S. A. (1989). *Aspects of quantum field theory in curved spacetime*. Number 17. Cambridge university press.

[32] González-Fernández, B. and Camacho, A. (2019). Accelerated observers emerging from a bose-einstein condensate through analogue gravity. *arXiv preprint arXiv:1904.02299*.

[33] Gradshteyn, I. S. and Ryzhik, I. M. (2014). *Table of integrals, series, and products*. Academic press.

[34] Griffiths, D. J. and Schroeter, D. F. (2018). *Introduction to quantum mechanics*. Cambridge university press.

[35] Gubser, S. S. and Klebanov, I. R. (1996). Four-dimensional greybody factors and the effective string. *Physical review letters*, 77(22):4491.

[36] Hawking, S. W. (1975). Particle creation by black holes. *Communications in mathematical physics*, 43(3):199–220.

[37] Headrick, M. (2019). Lectures on entanglement entropy in field theory and holography. *arXiv preprint arXiv:1907.08126*.

[38] Hill, C. T. (1986). One-loop operator matrix elements in the unruh vacuum. *Nuclear Physics B*, 277:547–574.

[39] Huerta, M. (2012). Numerical determination of the entanglement entropy for free fields in the cylinder. *Physics Letters B*, 710(4-5):691–696.

[40] Huerta, M. and Pedraza, L. A. (2018). Numerical determination of the entanglement entropy for a maxwell field in the cylinder. *arXiv preprint arXiv:1808.01864*.

[41] Islam, R., Ma, R., Preiss, P. M., Eric Tai, M., Lukin, A., Rispoli, M., and Greiner, M. (2015). Measuring entanglement entropy in a quantum many-body system. *Nature*, 528(7580):77–83.

[42] Jackson, J. D. (2021). *Classical electrodynamics*. John Wiley & Sons.

[43] Jannes, G. (2009). Emergent gravity: the bec paradigm. *arXiv preprint arXiv:0907.2839*.

[44] Jefferson, R. (2021). Qft in curved space, part 2: Bogolyubov transformations and the unruh effect. *Blogpost*.

[45] Katsinis, D., Pastras, G., and Tetradis, N. (2023). Entanglement of harmonic systems in squeezed states. *Journal of High Energy Physics*, 2023(10):1–71.

[46] Landau, L. D. and Lifshitz, E. M. (2013a). *Fluid mechanics: Landau And Lifshitz: course of theoretical physics, Volume 6*, volume 6. Elsevier.

[47] Landau, L. D. and Lifshitz, E. M. (2013b). *Quantum mechanics: non-relativistic theory*, volume 3. Elsevier.

[48] Liao, L., Van Der Wurff, E., Van Oosten, D., and Stoof, H. (2019). Proposal for an analog schwarzschild black hole in condensates of light. *Physical Review A*, 99(2):023850.

[49] Lohmayer, R., Neuberger, H., Schwimmer, A., and Theisen, S. (2010). Numerical determination of entanglement entropy for a sphere. *Physics Letters B*, 685(2-3):222–227.

[50] Long, D. and Shore, G. (1998a). The schrödinger wave functional and vacuum states in curved spacetime. *Nuclear physics B*, 530(1-2):247–278.

[51] Long, D. and Shore, G. (1998b). The schrödinger wave functional and vacuum states in curved spacetime. *Nuclear physics B*, 530(1-2):247–278.

[52] Mukhanov, V. and Winitzki, S. (2007). *Introduction to quantum effects in gravity*. Cambridge university press.

[53] Mukohyama, S., Seriu, M., and Kodama, H. (1998). Thermodynamics of entanglement in schwarzschild spacetime. *Physical Review D*, 58(6):064001.

[54] Müller-Lennert, M., Dupuis, F., Szehr, O., Fehr, S., and Tomamichel, M. (2013). On quantum rényi entropies: A new generalization and some properties. *Journal of Mathematical Physics*, 54(12).

[55] Muñoz de Nova, J. R., Golubkov, K., Kolobov, V. I., and Steinhauer, J. (2019). Observation of thermal hawking radiation and its temperature in an analogue black hole. *Nature*, 569(7758):688–691.

[56] Murphy, K. P. (2012). *Machine learning: a probabilistic perspective*. MIT press.

[57] Nielsen, M. A. and Chuang, I. L. (2010). *Quantum computation and quantum information*. Cambridge university press.

[58] Nishioka, T. (2018). Entanglement entropy: holography and renormalization group. *Reviews of Modern Physics*, 90(3):035007.

[59] Olver, F. W. J. and Maximon, L. C. (2010). *NIST Digital Library of Mathematical Functions*. National Institute of Standards and Technology. https://dlmf.nist.gov/.

[60] Peschel, I. (2003). Calculation of reduced density matrices from correlation functions. *Journal of Physics A: Mathematical and General*, 36(14):L205.

[61] Peschel, I. and Chung, M.-C. (1999). Density matrices for a chain of oscillators. *Journal of Physics A: Mathematical and General*, 32(48):8419.

[62] Pethick, C. J. and Smith, H. (2008). *Bose–Einstein condensation in dilute gases*. Cambridge university press.

[63] Pitaevski, L. P. (1998). Bose–einstein condensation in magnetic traps. introduction to the theory. *Physics-Uspekhi*, 41(6):569.

[64] Rottoli, F., Fossati, M., and Calabrese, P. (2024). Entanglement hamiltonian in the non-hermitian ssh model. *Journal of Statistical Mechanics: Theory and Experiment*, 2024(6):063102.

[65] Sakurai, J. (1994). *Modern Quantum Mechanics*. Addison-Wesley Publishing Company.

[66] Schmitt, A. (2015). Introduction to superfluidity. *Lect. Notes Phys*, 888(1).

[67] Soldati, R. (2019). Entanglement entropy in quantum field theory. Master's thesis.

[68] Srdinšek, M. (2023). *Numerical evaluation of Rényi entropy with path integrals*. PhD thesis, Sorbonne Université.

[69] Srednicki, M. (1993). Entropy and area. *Physical Review Letters*, 71(5):666.

[70] Srednicki, M. (2007). *Quantum field theory*. Cambridge University Press.

[71] Steinhauer, J. (2014). Observation of self-amplifying hawking radiation in an analogue black-hole laser. *Nature Physics*, 10(11):864–869.

[72] Stoof, H. T., Gubbels, K. B., and Dickerscheid, D. (2009). *Ultracold quantum fields*. Springer.

[73] Thebault, K. P. (2016). What can we learn from analogue experiments? *arXiv preprint arXiv:1610.05028*.

[74] Unruh, W. (1994). Dumb holes and the effects of high frequencies on black hole evaporation. *arXiv preprint gr-qc/9409008*.

[75] Unruh, W. G. (1981). Experimental black-hole evaporation? *Physical Review Letters*, 46(21):1351.

[76] Unruh, W. G. (1995). Sonic analogue of black holes and the effects of high frequencies on black hole evaporation. *Physical Review D*, 51(6):2827.

[77] Uriostegui, K. and Wolf, K. B. (2020). Discrete bessel functions and transform. *arXiv preprint arXiv:2005.06076*.

[78] Visser, M. (1993). Acoustic propagation in fluids: an unexpected example of lorentzian geometry. *arXiv preprint gr-qc/9311028*.

[79] Visser, M. (1998). Acoustic black holes: horizons, ergospheres and hawking radiation. *Classical and Quantum Gravity*, 15(6):1767.

[80] Walter, M. and Ozols, M. (2023). Lecture notes on quantum information theory.

[81] Watson, G. N. (1922). *A treatise on the theory of Bessel functions*, volume 2. The University Press.

[82] Wyatt, R. E. (2005). *Quantum dynamics with trajectories: introduction to quantum hydrodynamics*, volume 28. Springer Science & Business Media.

Appendix A

The Jacobi-Anger identity

According to [4], the Jacobi-Anger identity is given by

$$e^{iz\cos\theta} = \sum_m i^m J_m(z) e^{im\theta}, \tag{A.1}$$

where $J_m(z)$ is a Bessel function of the first type and $m \in \mathbb{Z}$. In the context of Ch.4, one can therefore write

$$e^{i\mathbf{k}\cdot\mathbf{x}} = e^{ikx\cos(\theta_r - \theta_k)} = \sum_m i^m J_m(kr) e^{im\theta_r} e^{-im\theta_k}, \tag{A.2}$$

where we have used the notation $k = |\mathbf{k}|$ and $x = |\mathbf{x}|$.

Appendix B

Bessel functions: properties and asymptotic expansion

B.1 Bessel functions and Rindler

A relationship between the Bessel functions of the first and second type, and the modified Bessel function of the second type, can be found in [1], given by

$$Y_\nu(z) = e^{\pm(\nu+1)\pi i/2} I_\nu(z e^{\mp \pi i/2}) - \frac{2}{\pi} e^{\mp \nu \pi i/2} K_\nu(z e^{\mp \pi i/2}). \tag{B.1}$$

Choosing the lower sign and using the identity

$$I_\nu(z) = e^{\nu \pi i/2} J_\nu(z e^{-\pi i/2}), \tag{B.2}$$

we find that the relation can be re-expressed as

$$Y_\nu(z) = -i J_\nu(z) - \frac{2}{\pi} e^{\nu \pi i/2} K_\nu(iz). \tag{B.3}$$

This expression can be rather easily rewritten to

$$J_\nu(z) - i Y_\nu(z) = \frac{2i}{\pi} e^{\nu \pi i/2} K_\nu(iz), \tag{B.4}$$

which is in the form sought in the Rindler example.

B.2 Kontorovich-Ledebev transform

According to [27, 51], for a function $f(x)$ and $y > 0$, one may write the Kontorovich-Lebedev tranform

$$f(x) = \frac{2}{\pi^2} \int_0^\infty \mathrm{d}x \, x \sinh(\pi x) f(x) \int_0^\infty \mathrm{d}y \, \frac{1}{y} K_{ix}(y) K_{ix}(y), \tag{B.5}$$

where $K_{ix}(y)$ is the modified Bessel function of the second type.

B.3 General properties and identities

B.3.1 Bessel differential equation

The differential equation solved by the Bessel function of the first type $J_\nu(x)$ and second type $Y_\nu(x)$ is given by

$$x^2\partial_x^2 f(x) + x\partial_x f(x) + (x^2 - \nu^2)f(x) = 0. \tag{B.6}$$

A similar differential equation to the one above is solved by the modified Bessel function of the first kind $I_\nu(x)$ and second kind $K_\nu(x)$:

$$x^2\partial_x^2 f(x) + x\partial_x f(x) - (x^2 + \nu^2)f(x) = 0. \tag{B.7}$$

B.3.2 Hänkel functions

The two Hänkel functions are defined as

$$H_n^{(1)}(x) = J_n(x) + iY_n(x) \tag{B.8}$$

$$H_n^{(2)}(x) = J_n(x) - iY_n(x) \tag{B.9}$$

B.3.3 Changing signs in modified Bessel functions

Let $z \in \mathbb{C}$ and $\nu \in \mathbb{C}$. For any modified Bessel function of the first kind it must hold [59] that

$$I_\nu(z) = e^{\mp i\nu\pi/2} J_\nu(ze^{\pm\pi i/2}). \tag{B.10}$$

Consider $\nu = -ic_0\omega$ and $z = i\omega x$. We can then rewrite the expression above as

$$I_{-ic_0\omega}(i\omega x) = e^{\mp c_0\omega\pi/2} J_{-ic_0\omega}(i\omega x e^{\pm i\pi/2}). \tag{B.11}$$

Choosing the lower sign simplifies the expression to

$$I_{-ic_0\omega}(i\omega x) = e^{c_0\omega\pi/2} J_{-ic_0\omega}(\omega x). \tag{B.12}$$

Next, we consider $z = -ic_0\omega$, but instead choose the upper sign, leading to

$$I_{-ic_0\omega}(-i\omega x) = e^{-c_0\omega\pi/2} J_{-ic_0\omega}(\omega x). \tag{B.13}$$

Isolating the Bessel function $J_\nu(x)$ and equating both expressions gives

$$I_{-ic_0\omega}(-i\omega x) = e^{-c_0\omega\pi} I_{-ic_0\omega}(i\omega x). \tag{B.14}$$

B.3.4 Complex conjugation

Let $z \in \mathbb{C}$ and $\nu \in \mathbb{C}$, then

$$(J_\nu(z))^* = J_{\bar{\nu}}(\bar{z}) \quad ; \quad (Y_\nu(z))^* = Y_{\bar{\nu}}(\bar{z}) \tag{B.15}$$

$$(I_\nu(z))^* = I_{\bar{\nu}}(\bar{z}) \quad ; \quad (K_\nu(z))^* = K_{\bar{\nu}}(\bar{z}) \tag{B.16}$$

B.3.5 Completeness

For a Bessel function of the first type with real argument and order, it holds that [42]:

$$\int_0^\infty \mathrm{d}x\, x J_m(\alpha x) J_m(\beta x) = \frac{\delta(\alpha-\beta)}{\alpha}. \tag{B.17}$$

B.4 Asymptotic expansions

The asymptotic expansion for large argument $z \to \infty$ and fixed order, up to leading order, is shown for all considered Bessel functions. The notation from [33, 59] has been adopted.

- Bessel functions:

$$J_\nu(z) \sim \sqrt{\frac{2}{\pi z}} \cos(z - \frac{\nu\pi}{2} - \frac{\pi}{4}) \tag{B.18}$$

$$Y_\nu(z) \sim \sqrt{\frac{2}{\pi z}} \sin(z - \frac{\nu\pi}{2} - \frac{\pi}{4}) \tag{B.19}$$

- Hänkel functions:

$$H_\nu^{(1)}(z) \sim \sqrt{\frac{2}{\pi z}} e^{z - \frac{\nu\pi}{2} - \frac{\pi}{4}} \tag{B.20}$$

$$H_\nu^{(2)}(z) \sim \sqrt{\frac{2}{\pi z}} e^{-(z - \frac{\nu\pi}{2} - \frac{\pi}{4})} \tag{B.21}$$

- Modified Bessel functions:

$$I_\nu(z) \sim \frac{1}{\sqrt{2\pi z}} \left[e^z + e^{\pm i\pi/2} e^{\pm\nu\pi i} e^{-z}\right] \tag{B.22}$$

$$K_\nu(z) \sim -\sqrt{\frac{\pi}{2z}} e^{-z} \tag{B.23}$$

For $z \to 0$, we have the following asymptotic expansion:

$$I_\nu(z) \sim \frac{(z/2)^\nu}{\Gamma(\nu+1)}. \tag{B.24}$$

B.5 Nicholson's integral

In line with the classic text [81], we denote Nicholson's integral (also known as Nicholson's formula) as

$$J_\nu^2(z) + Y_\mu^2(z) = \frac{8}{\pi^2}\int_0^\infty \mathrm{d}\alpha K_0(2z\sinh(\alpha))\cosh(2\nu\alpha), \tag{B.25}$$

where the real part of the argument $\Re(z) > 0$.

B.6 Cross-term integral

According to [59], the integral over $\mathcal{C}_\mu(z) = J_n(x)$ and $\mathcal{D}_\mu(z) = Y_n(x)$ can be shown to give

$$\int \mathrm{d}z\, zJ_\mu(\alpha z)Y_\mu(\alpha z) = \frac{z^2}{4}\{2J_\mu(\alpha z)Y_\mu(\alpha z) - J_{\mu-1}(\alpha z)Y_{\mu+1}(\alpha z) - J_{\mu+1}(\alpha z)Y_{\mu-1}(\alpha z)\}. \tag{B.26}$$

This result is non-zero and real for $\alpha \in \mathbb{R}$, $r \in \mathbb{R}$ and $\nu \in \mathbb{Z}$.

Appendix C

Entropy in classical information theory

As with many ideas in physics, the motivation behind entanglement entropy was inspired by developments in an entirely different field of research. Our hope was to rigorously connect the entropy measures from classical information theory to entanglement entropy as an interesting side-note, yet eventually this proved too great a distraction from what this dissertation set out to demonstrate in the first place. As such, we share a brief introduction to information measures in classical information theory in this humble appendix, since it would be a shame to let a good summary go to waste.

As in [21], we consider X to be some discrete random variable with an alphabet/state space $\mathcal{X}$. Furthermore, we take its probability mass function (henceforth: pmf) to be given by $p(x)$, with elements $x \in \mathcal{X}$. A natural question to ask in this context, is how much information about the system we gain upon observing the value of X. In [57] it is argued that such a measure should necessarily contain the probabilities of each element $x \in \mathcal{X}$, instead of their specific information content. This vision of 'gaining information' is captured by the Shannon entropy [57, 21], which is given by

$$S(X) = \mathbb{E}[\log(1/p(X))] = -\sum_{x\in\mathcal{X}} p_x \log p_x, \tag{C.1}$$

where we denote $S(X) \equiv S(p_1, ..., p_N)$. As a simple example to understand the usefulness of this measure of information, we consider the case of an 'unfair' coin toss, where the elements of $X = \{0, 1\}$ do not have an equal probability of occurring, *i.e.* $p(0) = \theta$ and $p(1) = 1 - \theta$. Hence, the coin-toss follows a Bernoulli distribution $X \sim \text{Ber}(x|\theta)$ [56]. In this case the Shannon entropy contains a 2-base logarithm and can be written as the binary cross-entropy

$$S(p) = -\theta \log \theta - (1 - \theta) \log(1 - \theta). \tag{C.2}$$

Maximizing this entropy shows that the greatest gain of information of the system comes from the case when $\theta = 1/2$. This is a natural example which is in line with our intuition; the *ab initio* outcome is maximally uncertain when both sides of the coin have equal probabilities. The Shannon entropy can in fact be interpreted as both of these statements; it measures the gain of information, but also acts as a measure of the uncertainty of X before observation. However, it is slightly optimistic to assume all of our systems of interest contain such a trivial alphabet. Instead, we also define the joint entropy of a pair $(X, Y) \sim p(x, y)$, where both X and Y are discrete random variables. This measure, in the light of the Shannon entropy, determines in what extend the content of X is related to Y. This form of entropy is given by

$$S(X,Y) = -\mathbb{E}[\log p(X,Y)] = -\sum_{x\in\mathcal{X}, y\in\mathcal{Y}} p(x,y)\log p(x,y). \tag{C.3}$$

Note that, if the random variables are unconditionally independent, the joint entropy separates into the sum of the Shannon entropy of both variables. Determining the joint-entropy provides information on the uncertainty of the pair (X, Y). However, what if we observed Y and want to infer the uncertainty of X? A measure for the conditional entropy can be found in [57, 21], and is based on the conditional probability $p(x, y) = p(x|y)p(y)$, where $p(y)$ is obtained by marginalizing over x. Hence, the conditional entropy is given by

$$\begin{aligned} S(Y|X) &= -\mathbb{E}[\log p(Y|X)] = -\sum_{x\in\mathcal{X}}\sum_{y\in\mathcal{Y}} p(x)p(y|x)\log p(y|x) \\ &= -\sum_{x\in\mathcal{X}}\sum_{y\in\mathcal{Y}} p(x,y)\log p(y|x). \end{aligned} \tag{C.4}$$

Using the properties of conditional probabilities, we can then rewrite this entropy to

$$S(Y|X) = -\sum_{x\in\mathcal{X}}\sum_{y\in\mathcal{Y}} p(x,y)\log p(y|x) = S(X,Y) - S(X), \tag{C.5}$$

where in the last line we use the symmetry $S(X, Y) = S(Y, X)$. This measure answers the question how much uncertainty about (X, Y) remains after observing of the discrete variables. Using these measures of entropy, we may now define a measure of the similarity between X and Y, *i.e.* how much the state spaces have in common, through the mutual information

$$I(X:Y) = S(X) + S(Y) - S(X,Y) = S(X) - S(X|Y). \tag{C.6}$$

This measure is quite easy to understand on a heuristic level; we take the uncertainty of the individual discrete states X and Y, and subtract their joint uncertainty. A slightly more insightful definition of the mutual information is obtained by defining the Kullback-Leibler divergence [57, 21, 56], which measures the inefficiency of assuming that the distribution is

$q(x)$, while the true distribution is $p(x)$:

$$\begin{aligned} D(p||q) &= \mathbb{E}[\log p(X)/q(X)] = \sum_{x\in\mathcal{X}} p(x)\log\frac{p(x)}{q(x)} \\ &= -S(X) - \sum_{x\in\mathcal{X}} p(x)\log q(x). \end{aligned} \tag{C.7}$$

Clearly, this measure is zero if $p(x) = q(x)$, and grows when the equality does not hold. The mutual information can be defined in terms of this measure [21], leading to

$$I(X:Y) = D(p(x,y)||p(x)p(y)) = \mathbb{E}_{x,y\sim p(x,y)}[\log p(X,Y)/p(X)p(Y)]. \tag{C.8}$$

There is an observation in order here which elucidates the function of the mutual information. If the random variables X and Y are unconditionally independent, *i.e.* their pmf factorizes as $p(x,y) = p(x)p(y)$, then the mutual information is seen to be zero. This makes sense: if the probability distributions do not overlap, the state spaces will not share any information content, and inferring values from X based on observations of Y becomes impossible. Once the pmf's share a greater degree of overlap, the mutual information increases accordingly.